

UNCLASSIFIED

AD NUMBER	
AD491310	
CLASSIFICATION CHANGES	
TO:	UNCLASSIFIED
FROM:	SECRET
LIMITATION CHANGES	
TO: Approved for public release; distribution is unlimited.	
FROM: Distribution authorized to DoD and DoD contractors only; Administrative/Operational Use; 10 MAY 1960. Other requests shall be referred to Defense Atomic Support Agency, Washington, DC.	
AUTHORITY	
DNA ltr 14 Sep 1995 ; DNA ltr 14 Sep 1995	

THIS PAGE IS UNCLASSIFIED

UNCLASSIFIED

AD 491310

DEFENSE DOCUMENTATION CENTER

FOR

SCIENTIFIC AND TECHNICAL INFORMATION

CAMERON STATION ALEXANDRIA, VIRGINIA



UNCLASSIFIED

NOTICE: When government or other drawings, specifications or other data are used for any purpose other than in connection with a definitely related government procurement operation, the U. S. Government thereby incurs no responsibility, nor any obligation whatsoever; and the fact that the Government may have formulated, furnished, or in any way supplied the said drawings, specifications, or other data is not to be regarded by implication or otherwise as in any manner licensing the holder or any other person or corporation, or conveying any rights or permission to manufacture, use or sell any patented invention that may in any way be related thereto.

WT-1404

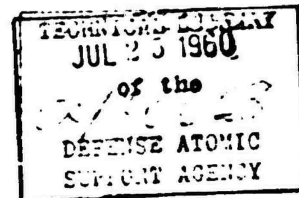
This document consists of 136 pages.

No. 150 of 180 copies, Series A

OPERATION PLUMB BOB



NEVADA TEST SITE
MAY-OCTOBER 1957



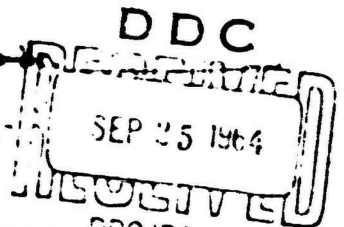
Project 1.4

GROUND-ACCELERATION, STRESS, and STRAIN
at HIGH INCIDENT OVERPRESSURES (U)

Issuance Date: May 10, 1960

Classification on () to **UNCLASSIFIED**
By Authority of *ASAC-3*
By *10/10/60*

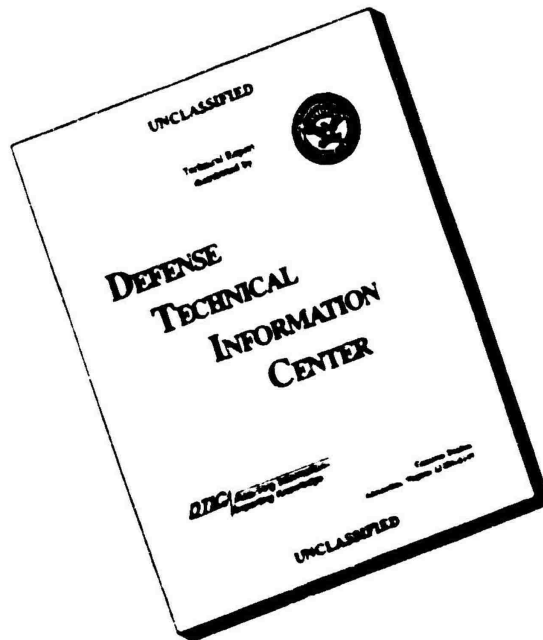
HEADQUARTERS FIELD COMMAND
DEFENSE ATOMIC SUPPORT AGENCY
SANDIA BASE, ALBUQUERQUE, NEW MEXICO



FORMERLY SELECTED DATA

UNCLASSIFIED

DISCLAIMER NOTICE



**THIS DOCUMENT IS BEST
QUALITY AVAILABLE. THE
COPY FURNISHED TO DTIC
CONTAINED A SIGNIFICANT
NUMBER OF PAGES WHICH DO
NOT REPRODUCE LEGIBLY.**

Inquiries relative to this report may be made to

Chief, Defense Atomic Support Agency
Washington 25, D. C.

When no longer required, this document may be
destroyed in accordance with applicable security
regulations.

DO NOT RETURN THIS DOCUMENT

Handwritten notes:
This document contains information
concerning the defense of the United States
and is to be kept confidential.
Do not discuss this information with
anyone outside your organization.
If you are not a member of the
organization, do not discuss this
information with anyone.

Handwritten notes:
CONFIDENTIAL

UNCLASSIFIED

WT-1404

OPERATION PLUMBBOB—PROJECT 1.4,

GROUND ACCELERATION, STRESS, and STRAIN
at HIGH INCIDENT OVERPRESSURES

L. M. Swift, ~~Project Officer~~
D. C. Sachs *and*
F. M. Sauer

Stanford Research Institute
Menlo Park, California

ALL INFORMATION CONTAINED HEREIN IS UNCLASSIFIED
DATE 10-10-80 BY 1043
EXCEPT WHERE SHOWN OTHERWISE
THIS DOCUMENT CONTAINS INFORMATION AFFECTING
THE NATIONAL DEFENSE OF THE UNITED STATES
WITHIN THE MEANING OF THE Espionage Laws,
TITLE 18, U.S.C. SECS. 793 AND 794, THE
TRANSMISSION OR REVELATION OF WHICH IN ANY
MANNER TO AN UNAUTHORIZED PERSON IS PRO-
HIBITED BY LAW.

UNCLASSIFIED

FOREWORD

This report presents the final results of one of the 46 projects comprising the military-effects program of Operation Plumbbob, which included 24 test detonations at the Nevada Test Site in 1957.

For overall Plumbbob military-effects information, the reader is referred to the "Summary Report of the Director, DOD Test Group (Programs 1-9)," ITR-1445, which includes: (1) a description of each detonation, including yield, zero-point location and environment, type of device, ambient atmospheric conditions, etc.; (2) a discussion of project results; (3) a summary of the objectives and results of each project; and (4) a listing of project reports for the military-effects program.

ABSTRACT

Project 1.4 objectives were to measure underground effects of a nuclear air burst (Shot Priscilla; 36.8 kt) as they vary with time, depth, and ground range, particularly in the region of high pressure; furnish, from these measurements, input data to other projects; and analyze these measurements with results of other tests. At 750 and 1,050 feet from ground zero, acceleration, stress, and strain measurements were made at several depths down through 50 feet, including two measurements each of horizontal acceleration and stress. At 450, 550, 650, 750, 850, 1,050, and 1,350 feet, vertical acceleration and stress were measured at 50- and 10-foot depths.

Records were obtained on 52 out of 64 gage channels installed. Losses were caused by mechanical failure of one oscillograph and by miscellaneous individual channel failures.

Wave forms of acceleration and velocity showed no ideal or classical shape but could be grouped in six categories according to their characteristics.

Outrunning occurred at the ground surface at 2,500-foot ground range from a signal originating at 1,900-foot ground range. However, outrunning can occur at closer ranges for deep measurements, and refracted signals may be recorded after arrival of local effects, as evidenced by acceleration measurements.

Attenuation of maximum downward acceleration at 5- and 10-foot depths varied between 30 and 45 percent except at 550- and 650-foot ranges where it was negligible. At greater depths, wave theory concerning energy transfer at an interface between two materials was borne out. Horizontal (outward) acceleration at 10- and 50-foot depths was attenuated less with depth than was the corresponding peak downward acceleration.

Peak downward velocity followed an exponential decay law rather than a power law decay characteristic of downward acceleration. At 275-psi level, horizontal (outward) velocity showed somewhat less attenuation with depth than the downward component. At the 100-psi level, peak outward velocity at 50-foot depth was twice that at 10-foot depth, owing to signals from sources closer to ground zero.

Attenuation of peak displacement corresponded closely to attenuation of peak velocity.

Attenuation of maximum vertical stress was slight between the surface and 5-foot depth, and stress decreased by half for every 10-foot increase in depth, except at 50-foot depth where it increased. Stress measurements on this project were not considered entirely successful, despite extreme caution exercised in gage placement and backfill procedure.

At 275-psi overpressure, peak strain decreased abruptly between 1- and 30-foot depths, leveling off to a constant value at greater depths. At 100-psi overpressure, vertical strain showed almost no change with depth. This difference between the two stations could probably be traced to the longer rise time of the overpressure at 100 psi than at 275 psi.

The velocity-jump peak overpressure ratio increased with decreasing pressure, with no apparent systematic variation with yield, overpressure level or wave form, or test area. Experimental ratios agreed well with the theoretical result. Peak vertical displacement-overpressure impulse ratio data were too scattered to allow firm conclusions.

From displacement-response spectra, the change in the character of the response appeared to be associated with the interference of the refracted ground-transmitted wave and not with the local ground wave. Normalized velocity spectra for 5-, 10-, and 50-foot depths showed similar maxima although the frequency at which this maximum occurred decreases with increasing depth.

In stress-strain relations, it was tentatively concluded that laboratory triaxial tests were more useful in correlation with blast results than were compaction tests.

PREFACE

The planning and execution of Project 1.4 were under the direction of L. M. Swift, with L. H. Inman serving as field party chief and W. M. Wells as assistant to the project leader. Other members of the field party included R. E. Aumiller, V. E. Krakow, J. Milless, R. V. Ohler, C. M. Westbrook, and H. Wuner. Miss Barbara Ames, Miss Phyllis Flanders, Mrs. Elizabeth Hearn, Miss Sherry Ward, Mrs. Barbara Wells, and Mrs. Mona Wise assisted in the data analysis and preparation of the report.

The excellent planning and cooperation of Maj H. T. Bingham, USAF, Lt Col J. A. Kodis, USAF, and LCDR J. F. Clarke, AFSWP (DASA) Field Command, are gratefully acknowledged. The assistance and cooperation of T. B. Goode and his party, of Project 3.8, in the control of backfill procedures are also especially recognized.

CONTENTS

FOREWORD	4
ABSTRACT	5
PREFACE	6
CHAPTER 1 INTRODUCTION	13
1.1 Objectives	13
1.2 Background	13
1.3 Theory	14
1.3.1 Models for Soil Reacting to Stress	14
1.3.2 Homogeneous Elastic Solid	18
1.3.3 Effects from Remote Sources	19
1.4 Seismic Measurements	21
CHAPTER 2 PROCEDURE	24
2.1 Predictions	24
2.1.1 Input Predictions	24
2.1.2 Earth Stress	24
2.1.3 Seismic Velocity	24
2.1.4 Earth Strain	25
2.1.5 Earth Acceleration	25
2.2 Instrumentation	26
2.2.1 Central Station	26
2.2.2 Stress Gages	27
2.2.3 Strain Gages	27
2.2.4 Accelerometers	27
2.2.5 Instrument Response	27
2.2.6 Calibration	29
2.3 Experiment Plan	30
2.3.1 Gage Placement	30
2.3.2 Gage Cabling	30
2.3.3 Gage Layout	30
2.3.4 Seismic Measurements	30
2.4 Field Operations	32
CHAPTER 3 RESULTS	34
3.1 Instrumentation Performance	34
3.2 Data Reduction Procedures	34
3.2.1 General	34
3.2.2 Integration Procedures	34
3.3 Gage Records and Tables of Results	35
3.3.1 Overpressure	35
3.3.2 Earth Accelerations	35
3.3.3 Earth Velocity	42
3.3.4 Earth Displacement	47

3.3.5 Earth Stress - - - - -	52
3.3.6 Earth Strain - - - - -	52
3.4 Seismic Measurements - - - - -	55
3.4.1 In Situ Seismic Velocities - - - - -	61
3.4.2 Velocities in Backfill - - - - -	62
CHAPTER 4 DISCUSSION - - - - -	65
4.1 Acceleration and Velocity Wave Forms - - - - -	65
4.2 Signals from Remote Sources - - - - -	66
4.3 Attenuation of Ground Shock with Depth - - - - -	67
4.3.1 Acceleration (Attenuation with Depth) - - - - -	67
4.3.2 Velocity (Attenuation with Depth) - - - - -	71
4.3.3 Displacement (Attenuation with Depth) - - - - -	77
4.3.4 Stress (Attenuation with Depth) - - - - -	77
4.3.5 Strain (Attenuation with Depth) - - - - -	82
4.4 Ground Shock and Overpressure - - - - -	82
4.4.1 Acceleration (and Overpressure) - - - - -	82
4.4.2 Velocity (and Overpressure) - - - - -	87
4.4.3 Displacement (and Overpressure) - - - - -	91
4.4.4 Strain (and Overpressure) - - - - -	95
4.5 Response Spectrum of Ground Motion - - - - -	95
4.5.1 Theory - - - - -	95
4.5.2 Measurements - - - - -	99
4.5.3 Correlation and Scaling - - - - -	103
4.6 Soil Stress-Strain Considerations - - - - -	112
4.6.1 Soil Survey Tests - - - - -	112
4.6.2 Deduced Stress-Strain - - - - -	116
CHAPTER 5 CONCLUSIONS AND RECOMMENDATIONS - - - - -	117
5.1 Conclusions - - - - -	117
5.1.1 Instrument Performance - - - - -	117
5.1.2 Acceleration and Velocity Wave Forms - - - - -	117
5.1.3 Signals from Remote Sources - - - - -	117
5.1.4 Attenuation of Ground Shock with Depth - - - - -	118
5.1.5 Ground Shock and Overpressure - - - - -	119
5.1.6 Response Spectrum of Ground Motion - - - - -	119
5.1.7 Soil Stress-Strain Considerations - - - - -	120
5.2 Recommendations - - - - -	120
APPENDIX A SYMBOLS AND OVERPRESSURE WAVE FORM CLASSIFICATION - - -	121
A.1 Symbols - - - - -	121
A.2 Overpressure Wave Form Classification - - - - -	122
APPENDIX B CATALOG OF GROUND MOTION MEASUREMENTS - - - - -	124
APPENDIX C RECORD INTEGRATION AND INSTRUMENT RESPONSE - - - - -	127
C.1 Acceleration Baseline Shift - - - - -	127
C.2 Instrument Response - - - - -	130
APPENDIX D SCALING OF POSITIVE OVERPRESSURE IMPULSE AND DURATION - - - - -	131

TABLES

1.1 Refinements of Linear Elastic Theory	16
1.2 Phenomena Explained by Various Models of Soil Behavior	18
1.3 Approximate Overpressures at which Outrunning of Ground Wave Occurs, Large Yield Surface Bursts	21
1.4 Poisson's Ratio for Some Materials	23
2.1 Shot Priscilla Input Predictions	25
2.2 Gage Layout	31
3.1 Summary of Peak Surface Overpressure, Shot Priscilla	35
3.2 Summary of Corrected Acceleration, Velocity and Displacement Data, Shot Priscilla	41
3.3 Summary of Stress Data, Shot Priscilla	54
3.4 Summary of Strain Data, Shot Priscilla	61
4.1 Examples of Vertical Acceleration Wave Form Types Shown in Figure 4.1	67
4.2 Maximum Strain, Shot Priscilla	83
4.3 Average Propagation Velocity of Direct Wave, 0 to 10 Feet, Shot Priscilla	91
4.4 Comparison of Maximum Transient-Vertical Displacement, Shot Priscilla	95
4.5 Maximum of Normalized Velocity Spectrum, Shot Priscilla	112
4.6 Project 3.8 Soil Survey Results	116
B.1 Summary of Nevada Surface and Air Nuclear Bursts on which Strong Ground Motion was Measured	124
B.2 Number of Ground Motion Measurements, NTS	125
B.3 Number of Ground Motion Measurements, EPG	126
B.4 Summary of Mole Rounds (256-pound TNT)	126
B.5 Number of Ground Motion Measurements, Jangle HE-4	126
C.1 Baseline Corrections, Shot Priscilla	128

FIGURES

1.1 Typical stress and strain diagrams for various models of soil behavior	15
1.2 Schematic stress-strain relation for a plastic material	16
1.3 Actual record of stress versus strain in typical silty clay	17
1.4 Schematic diagram of superseismic wave front	19
1.5 ϕ versus U/C_L and Poisson's ratio	20
1.6 Construction of ground motion arrival time curves, Tumbler Shot 1	20
1.7 Seismic velocity ratios versus Poisson's ratio	22
2.1 Earth stress gage	28
2.2 Schematic, earth strain gage	28
2.3 Earth strain gage, unassembled	29
2.4 Earth strain gage, installed	29
2.5 Gage layout	32
2.6 Seismic locations	33
3.1 Surface overpressure versus time, Stations 1 to 7, Shot Priscilla	36
3.2 Vertical acceleration versus time, Stations 1, 2 and 3, Shot Priscilla	37
3.3 Vertical acceleration versus time, Station 4, Shot Priscilla	38
3.4 Horizontal acceleration versus time, Station 4; vertical acceleration versus time, Station 5; Shot Priscilla	38
3.5 Vertical acceleration versus time, Station 6, Shot Priscilla	39
3.6 Horizontal acceleration versus time, Station 6; vertical acceleration versus time, Station 7; Shot Priscilla	40
3.7 Vertical velocity versus time, Station 1, Shot Priscilla	42
3.8 Vertical velocity versus time, Station 2, Shot Priscilla	43

3.9 Vertical velocity versus time, Station 3, Shot Priscilla - - - - -	43
3.10 Vertical velocity versus time, Station 4, Shot Priscilla- - - - -	44
3.11 Horizontal velocity versus time, Station 4; vertical velocity versus time, Station 5; Shot Priscilla - - - - -	45
3.12 Vertical velocity versus time, Station 6, Shot Priscilla- - - - -	46
3.13 Horizontal velocity versus time, Station 6; vertical velocity versus time, Station 7; Shot Priscilla - - - - -	47
3.14 Vertical displacement versus time, Stations 1, 2 and 3, Shot Priscilla - - - - -	48
3.15 Vertical and horizontal displacement versus time, Stations 4 and 5, Shot Priscilla- - - - -	49
3.16 Vertical displacement versus time, Station 6, Shot Priscilla - - - - -	50
3.17 Horizontal displacement versus time, Station 6; vertical displacement versus time, Station 7; Shot Priscilla - - - - -	51
3.18 Vertical stress versus time, Stations 1 and 2, Shot Priscilla- - - - -	52
3.19 Vertical stress versus time, Station 3, Shot Priscilla- - - - -	53
3.20 Vertical stress versus time, Station 4, Shot Priscilla- - - - -	53
3.21 Horizontal stress versus time, Station 4; vertical stress versus time, Station 5; Shot Priscilla - - - - -	55
3.22 Vertical stress versus time, Station 6, Shot Priscilla- - - - -	56
3.23 Vertical and horizontal stress versus time, Station 6, Shot Priscilla- - - - -	58
3.24 Vertical strain versus time, Stations 4 and 6, Shot Priscilla - - - - -	59
3.25 Travel-time data, Shot Point 1, Frenchman Flat - - - - -	60
3.26 Travel-time data, Shot Point 2, Frenchman Flat - - - - -	60
3.27 Travel-time data, Shot Point 3, Frenchman Flat - - - - -	62
3.28 Refraction survey, travel-time data, and wave front diagram, Frenchman Flat - - - - -	63
3.29 Refraction survey, short-span instrument array, Frenchman Flat - - - - -	64
4.1 Schematic diagrams of vertical acceleration and velocity wave forms - - - - -	66
4.2 Uncorrected and corrected vertical velocities, 5-psi overpressure, Tumbler Shot 1 - - - - -	68
4.3 Vertical velocity versus ground range, Tumbler Shot 1, 5-foot depth - - - - -	68
4.4 Air-blast time of arrival, Shot Priscilla, and seismic soil survey, Frenchman Flat - - - - -	69
4.5 Earth acceleration versus depth, Shot Priscilla- - - - -	70
4.6 Attenuation of vertical acceleration with depth, Nevada Test Site (power law attenuation) - - - - -	71
4.7 Attenuation of vertical acceleration with depth, Nevada Test Site (exponential law attenuation)- - - - -	72
4.8 Attenuation of vertical acceleration with depth, Nevada Test Site - - - - -	73
4.9 Attenuation of downward velocity with depth, Nevada Test Site - - - - -	73
4.10 Increase in vertical velocity rise time with depth, Frenchman Flat - - - - -	74
4.11 Overpressure, particle velocity, earth stress, normalized to maximum value, Stations 1 through 3, Shot Priscilla - - - - -	75
4.12 Overpressure, particle velocity, earth stress, normalized to maximum value, Stations 3 and 4, Shot Priscilla - - - - -	75
4.13 Overpressure, particle velocity, earth stress, normalized to maximum value, Station 4, Shot Priscilla- - - - -	76
4.14 Overpressure, particle velocity, earth stress, normalized to maximum value, Stations 5 and 6, Shot Priscilla - - - - -	78
4.15 Overpressure, particle velocity, earth stress, normalized to maximum value, Stations 6 and 7, Shot Priscilla - - - - -	79
4.16 Attenuation of vertical displacement, Frenchman Flat- - - - -	80
4.17 Maximum earth stress versus gage depth, Shot Priscilla- - - - -	80

4.18	Earth strain versus depth, Shot Priscilla -----	84
4.19	Vertical acceleration, Frenchman Flat, 5-foot depth -----	85
4.20	Vertical acceleration, Tumbler Shots 1 and 2, 5-foot depth -----	85
4.21	Vertical acceleration, Tumbler Shots 2, 3, and 4, 5-foot depth -----	86
4.22	Vertical acceleration at 5-foot depth versus ground range, Tumbler -----	86
4.23	Vertical acceleration, Jangle HE-4, 5-foot depth -----	88
4.24	Vertical acceleration, Jangle S -----	88
4.25	Vertical acceleration, Project Mole, Nevada sand and gravel mix, 5-foot depth -----	89
4.26	Vertical acceleration, Project Mole, Utah dry clay, 5-foot depth -----	89
4.27	Vertical velocity, 5-foot depth, summary of superseismic data -----	90
4.28	Vertical velocity, Tumbler Shot 1, 5-foot depth -----	90
4.29	Vertical velocity, Tumbler Shot 2, 5-foot depth -----	92
4.30	Vertical velocity, Tumbler Shot 3, 5-foot depth -----	92
4.31	Vertical velocity, Tumbler Shot 4, 5-foot depth -----	93
4.32	Vertical velocity, Frenchman Flat, 5-foot depth -----	93
4.33	Summary of vertical displacement, Nevada Test Site -----	94
4.34	Summary of reed-gage data (displacement spectra), Nevada Test Site -----	94
4.35	A linear, single-degree-of-freedom system -----	98
4.36	Schematic diagram of ground particle velocity -----	98
4.37	Schematic diagram of velocity spectrum -----	98
4.38	Shot Priscilla vertical displacement spectra -----	100
4.39	Shot Priscilla horizontal displacement spectra -----	102
4.40a	Vertical velocity spectra, 5-foot depth, Shot Priscilla -----	103
4.40b	Vertical velocity spectra, 10-foot depth, Shot Priscilla -----	104
4.40c	Vertical velocity spectra, 275 psi, Shot Priscilla -----	105
4.40d	Vertical velocity spectra, 100 psi, Shot Priscilla -----	106
4.41a	Horizontal velocity spectra, 275 psi, Shot Priscilla -----	107
4.41b	Horizontal velocity spectra, 100 psi, Shot Priscilla -----	108
4.42	Shot Priscilla vertical acceleration spectra -----	109
4.43	Normalized vertical velocity spectra, Priscilla 5-foot depth -----	110
4.44	Normalized vertical velocity spectra, Priscilla 10-foot depth -----	110
4.45	Normalized vertical velocity spectra, Priscilla 50-foot depth -----	111
4.46	Normalized horizontal velocity spectra, Priscilla 10-foot depth -----	111
4.47	Normalized horizontal velocity spectra, Priscilla 50-foot depth -----	113
4.48	Stress-strain curves, undisturbed soil, Frenchman Flat -----	113
4.49	Project 1.4 constant ratio of applied stress, triaxial tests, undisturbed soil, 50-foot depth -----	114
4.50	Stress-strain diagram, Station 4, Shot Priscilla -----	115
4.51	Stress-strain diagram, Station 6, Shot Priscilla -----	115
C.1	Typical velocity-time wave forms from Types a, b, or c acceleration-time wave forms -----	129
C.2	Uncorrected and corrected vertical velocities -----	129
C.3	Comparison of ERA and Wiancko accelerometer data, Tumbler Shot 1, 5-foot depth -----	130
D.1	Positive overpressure impulse versus peak overpressure -----	132
D.2	Positive overpressure duration versus peak overpressure -----	132

SECRET

Chapter 1 **INTRODUCTION**

1.1 OBJECTIVES

The objectives of Project 1.4 were to: (1) measure underground effects of a nuclear air burst as they varied with time, depth, and ground range, particularly in the region of high pressure; (2) use these measurements to furnish input data to other projects; and (3) analyze these data in combination with the results of other tests to establish criteria for the prediction of underground effects.

The quantities measured were earth acceleration, earth stress, and earth strain.

In addition, to obtain more information on the test medium, seismic studies were performed at Frenchman Flat.

1.2 BACKGROUND

Underground effects of a nuclear air burst, as opposed to underground effects of an underground burst, have not been extensively investigated. The most complete full-scale study of these effects was on Operation Upshot-Knothole (Reference 1), when detailed measurements of earth acceleration, stress, and strain were made at one depth and at one ground range on two shots and when measurements of earth stress were made at three depths at several ground ranges on the same shots. On Operation Tumbler (Reference 2), earth acceleration was measured on four shots; measurements were made at two depths on one shot and at three depths at two ground ranges on all four shots. Only one of these shots was in Frenchman Flat; the other three were in the Yucca Flat T7 area, where geological conditions were considerably different. All these measurements were made at pressure levels considerably lower than the regions of present interest. Small-scale studies of similar phenomena conducted by Stanford Research Institute (SRI) on Project Mole (Reference 3) and by SRI on the high-explosives series of Operation Buster-Jangle (Reference 4) provided little useful information; the limited frequency response of the instruments used resulted in under-registration of the phenomena. Therefore, extrapolation of these small-scale results to full-scale effects was probably not useful.

Rather extensive small-scale and full-scale studies of underground effects of underground high explosives have been conducted, but the transmission and loading mechanisms under high-explosive test conditions differed so markedly from those of the conditions of this project that extension of their results to these problems was difficult if not impossible.

Requirements have been set up for criteria for protective construction against large air and surface bursts in the pressure regions of 100 psi and above. Such requirements imply that, wherever possible, underground construction must be used for maximum protection. It is believed that most of the loading of underground structures in these pressure regions from such shots will be produced by the air-blast slap on the surface in the immediate vicinity of the structure (local effects), rather than by energy transmitted through the ground from the regions closer to ground zero (remote effects). This project was established to obtain quantitative data on underground phenomena in these regions and to explore these phenomena sufficiently to permit at least a tentative application of the results to similar effects in soils other than those characteristic of Frenchman Flat. Because of limitations imposed at the Nevada Test Site (NTS),

SECRET

FORMERLY RESTRICTED DATA

it was not possible to plan a large surface shot; therefore these studies were based on the effects of a moderately large (35 to 40 kt) air burst.

A complete description of the ground motion induced by air blast from a high-explosive or nuclear detonation requires spatial and temporal specification of both the horizontal radial (hereafter referred to simply as the horizontal component) and vertical components of: (1) particle acceleration; (2) particle velocity; (3) particle displacement; and (4) earth strain. Theoretically, only one of these need be presented along with earth stress since any one of the first three may be derived from the other by differentiation or integration with respect to time, and strain may be found by differentiation of displacement with distance and vice versa. Together these parameters form a redundant set of data since the relationship between them is simply one of geometry. On the other hand, if the medium exhibits inelastic behavior, the relationship of stress to particle velocity, for example, requires a great deal more knowledge than is now available. Furthermore, if the medium is strain-rate sensitive (as soil is suspected to be) or possesses visco-elastic properties, then stress depends not only on the instantaneous values of strain and/or particle velocity but on their past history as well.

From a practical standpoint, specification of ground motion as a single parameter is seriously limited by the small number and low density of observations made on any one experiment and also by the inherent complexity of soil-particle motion compared with that of air. At present, ground motion must be specified as positive and negative peak values, time durations, and representative pulse shapes. Hence, salient features of acceleration, velocity, displacement, and strain may be lost. If these salient features are required, as in computation of response spectrum (see Chapter 4), it is necessary to refer to the original records.

In seeking a valid correlation of ground motion data with air blast input data, answers to several fundamental questions are required. These may be set forth as follows:

1. What relationships are to be expected between the various elements of ground motion and air-blast input? How are these relationships modified by soil properties and by variation of soil properties with depth?
2. Are the above relationships expected to vary with yield of the device, ground range, and/or stress level? If so, are these variations of major importance?
3. For a particular test area, i.e., a relatively fixed set of soil properties, are data from various experiments internally consistent?
4. Do systematic differences in the correlations appear when data from one test area are compared with those from another? Are these differences consistent with known variations of soil properties?

Obviously the answers to Items 1, 2, and 3 depend a great deal on theoretical knowledge of the problem since the number of measurements involved are not sufficient to form an independent empirical evaluation of all factors involved.

1.3 THEORY

Adaption of historical theories of the propagation of stress through soil is limited in that either (1) flows are slow under applied loads or stresses (soil statics), or (2) stress waves are of low intensity (exploration and earthquake seismology). The present need is for theories and special experiments that consider stress waves of high intensity and rapid rates of loading.

1.3.1 Models for Soil Reacting to Stress. In this section are reviewed the well-known mathematical models (Figure 1.1) for solids which are subjected to stress, and the limitations and range of applicability of these models are described.

Linear Elasticity: Statics. For the study of small strains, linear elasticity may be a satisfactory model (Column 1 of Figure 1.1). In this model, soil is assumed to act essentially as a linear spring supporting a mass. Because of the success of this model in studying complicated problems involving steel, it has received a tremendous amount of attention.

The theory of elasticity without further qualification may be understood to mean a theory based on the assumption that there is a unique relationship between stress and strain; more

explicitly, that for the material under consideration, each component of stress can be calculated solely from a knowledge of the local strain. This assumption is believed to be false for all known materials; but it is a useful approximation. In actual practice, the previous history of the material, the rate of strain, and even the derivative of the rate of strain can affect the values of the stress at each point. Spectacular examples of dependence on these quantities are

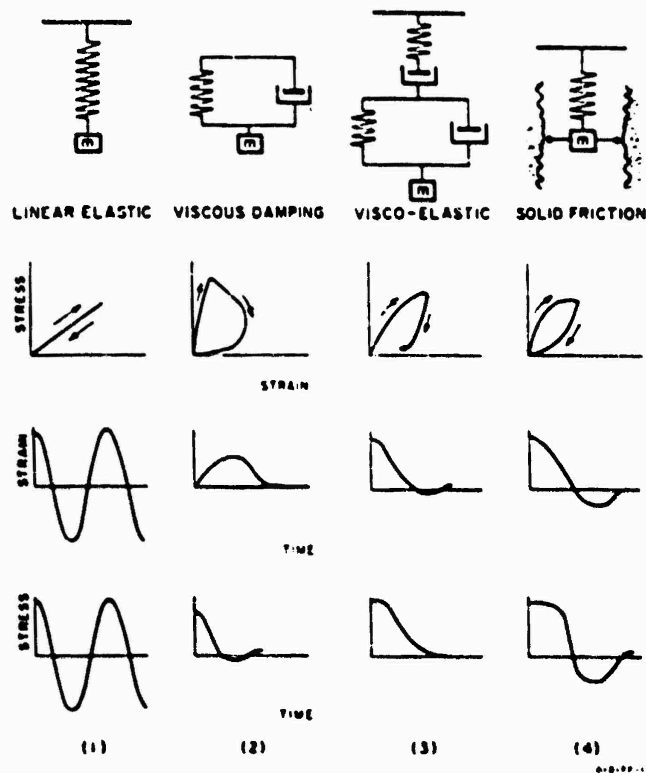


Figure 1.1 Typical stress and strain diagrams for various models of soil behavior (sudden stress).

given by bouncing putty, bread dough, natural rubber, and synthetic plastics.

The complications or modifications of pure (linear) elastic theory which must be considered can be separated into two classes (Table 1.1). The first class is the set of complications in space, e. g., vertical anisotropy. The second class is the set of complications which are intrinsic in every cubic millimeter of the soil. Certainly the two types of complications can be combined: viscosity of soil can change with depth, etc.

Nonlinear Elasticity. It is possible to conceive of a substance in which the Lamé constants, or (since they are related) in which Young's modulus and Poisson's ratio, depend on the strain. A simple example of such a substance is a spring which becomes stiffer in compression. A helical spring will exhibit this characteristic when it closes coil to coil.

For a spring which becomes stiffer with increasing strain, the mathematical model is that of a substance which consists of various fibers, some of which offer no resistance to strain until the strain reaches a finite value. A corresponding model is possible for a spring which becomes less stiff with increasing strain. These models can even be combined to give a model of a substance, the stiffness of which first decreases and then increases with increasing strain. For all these models, the supposition is that the strain is completely recovered when stress is relieved. These models can probably be used successfully for certain analyses; since they are too simple

to explain certain other experimental results, they seem not to have been used extensively in the literature.

Plasticity. By nonlinear behavior is meant usually a medium which has properties different even from those of the paragraph above. If a solid undergoes permanent deformation or set when it is strained, it is said to be plastic (clay, for example). A schematic stress-strain relation for a plastic material is that of Figure 1.2.

This diagram is similar in some respects to Figure 1.3 which is a stress versus strain curve determined from dynamic measurements obtained in typical silty clay soil.

In Figure 1.2, the material is called perfectly plastic if AB is a horizontal line and OA and BC are parallel straight lines. Such a material behaves as a linear elastic material with no per-

TABLE 1.1 REFINEMENTS OF LINEAR ELASTIC THEORY

Complications in Space	Complications Intrinsic to the Medium
Space-Dependent Velocities	Nonlinearity
Interfaces	Viscosity
Free Surfaces	Visco-Elasticity
Layering	Intrinsic Anisotropy
Refractions	(as in crystals)
Reflections	
Interference	
Lenses	
Boulders	
Inhomogeneities	

manent set if the stress remains below a yield value; the stress can never exceed this yield value; when the yield value is reached, the material flows plastically. A more general curve, such as that of Figure 1.2 would be obtained by postulating a model with several fibers; each fiber is perfectly plastic, but the fibers have different yield values.

Viscosity. It is convenient to study the propagation of waves in a plastic substance by assuming that a certain amount of strain energy is dissipated at the wave front. One possible mode of dissipation, which seems physically reasonable, is that the rate of loss of energy de-

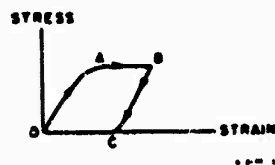


Figure 1.2 Schematic stress-strain relation for a plastic material.

pends on particle velocity; this is viscous friction. The mechanical analog for this mode is that of a spring and dashpot in parallel (see Column 2 of Figure 1.1). For this model, the attenuation per cycle is a function of the frequency.

Visco-Elasticity. If stress is applied to a sample of soil rapidly and then suddenly removed, the graph of strain against time is like that in Column 3 of Figure 1.1. A plausible model is that at the top of the column. The upper spring and dashpot allow for permanent set and rapid relief of stress; the spring and dashpot in parallel allow for gradual relief of the remaining portion of stress. Indeed, any number of parallel spring-dashpot units (Voigt units) can be connected in series to make a still more complicated model. The model in question can be thought of as a system of three Voigt units in series. The dashpot constant in the first unit is zero: it is effectively a spring alone. The spring constant in the second unit is zero: it is effectively a dashpot alone. In the third unit, the spring constant and the dashpot constant are both different from zero.

Solid Friction. In a solid friction model, (Column 4, Figure 1.1) dissipation of energy is assumed to depend on particle displacement but not on particle velocity. The attenuation per cycle is thus independent of the frequency. Certain laboratory experiments of Born (Reference 5) on oven-dried rocks support this model. For wet rocks, Born shows that viscous as well as solid friction damping is present. This result will probably be true for clay soil as well. In the model for solid friction used by Born, the damping force is taken to be proportional to displacement from the neutral position. This is not stated by him, but can be inferred from the formulas which he uses. This kind of damping is also termed structural damping.

Other Mathematical Models. Besides the possibility, already alluded to, of using more than three Voigt units in series, the above schemes are not the only ones that have to be considered in making mechanical models of the behavior of soil. Unfortunately soil is not isotropic. The most common variation in properties which it is necessary to take into account is horizontal layering. For example, there can be horizontal layers, in which seismic velocities are widely different. It is frequently true also that in any one stratum the horizontal velocity is not the same as the vertical velocity.

The propagation of waves in a layered medium is a special topic. Some wave paths which enter the medium can be refracted and returned to the surface. Even the most straightforward problems in wave propagation in a layered (linear) elastic medium are difficult.

Table 1.2 gives practical limitations of some of the theories which are discussed here. The table shows two things: (1) no single, simple model will explain all the phenomena observed when shock waves pass through soil; and (2) the model to use in studying particular types of

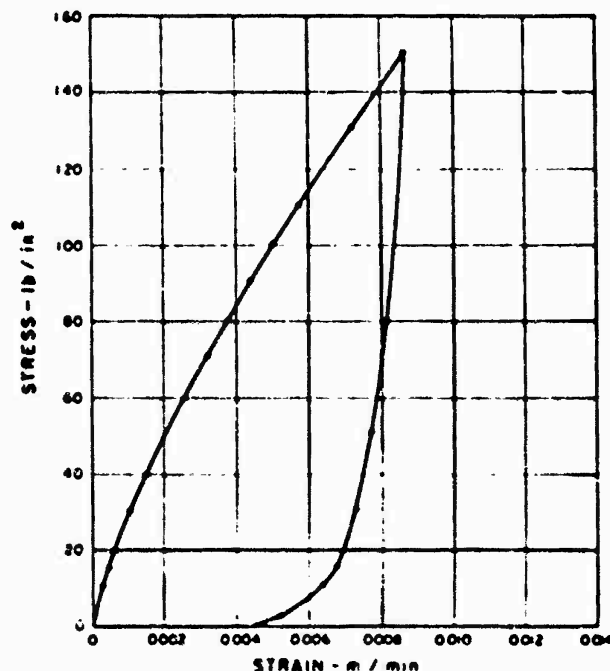


Figure 1.3 Actual record of stress versus strain in typical silty clay.

problems must be a compromise between the faithfulness with which one wants to portray all elements of soil behavior and the economics of producing many numerical solutions. This is to say that the least complicated model which will give reasonably good agreement with experimental facts is the model to use. However, some rudimentary numerical solutions will always be necessary before one can choose the simplest and yet the most appropriate model for a given problem.

1.3.2 Homogeneous Elastic Solid. Within the framework of present theoretical knowledge, several postulated relationships derived from analysis of a homogeneous elastic solid can be set down (Reference 6).

The assumptions under which this analysis was derived are as follows. First, the plan radius of curvature of the air-blast wave is large compared with the depth under investigation so that induced ground motion may be regarded as two-dimensional. Second, it is assumed that the air-

TABLE 1.2 PHENOMENA EXPLAINED BY VARIOUS MODELS OF SOIL BEHAVIOR

Model	Dissipation of Energy	Permanent Set	Return of Wave Paths to Surface	Dispersion of Surface Waves
Linear Elastic (isotropic medium)	No	No	No	No
Nonlinear Elastic (isotropic medium)	No	No	Yes *	Yes *
Elastic with Vertical Anisotropy (including discontinuous layers)	No	No	Yes	Yes
Solid (structural) Friction	Yes	No	No	No
Viscosity	Yes	No	No	No
Visco-Elastic	Yes	Yes	No	No

* These entries imply possible explanation of the phenomena, especially in connection with waves of high stress.

blast wave of invariant magnitude is moving at a constant velocity, U , and that sufficient time has elapsed so that a steady ground disturbance pattern appears to an observer fixed in the coordinates of the moving blast wave.

An elastic solid exhibits two wave speeds: one corresponding to the propagation of waves of dilatation (or compression) C_L , the seismic L (longitudinal) wave velocity, and another corresponding to propagation of components of rotation, C_S , the seismic S (transverse, shear) wave velocity. Three distinct theoretical cases are present in the above situation,

1. $U < C_S < C_L$, the subseismic case.
2. $C_S < U < C_L$, the transseismic case.
3. $C_S < C_L < U$, the superseismic case.

The theory in Cases 1 and 2 says that the ground motion outruns the air-blast wave; the earth moves downward and away from ground zero. Although ground motion outrunning is observed in the field, the initial motion of the earth is generally upward and away from ground zero. This motion is the result of refraction of the wave front due to the vertical gradient of seismic velocity. The overpressure at which outrunning occurs depends on the device yield and the seismic velocity gradient (Section 1.3.3). For the yields and seismic velocity gradients at the NTS (Frenchman Flat), this overpressure is approximately 10 psi.

At higher overpressures, the blast-wave velocity is large enough so that it moves superseismically (Case 3) and the ground motion lags progressively behind that at the surface as in Figure 1.4. At the surface, the vertical ground motion and the blast wave are related simply, viz.,

$$A_V = \frac{1}{\rho C_L} \frac{dP}{dt} \cdot \left(\frac{U}{C_L} \right)$$

$$U_V = \frac{P}{\rho C_L} \cdot \left(\frac{U}{C_L} \right)$$

$$D_V = \frac{1}{\rho C_L} \int P dt + \left(\frac{U}{C_L} \right)$$

Where A_V , U_V , and D_V are the vertical particle acceleration, vertical particle velocity, and vertical particle displacement; ρ is the soil density; P is overpressure; and t is time. The function, Φ (derived from results in Reference 6), is shown in Figure 1.5 and is nearly unity for $U/C_L > 1.5$. At small depths, one would expect the peak negative displacement to be proportional to the positive overpressure impulse and the peak negative velocity to be proportional to the peak overpressure, P_M . (The usual convention is preserved; positive motion is upward and outward [away from ground zero] and negative motion is downward and inward [toward ground zero].) The peak acceleration depends on the overpressure wave form and for an ideal shock wave would be infinite. In reality, all shocks have a finite rise time, t_r , so that

$$A_V \approx \frac{1}{\rho C_L} \cdot \frac{P_M}{t_r}$$

If one postulates that all nonprecursor shocks have approximately the same rise time, then one might expect the acceleration to be also proportional to the peak overpressure.

These simple statements form the basis of correlation of near-surface ground motion. Attenuation of ground motion with depth must at present be treated empirically.

1.3.3 Effects from Remote Sources. When the propagation velocity of the air blast is larger than the compressional (L) wave velocity of the ground, signals will not be observed underground prior to arrival of the wave front (Figure 1.4). In a homogeneous medium, the wave front will be bent upward at increased depths (Curve a, Figure 1.4); however, if the seismic velocity increases with depth, the wave front will tend to be bent downward (Curve b, Figure 1.4).

As the air-blast velocity decreases with distance from ground zero, the information given the earth will eventually arrive prior to arrival of the direct signal. This may happen either

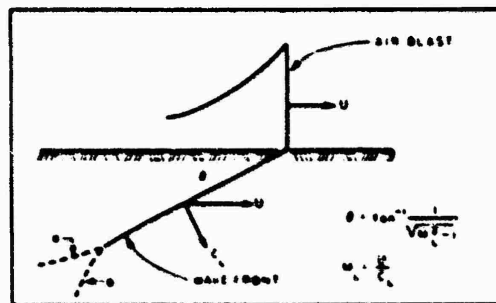


Figure 1.4 Schematic diagram of supersonic wave front.

when a near-surface seismic velocity is greater than the air-blast velocity or by ground transmission along a curved path which dips into the higher velocity, lower earth strata, i.e., by seismic refraction. The former corresponds to the trans seismic case (Case 2), and the initial signal is down and outward as in the supersonic case. The onset of acceleration is, however, more gradual. The latter is distinguished by an upward and outward first signal and is by far the predominant type of outrunning observed at both the NTS and the EPG.

The outrunning signal arriving at a gage by refraction is generally called the air-induced, ground-transmitted wave, or, simply, the remote effect. The signal arriving by the direct path as the air blast passes over the gage is called the air-induced, direct wave, or, simply, the local effect. It is a misnomer to describe only the latter as the air-blast-induced wave

since both classes of motion are air-blast induced, with the only difference being the point of origin and the transmission path. (Since the air-induced remote effect is due to an extended source, it should not be confused with the directly-induced ground motion resulting from an underground detonation.)

Outrunning of the ground wave has considerable importance in that the character of the ground motion changes when this occurs. If a seismic refraction survey has been made of the area, the

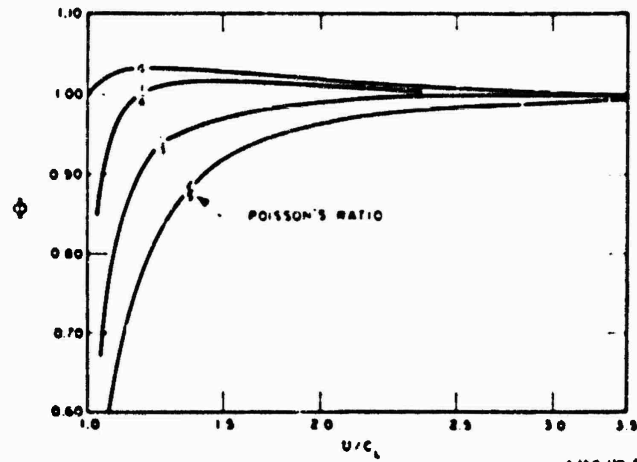


Figure 1.5 ν versus U/C_L and Poisson's ratio.

technique of constructing the ground motion arrival time distance is simple (Figure 1.6).

In the lower portion of Figure 1.6 is shown the measured refraction survey of Frenchman Flat made during 1957. The concave portion of the refraction arrival time curve is due to the increase of seismic velocity with depth. The air-blast arrival curve is first constructed. At each point along this curve a signal is generated which travels outward at the rate prescribed

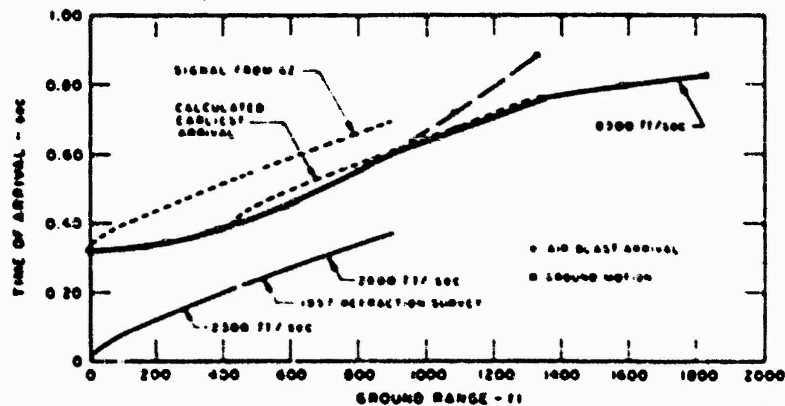


Figure 1.6 Construction of ground motion arrival time curves, Tumbler Shot 1, 5-foot depth.

by the refraction arrival curve, e.g., the signal from ground zero. From the envelope formed by superimposing the arrival time curves for all signals generated by the air blast, the earliest arrivals are selected. This curve then defines the ground range at which outrunning occurs, e.g., 920 feet in Figure 1.6.

The measured air-blast and ground motion arrivals at 5-foot depth for Operation Tumbler Shot 1 (Reference 2) are shown in Figure 1.6. Before outrunning, the ground motion lags the air blast slightly since the air blast is supers seismic. After outrunning, the ground motion pre-

cedes the calculated values by a small amount as the refracted wave travels upward to the surface. The differences are not important at 5-foot depth; however, at much greater depths they will be significant. The 8,300-ft/sec propagation velocity is the result of refraction from the basement rock. The 1957 refraction survey did not extend sufficiently to pick up these arrivals.

From seismic velocities associated with strata of known thickness, the refraction curve may be reconstructed. Details of this procedure may be found in any text on geological exploration.

As the device yield increases, the near-surface seismic velocity becomes less important in the calculation of outrunning. The seismic velocities at depth play the dominant role, and hence the overpressure at which outrunning would be expected to occur will generally increase as device yield increases. For surface bursts over shallow weathered layers or for large yield devices detonated over deep weathered layers, the approximate values of Table 1.3 apply. This indication of early outrunning for the most common materials focuses more than casual attention to the behavior of the ground-transmitted wave.

1.4 SEISMIC MEASUREMENTS

The elastic properties of a soil are related to and may be determined from an accurate knowledge of the seismic velocities. The main elastic waves which are of interest in this program

TABLE 1.3 APPROXIMATE OVERPRESSURES AT WHICH OUTRUNNING OF GROUND WAVE OCCURS, LARGE YIELD SURFACE BURSTS

Formation	Overpressure psi	Formation	Overpressure psi
Alluvium	< 40	Shale	650 to 2,500
Gravel, dry	10 to 100	Limestone	> 1,500
Gravel, wet	40 to 500	Metamorphic	> 1,000
Sandy Clay	100 to 500	Granite	> 3,000
Sandstone	500 to 2,000		

are longitudinal or compressional waves (L) and transverse or shear waves (S). Other seismic waves that may or may not be of interest are the Rayleigh and Love waves.

The compressional wave (L) is characterized by an in-line particle motion with particle displacement parallel to the direction of propagation. Of the elastic waves, the compressional wave has the highest velocity.

The shear wave (S) is also linear, but the direction of particle motion is perpendicular to the direction of propagation. The shear wave, because of its property of polarization, can be further subdivided into S_H and S_V type depending on whether the displacement is horizontal or vertical, both waves traveling with the same velocity but lower than the L wave velocity.

The Rayleigh wave (R) is a surface wave which is a combined compressional and shear wave with a plane of oscillation at right angles to the surface and parallel to the direction of propagation. Its velocity is dependent on frequency and is dispersive. Shear-wave velocity for shallow depths may be estimated from these surface-wave velocities. An approximate relation between C_S and C_R is:

$$C_R = [0.87 + 0.8 \nu] C_S$$

The elastic properties of a solid may be described by two elastic constants. Three of these constants are the bulk modulus (k), the modulus of rigidity (u), and Poisson's ratio (ν). The bulk modulus (k) is defined as the ratio between applied pressure and fractional change in volume for a uniform hydrostatic compression. The rigidity modulus (u) is defined as the ratio between shear stress and shear strain. Poisson's ratio is defined as the ratio between lateral contraction and longitudinal extension of a solid with free lateral surfaces. It is related to (k) and (u) by

$$\sigma = \frac{1}{2} \frac{k - \frac{2}{3}u}{k + \frac{1}{3}u} \quad (\text{Equation 1.1})$$

The compressional and shear-wave velocities C_L and C_S , measured by seismic methods, are

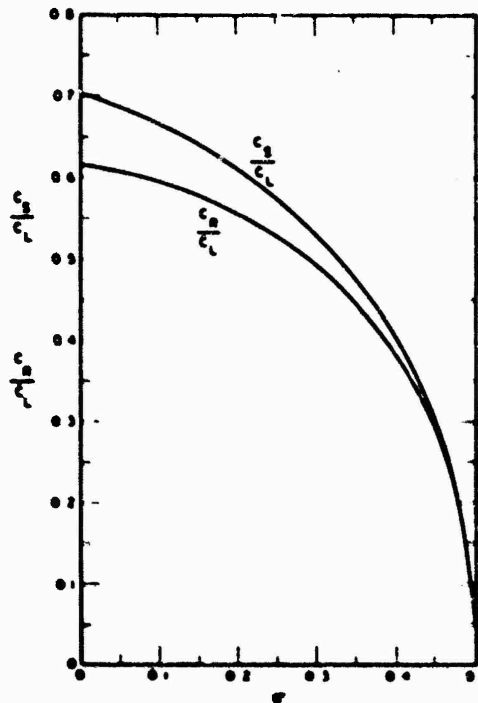


Figure 1.7 Seismic velocity ratios versus Poisson's ratio.

$$C_L = \left[\frac{k + \frac{1}{3}u}{\rho} \right]^{1/2} = \left[\frac{E(1-\sigma)}{\rho(1+\sigma)(1-2\sigma)} \right]^{1/2} \quad (\text{Equation 1.2})$$

$$C_S = \left[\frac{u}{\rho} \right]^{1/2} = \left[\frac{E}{2\nu(1+\sigma)} \right]^{1/2} \quad (\text{Equation 1.3})$$

Where ρ is the density and E is Young's modulus. Inserting Equations 1.2 and 1.3 in Equation 1.1

$$\sigma = \frac{1 - 2(C_S/C_L)^2}{2 - 2(C_S/C_L)^2}$$

For perfect fluids, $u = 0$, $C_S = 0$ and $\sigma = \frac{1}{2}$.

TABLE 1.4 POISSON'S RATIO FOR SOME MATERIALS

A plot of σ versus C_S/C_L and C_R/C_L is shown in Figure 1.7.

Gravel	0.47	Reference 7
Loess, dry	0.44	Reference 7
River Deposits	0.45	Reference 7
Clay, dry	0.47	Reference 8
Clay, wet	0.38	Reference 8
Limestone	0.28	Reference 7
Granite	0.23	Reference 7
Sandstone	0.12	Reference 7

For incompressible materials, k becomes large and $\sigma = \frac{1}{2}$. For elastic solids, $0 < \sigma < \frac{1}{2}$. Values of σ for some common materials are shown in Table 1.4.

Chapter 2

PROCEDURE

Project 1.4 participated on Shot Priscilla of Operation Plumbbob. Many other projects participated on this shot, including Project 1.3, which provided input data for this project; and Project 1.5, which made measurements similar to this project. There were also a number of structural projects for which Project 1.4 was designed to provide free-field input data.

2.1 PREDICTIONS

In planning an experiment of this type, it is necessary to predict the values of the functions to be measured to an accuracy sufficient to allow the sensitivity of each channel of instrumentation to be set closely enough that satisfactory deflection may be obtained. For best results these values should be within a factor of two of the true values. A greater range is acceptable on channels where dual-sensitivity galvanometers are used. Predictions are also important in the selection of gage ratings to ensure that gages are not over-ranged, thereby introducing nonlinearities. This section (2.1) is presented as written before the test; it has not been modified in the light of the actual data obtained.

Directly applicable data, taken in the Frenchman Flat area on underground effects of above-ground shots, are limited to those from Tumbler Shot 1 (Reference 2), and Upshot-Knothole Shots 9 (Reference 1) and 10 (Reference 9). The majority of these data were taken from shock waves at relatively low pressure levels, except some from Upshot-Knothole Shot 10 at levels up to 100 psi with precursor wave forms. Reference 10 gives some seismic velocities in the Frenchman Flat area.

2.1.1 Input Predictions. Subsurface phenomena are assumed to be a result of the overpressure appearing at the surface in the immediate vicinity of the station. Table 2.1 shows some of the predicted parameters of interest obtained from analyses carried out on the basis of previous data (Reference 11).

2.1.2 Earth Stress. In general, vertical earth stress may be assumed to be the same as the applied pressure. There will be a small change in the slope of the front with depth. At Stations 1, 2, and 3, the sharp decay of overpressure behind the front may eat away the peak slightly, with an estimated decrease of 25 percent, which is insignificant for range-setting purposes. Horizontal earth stress is assumed to be one fifth the vertical. This is consistent with some of the previous experimental experience and with probable values of Poisson's ratio.

2.1.3 Seismic Velocity. Seismic velocity is not important per se, but it is important in prediction of strain and acceleration. If one assumes that $\rho = 100$ pci and that $\sigma = 0.25$, then with peak stress equal to peak surface overpressure P , P_M (psi), $V_{max} = 55.6 P_M / C_L$ (in the early part of the wave), or $C_L = 55.6 P_M / V_{max}$, where V_{max} is the peak particle velocity at the ground surface.

Data from Tumbler-Snapper Shot 1 and Upshot-Knothole Shot 9 in the Frenchman Flat area give average value of C_L of 730 ft/sec at 1-foot depth, 1,220 ft/sec at 5-foot depth, and 2,460 ft/sec at 50-foot depth. These values for C_L at the three depths of measurement covered by the data are represented best by an exponential form of empirical equation:

$$C_L = 750 y^{0.30}$$

(Equation 2.1)

Where y denotes the vertical dimension.

Reference 10 gives the following seismic velocities in the Frenchman Flat area:

Depth, ft	Velocity, ft/sec
0 to 10	1,200
10 to 175	2,600
175 to 650	3,600
Below 650	10,000

While these values match well the average C_L results at 5 and 50 feet, they show no difference between 1 and 5 feet. This is unrealistic; particularly since the abrupt velocity change at 10 feet is not consistent with the profile of soil observed in excavations.

It must be observed that these data were derived from a refraction survey, where the pri-

TABLE 2.1 SHOT PRISCILLA INPUT PREDICTIONS

Station	Ground Range ft	Arrival Time msec	Horizontal Velocity ft/sec	Wave Form	P_{max} psi	P_1 psi	P_2 psi	T_1 msec	T_2 msec
1	450	99	6,400	0	750	750	—	0	—
2	550	117	5,000	0	600	600	—	0	—
3	650	137	6,700	0	450	450	—	0	—
4	750	152	6,100	1	320	280	40	5	7.5
5	850	167	5,600	1	200	110	120	5	12.5
6	1,050	205	4,800	1	100	60	70	5	20
7	1,350	275	3,900	1	50	30	40	5	20

mary data were arrival time versus ground range from small shots. When these primary data are reconstructed from the reported conclusions, they fit well an empirical exponential equation,

$$t_x = 0.0015 x^{0.88} \quad (\text{Equation 2.2})$$

Where x denotes the horizontal dimension. According to Blondeau's derivation (Reference 12), this would correspond to a vertical variation of velocity,

$$C_L = 1,160 y^{0.2} \quad (\text{Equation 2.3})$$

There is a considerable difference between Equations 2.1 and 2.3, but the best compromise, which does serious violence to neither, appears to be:

$$C_L = 1,000 y^{0.25} \quad (\text{Equation 2.4})$$

2.1.4 Earth Strain. With the same assumptions used for calculations of C_L , it may be shown that vertical strain, S , may be expressed as:

$$S = 55.6 P_M / C_L^3 = 5.6 \times 10^{-5} P_M y^{-0.75} \quad (\text{Equation 2.5})$$

2.1.5 Earth Acceleration. Data from Operations Tumbler-Snapper and Upshot-Knothole of the average values of $P_M A$ (ratio peak overpressure in psi to peak vertical acceleration in g-units) fit well the exponential equation,

$$A = 1.64 P_M y^{-0.35} \quad (\text{Equation 2.6})$$

This is for shock-wave input at pressure levels between 10 and 25 psi. If the rise time were

constant, A might be expected to vary inversely as the seismic velocity, i.e., in the same way as V_{\max} .

From Equations 2.1 and 2.5,

$$V_{\max} = 0.056 P_M y^{-0.25} \quad (\text{Equation 2.7})$$

From normal mechanics, if one assumes the rise of velocity to resemble a half cosine-wave,

$$A = 0.0975 V_{\max}/T_R \quad (\text{Equation 2.8})$$

From Equations 2.6, 2.7 and 2.8, then

$$T_R = 0.0033 y^{0.6} \quad (\text{Equation 2.9})$$

In other words, the steeper slope of acceleration with depth is explained by the increase of T_R with depth. Since T_R is the duration of the rise of particle velocity, V , it should also be the duration of the first acceleration pulse. Data on T_R yield average values of 3.25, 7.5, and 30 msec at 1, 5, and 50 feet, respectively, corresponding to the exponential $T_R = 0.00325 y^{0.67}$, a negligible difference from Equation 2.9.

Equation 2.6 can be used to predict peak accelerations at Stations 1, 2, and 3. At subsequent stations, however, T_R is affected by the finite rise time of the input-pressure wave. In the case of a precursor-type wave form, the rise time of the input wave can be quite long. If one can add geometrically, the influence of depth and input pressure upon rise time, ($T_R = \sqrt{T_y^2 + T_p^2}$), then one may calculate T_R for each depth and calculate A from Equations 2.4 and 2.5.

$$A_{\max} = 0.00542 P_M y^{-0.25}/T_R \quad (\text{Equation 2.10})$$

Horizontal accelerations are arbitrarily taken as one third the vertical. Although experience to date indicates a considerable scatter in this ratio, it appears to be always less than one.

2.2 INSTRUMENTATION

2.2.1 Central Station. All central-station channels of instrumentation used on Project 1.4 were essentially identical to those used on a number of previous projects, including Operation Teapot Project 1.10 (Reference 13). Wiancko 3-kc oscillators supplied carrier power to the transducers themselves and to modified Wiancko demodulators. The demodulated signal was applied to William J. Miller Corporation oscillograph recorders. Provisions were included for applying automatically a synthetic calibrating signal to each channel immediately prior to zero time to compare the final deflection on the record with the deflection produced by the same signal at the time of calibration. An accurate timing signal of 100 cps and 1,000 cps was also applied to all recorders simultaneously from a single source having a time accuracy of better than 10 parts per million. This provided means for time correlation of records to a high degree of accuracy. Since the same central station equipment was used for Projects 1.3, 1.7, and 3.5, this time correlation could be extended to include data obtained on Project 1.4.

The prime power supply for all instruments during the shot was a bank of storage batteries. Suitable converters were used to produce 115-volts ac for components requiring this power source. An individual converter was used for each rectifier power supply, thus minimizing the possibility of gross failure due to converter failure.

On this project, 62 gage channels were connected. Of these, 22 were connected to dual-recording systems, consisting of one galvanometer on each of two recorders. These dual channels were assigned to those gages which were considered to be most important to minimize loss of important data due to any recorder failure. On 6 of these 22 channels, one of the galvanometers used had a natural frequency of 200 cps, and the remainder had a natural frequency of 300 cps. The channels incorporating one 200-cps galvanometer were used on gages where uncertainty of the predicted peak was greatest and where the expected signal was such as not to

be degraded appreciably by the reduced response of the lower frequency galvanometer. Since there was an appreciable difference in the sensitivity of the galvanometers thus used on a single channel, a wider range of input signal could be accommodated without loss of data (provided both recorders operated properly).

Instruments were powered at suitable times before zero time by Edgerton, Germeshausen, and Grier (EG&G) relay circuits, with lock-in relays controlled by a time-delay relay to continue operation for approximately 1 minute after zero time, even though EG&G relays dropped out sooner. Utmost attention was paid to circuitry and procedures to insure maximum reliability of operation. Dual-relay contacts or dual relays were used wherever feasible.

A multipen recorder was connected to provide a record of time and sequence of operation of various elements so that any failure which might occur could be traced to its source in a posttest study.

The recording shelter was buried to a depth sufficient to reduce the integrated radiation dosage within the shelter to below 10 r to avoid radiation fogging of the recording paper.

2.2.2 Stress Gages. The basic earth-stress gage used in these tests was a modification of that originally designed by R. W. Carlson for the measurement of static stress in foundations and grades. The gage consisted of two flat circular plates with thin flexible edges attached at the edges so as to be separated by a narrow space filled with oil. A pressure gage was arranged to measure the pressure in this oil as a measure of the actual component of the stress in the medium in which the gage was buried.

Two variations of this gage were used. For the low pressures, a Wiancko variable-reluctance pressure gage covered by a housing was used in an identical construction to those used on previous projects (Reference 3). For pressures above 300 psi, a special diaphragm-type transducer, manufactured by Ultradyne Engineering Company, was used in place of the Wiancko transducer (Figure 2.1) This variable-reluctance transducer was electrically similar to the Wiancko, but was mechanically smaller in size so that the projecting housing was smaller.

2.2.3 Strain Gages. The earth-strain gages used were of a new type designed for the purpose and shown in schematic form in Figure 2.2. The gage is shown unassembled in Figure 2.3 and is shown installed in Figure 2.4. Fundamentally, the gage consisted of a linear differential transformer, which measured the change in spacing between two anchors, separated by 2 or 3 feet, set into the side of a large hole before the hole was backfilled. One of these anchors supported the body of the transformer enclosed in a protective housing, and the other carried a light tubular rod, at the far end of which was attached the movable core of the transformer. The position of this core could be adjusted after installation. For calibration, the adjusting nuts could be used as a micrometer by turning them one full turn at a time. The linear differential transformer was connected through a transformer to the normal Wiancko half-bridge circuit by the standard three-conductor cable.

2.2.4 Accelerometers. Accelerometers used were the standard Wiancko variable-reluctance accelerometers used on previous tests (Reference 2). They were enclosed in protective canisters of two types: one type carried a single vertical accelerometer; the other was used where horizontal as well as vertical measurements were desired and carried two mutually perpendicular accelerometers.

2.2.5 Instrument Response. The Wiancko gage and its associated recording system was basically flat down to steady-state conditions, due to its design as a carrier-demodulator system. No corrections were required therefore for its low-frequency response. The high-frequency response was limited either by the characteristics of the galvanometers used or by the dynamic characteristics of the transducers. The (nominal) 300-cps galvanometers had an undamped natural frequency of 315 to 340 cps and were damped to have an overshoot of approximately 7½ percent. This corresponded to a damping factor of approximately 0.65 critical and provided a

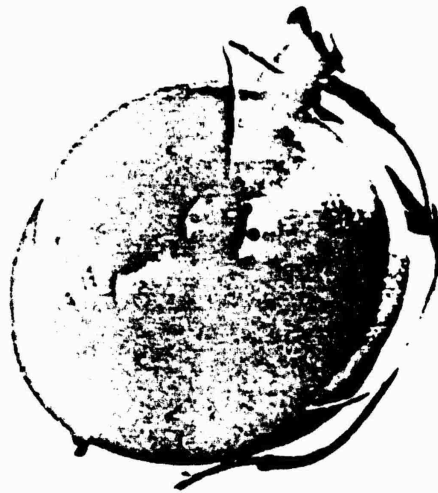


Figure 2.1 Earth stress gage:

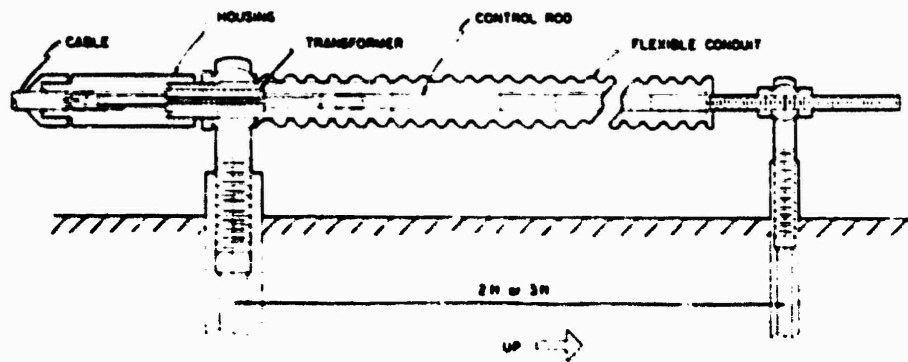


Figure 2.2 Schematic, earth strain gage.

nominal rise time of 1.3 msec. The nominal 200-cps galvanometers had a correspondingly longer rise time of approximately 1.8 msec.

The accelerometers varied widely in sensitivity and maximum range and consequently in undamped natural frequency. In general, those used at high-pressure stations and near the surface were low-sensitivity, high-range instruments with a high natural frequency; and those used at low-pressure stations, particularly at greater depths, were more sensitive instruments with lower natural frequencies. Where the high-range instruments were used, the overall frequency response was limited by the galvanometer response. Where the low-range instruments were used, the limiting frequency response was generally that of the accelerometer.

The frequency-response characteristics of the Carlson stress gages were difficult to deter-

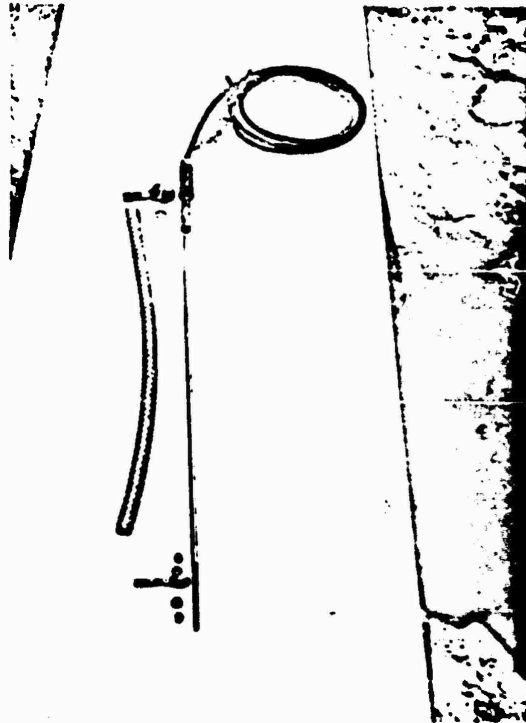


Figure 2.3 Earth strain gage, unassembled.

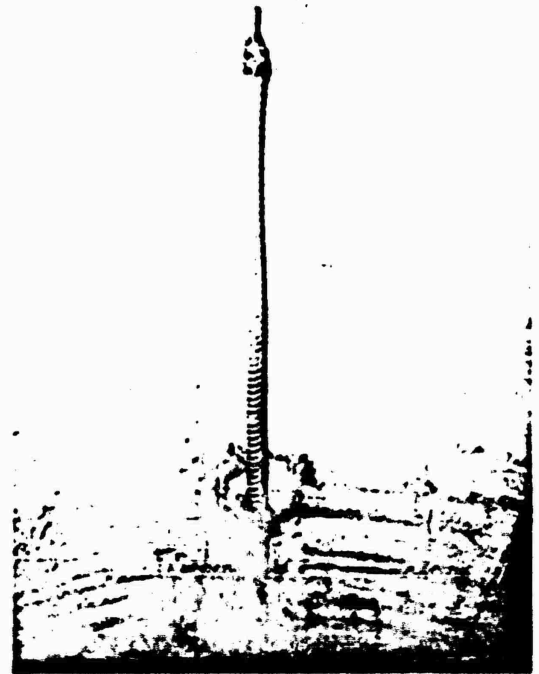


Figure 2.4 Earth strain gage, installed.

mine implicitly since they were affected significantly by loading of the earth on the gages; however, the basic gage was known to have a response similar to that of the pressure gage alone. It is believed that the overall response was limited by that of the galvanometers. Similarly, the response time of the earth-strain gages was difficult to ascertain exactly, but measurements indicated that for the short span used the response time was far shorter than the rise times indicated on the final records; therefore, no distortion from this cause was attributed to the gages.

2.2.6 Calibration. Each gage was calibrated in the field after it had been connected to its associated cable and recording equipment and immediately prior to its final installation in the earth. Carlson stress gages were calibrated by the application of direct air pressure. Accelerometers were calibrated by the use of a spin table which produced accelerations up to about 200 g. Where higher accelerations than 200 g were anticipated, gages were calibrated to that figure in the field, and this calibration was extrapolated on the basis of linearity checks made previously in the laboratory. Earth-strain gages were calibrated by the introduction of directly-measured deflections on the gages in place.

In the calibration procedure several deflections ranging from zero to well above the expected

peak (where possible) were applied to each gage in sequence. Each galvanometer deflection was noted and recorded. In addition, the deflection caused by an artificial signal (cal signal) injected into the gage circuit was recorded. From the former deflection, a calibration curve of deflection versus peak reading could be constructed. The cal signal served to correct for any changes of sensitivity of the recording system between calibration and the final test since an identical signal was injected on the final record about 10 seconds before zero time.

2.3 EXPERIMENT PLAN

2.3.1 Gage Placement. Gages were located at several depths in two sizes of holes. At five stations, the holes were 30 inches in diameter by 10 feet deep, and at two other stations the holes were 5 feet in diameter by 50 feet deep. Stress gages and accelerometers were placed in small excavations in the sides of the holes, and backfill material was carefully tamped around the gages by hand to ensure proper contact with the formation before the general backfilling proceeded. Strain-gage anchors were cemented into the walls of the large holes to make good contact with the undisturbed formation and to minimize the effect of the difference between characteristics of the backfill and of the original formation. In addition, every effort was made in backfilling to return the material as nearly as possible to its original condition.

The specifications for preparation of backfill material and for tamping procedures were set up by Project 3.8 (Reference 14) on the basis of laboratory tests conducted at Waterways Experiment Station (WES) on samples of material from the area. These specifications were directed toward restoring the dynamic modulus rather than the density and required careful control of the water content at slightly below Proctor optimum, with somewhat greater than normal tamping effort. During backfilling, control of procedure was assisted by the frequent sampling and analysis of the backfill in the field by Project 3.8. Samples for record were also taken by that project and are reported in Reference 14.

2.3.2 Gage Coding. For identification of channels and recorded traces with their proper gages, a systematic coding was adopted. A station number was assigned to each gage station; these numbers were used as a first part of the gage code. The second part of the gage code was a letter indicating the type of measurement. For this project V was used for vertical acceleration, H for horizontal acceleration, CV for vertical stress, CH for horizontal stress, and SV for vertical strain. A third part of the code indicated the depth of the gage (in feet) below the surface.

Typical gage code numbers would then be 3V5 for Station 3 vertical acceleration at 5-foot depth; 4CV30 for Station 4 vertical stress at 30-foot depth, etc.

2.3.3 Gage Layout. The gage layout (Figure 2.5 and Table 2.2) was selected to provide the maximum of basic data on phenomenology and at the same time to provide maximum coordination with other projects. Stations 4 and 6 were placed at ground ranges where predicted peaks of applied pressure of approximately 300 and 100 psi, respectively, were expected. At these locations, measurements were made of acceleration, stress, and strain, at a number of depths down to 50 feet, including two measurements each of horizontal acceleration and horizontal stress. The remaining stations were chosen to correspond to aboveground stations of Project 1.3 and to cover a wide range of input pressure levels. At these stations, measurements were made of vertical acceleration and stress at depths of 5 and 10 feet only.

2.3.4 Seismic Measurements. It was considered desirable to obtain data on seismic propagation velocities and their variation with depth, particularly in the first 100 feet, to assist in interpretation of final data from this project. To obtain these seismic data, a program was conducted in the area during the preparational phase of operations prior to the shot. Figure 2.6 shows the location of shot holes and lines used in this work. Shot Points 1 and 2 were 200-foot holes, originally drilled dry, but flooded before use (Section 2.4). Shot Point 3 was a similar 100-foot hole drilled later to check the results from the first two. In these holes, small charges

TABLE 2.2 GAGE LAYOUT

Station		Ground		Galvanometer		Station		Ground		Galvanometer	
Number	Range	Gage Code	Peak	Frequency	Peak	Number	Range	Gage Code	Peak	Frequency	Peak
		fl			cps			fl			cps
1	450	1V5	270 g	300		5	850	5V5	39 g	300	
		1V10	140 g	300				5V10	22 g	300	
		1CV5	750 psi	300				5CV5	200 psi	300	
		1CV10	750 psi	300				5CV10	200 psi	300	
2	550	2V5	220 g	300		6	1,050	6V1	54 g	300	
		2V10	120 g	300				6V5	22 g	300	
		2CV5	600 psi	300				6V10	13 g	300	
		2CV10	600 psi	300				6V20	7.2 g	300	200
3	650	3V5	160 g	300				6V30	5.0 g	300	200
		3V10	85 g	300				6V50	3.3 g	300	200
		3CV5	450 psi	300				6I110	4.2 g	300	
		3CV10	450 psi	300				6I150	1.1 g	300	
4	750	4V1	150 g	300				6CV1	100 psi	300	
		4V5	62 g	300				6CV5	100 psi	300	
		4V10	36 g	300				6CV10	100 psi	300	300
		4V20	20 g	300				6CV20	100 psi	300	300
		4V30	15 g	300				6CV30	100 psi	300	300
		4V50	10 g	300				6CV50	100 psi	300	300
		4I110	11 g	300				6C110	18 psi	300	
		4I150	3 g	300				6C1150	18 psi	300	300
		4CV1	320 psi	300				6SV5	3.8 ppk	300	
		4CV5	320 psi	300				6SV10	2.8 ppk	300	
		4CV10	320 psi	300				6SV20	1.6 ppk	300	300
		4CV20	320 psi	300				6SV30	1.8 ppk	300	300
		4CV30	320 psi	300				6SV50	5.0 ppk	300	300
		4CV50	320 psi	300				7V5	11 g	300	
		4CH10	60 psi	300			1,350	7V10	6.3 g	300	
		4CH50	60 psi	300				7CV5	50 psi	300	
		4SV5	12 ppk	300				7CV10	50 psi	300	
		4SV10	9 ppk	300							
		4SV20	5.1 ppk	300							
		4SV30	5.8 ppk	300							
		4SV50	16. ppk	300							

were set off at various depths in the holes, and geophones were placed near the top of the hole and at 50 and 100 feet from the hole to measure the arrival times to determine vertical compressional wave velocities.

Shot Point 4 was a 10-foot hole used in an experimental program in an effort to measure shear wave velocities. Shot Points 1R, 2R, and 3R were also 10-foot holes used for a refrac-

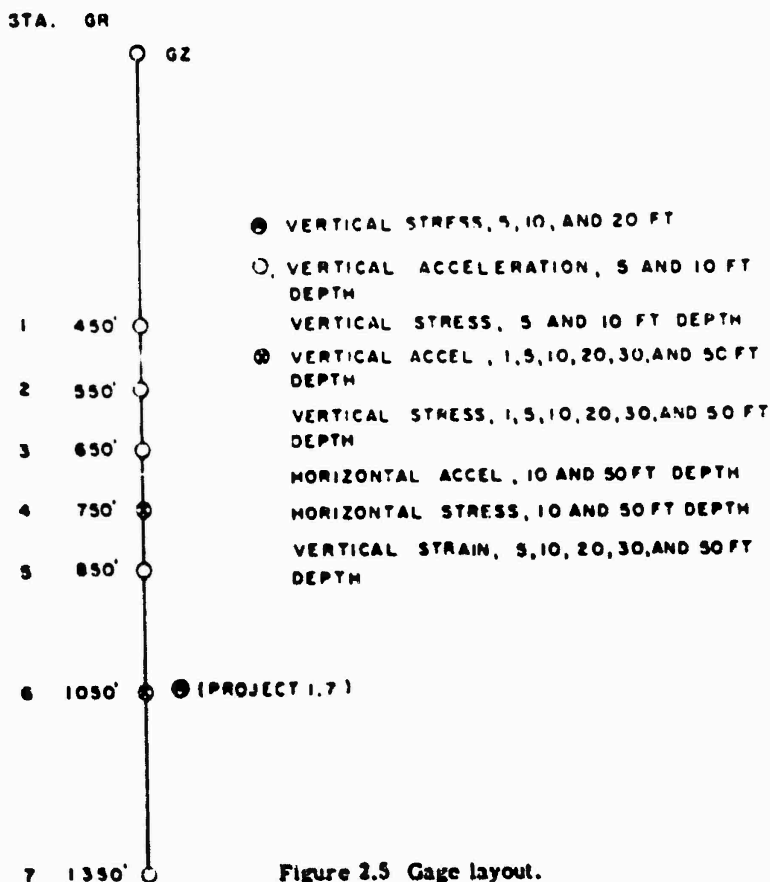


Figure 2.5 Gage layout.

tion profile to determine horizontal velocities. In making the refraction profile, the geophone spread was left in one position and the shot point moved progressively out to a final offset of 900 feet from the end of the spread.

Results of these measurements are reported in Chapter 3.

2.4 FIELD OPERATIONS

Field operations on this project were concurrent with those for Projects 1.3, 3.5, and the instrumentation for Project 1.7 and were performed by the same personnel. A common recording shelter was used, and the data channels were intermingled. In most cases, common cable trenches were used.

At the time the field crew arrived at the NTS, the only construction requirements completed for this project were the drilling of the 50-foot holes for gages and of two 200-foot holes for seismic measurements. The former were protected by local dikes from a subsequent general flood, but the latter were covered with water for several days.

The recording shelter was ready for occupancy 10 days after the crew arrived at the test site, and equipment was promptly installed. Cable-trenching operations were delayed so that, to meet schedules, it was necessary to start planting and backfilling of underground gages.

Most of these gages were therefore calibrated with cables only partly in place and without the full complement of cables and gages connected.

It is not certain whether this procedure has any effect on the accuracy of calibrations, but it was certainly not optimum. Calibration and planting of gages and backfilling of holes was completed about 8 weeks after project personnel arrived in the field.

Seismic measurements were made as opportunities arose. The two deep shot holes (200 feet)

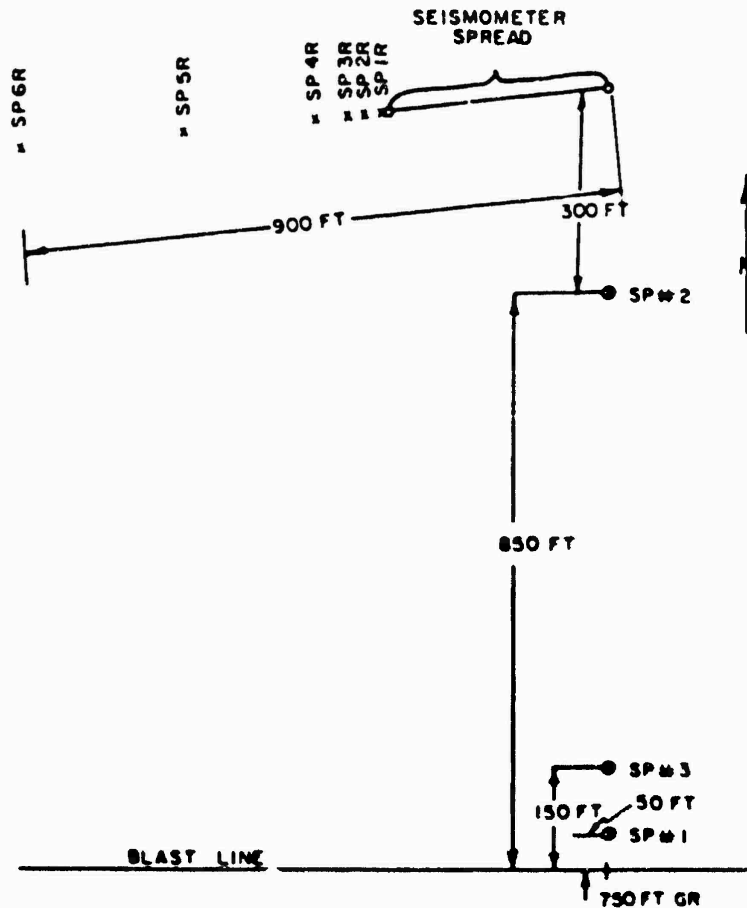


Figure 2.6 Seismic locations.

were shot after they had been flooded for several days. To check the possibility that the results were affected by water intrusion, another 100-foot hole was drilled by Project 3.8 and was shot later. Additional seismic shooting was done on a noninterference basis.

The records were recovered from the shelter on the afternoon of D-day. The recovery operation required five persons to be in about a 300-mr/hr radiation field for approximately 20 minutes.

Chapter 3

RESULTS

3.1 INSTRUMENTATION PERFORMANCE

Of the 64 gage channels installed on this project, 52 gave usable records, although four records were incomplete due to cable breaks during the active period of recording. Of the four cables broken, three were associated with the gages at one station (Station 5, 850-foot ground range). The only apparent explanation for this behavior was that the finger cable trenches off the main 8-foot deep trench were too shallow at this station for adequate protection of the gage cables.

Of the 52 usable gage records, one record (6CV20) showed a peculiar wave form indicative of gage overload; although its value was limited, some information may be obtained from this record.

Of the 12 channels producing no record, six were lost due to failure of one oscillograph to pull recording paper throughout the run. This camera ran for about 10 seconds after turn-on (until minus 5 seconds) before the recording paper tore and jammed. The other six failures were apparently due to breaks in the cables or faulty cable-plug connections. Some of these difficulties were detected before the shot, but too late to repair; some were apparently caused by strains or jarring introduced during the backfilling operations. It appears that the strain-gage design used on this project was particularly susceptible to electrical shorts and/or cable-continuity difficulties. Much of this might be eliminated by an improved cable-connection system.

There was no definite evidence of record disturbance caused by the electromagnetic transient at zero time. All traces remained within the boundaries of the recording paper. Some gages, particularly the stress and intermediate depths, produced small deflections which reduced the accuracy of the data obtained.

No evidence of radiation fogging was observed on any of the recordings obtained on this project. The data obtained for Project 1.7 was transmitted to the appropriate agency for analysis.

3.2 DATA REDUCTION PROCEDURES

3.2.1 General. After each gage record was identified on the oscillograms, they were read (inches of deflection of record versus time) with an electromechanical reader, Benson-Lehner "Oscar" Model J. The reader output was fed into an IBM card punch, which produced the data cards. These deflection versus time data cards, along with appropriate calibration cards, were processed by an IBM Model 650 electronic computer. The final reduced data came out in the form of parameter (e.g., acceleration) versus time listings corresponding to each gage record. These listings were then plotted to give data upon which this report is based.

3.2.2 Integration Procedures. It was desirable for the earth acceleration versus time records to successively integrate the results to obtain, first, the particle velocity versus time, and second, the particle displacement versus time. It becomes apparent after only a few attempts at this integration process that there is a great deal of judgment involved in obtaining a meaningful result. The main problems and their solutions are discussed fully in Appendix C of this report.

Suffice it to say that the integration procedure involved the following operations:

1. Integration of the as-read acceleration-time record to obtain as-read velocity-time.

2. Adjustment of the as-read velocity-time baseline to obtain zero velocity at an appropriate time; called corrected velocity-time.

3. Adjustment of the acceleration-time baseline to be consistent with the velocity-time adjustment cited in Item 2 above.

4. Integration of the adjusted velocity-time record to obtain the displacement-time trace, called corrected displacement-time.

As explained in Appendix C, the corrections as applied usually have little effect upon the as-read acceleration, more on the as-read velocity, and most upon the displacement.

The results of the Project 1.4 experiment will be presented in terms of the corrected values only; however, the figures and tables will indicate the magnitude of the corrections (Table 3.1).

3.3 GAGE RECORDS AND TABLES OF RESULTS

Figures 3.1 through 3.24 present the significant portions of the replotted gage records obtained on this project. Figure 3.1 presents the overpressure-time records obtained on Project 1.3 and represents the input air pressure at the ground surface on this shot. The remaining

TABLE 3.1 SUMMARY OF PEAK SURFACE OVERPRESSURE, SHOT PRISCILLA
CB, cable break.

Gage	Ground Range	Arrival Time	Maximum Precursor		Maximum		Positive Phase Duration	Positive Phase Impulse	Wave Form
			Pressure	Time	Pressure	Time			
	ft	sec	psi	sec	psi	sec	sec	psi-sec	
1B	450	0.103	None	None	551.2	0.104	CB	—	0
2B	550	0.116	39.2	0.118	366.0	0.126	CB	—	1
3B	650	0.131	31.4	0.134	342.3	0.146	0.169	12.2	1
4B	750	0.146	26.0	0.150	228.7	0.175	0.200	10.1	1
5B	850	0.163	25.6	0.166	220.9	0.201	0.237	11.2	1
6B	1,050	0.201	20.8	0.223	104.0	0.275	0.329	9.2	1
7B	1,350	0.268*	12.0*	0.308*	59.1*	0.394*	0.783*	6.62*	1

* Sandia (Project 1.5) data.

figures present acceleration-time, velocity-time, displacement-time, stress-time, and strain-time data in that order. Included in these figures are the times of arrival; designation of peak values; and where applicable, the air-pressure arrival (AB) at the ground surface over the gage.

All the records are plotted to the same time scale; however, to obtain the best compromise between economy of space and faithful reproduction of the details of the records, it was necessary to group the records and use several different ordinate scales.

3.3.1 Overpressure. The pertinent overpressure-time records from Project 1.3 are presented in Figure 3.1, and the data are listed in Table 3.1. Referring to the pressure-time plots, it is apparent that, although a definite precursor wave formed on the Shot Priscilla main blast-line, the ground level overpressure at Station 1 (450-foot range) was characterized by a clean (Type 0; see Appendix A) wave form. However, the longer than normal rise time of about 5 msec gave some evidence of thermal disturbance at this station. The record at Station 2 (550-foot range), although incomplete due to a cable break, showed that the precursor wave formed between the 450- and 550-foot range. Subsequent pressure records documented the development of the precursor wave in detail. One of the most significant characteristics of this set of records with respect to ground motion was that the rise time to peak pressure associated with the main pulse increased with increasing ground range and decreasing peak pressure. Also as the distance from ground zero increased, the precursor wave front led the main shock by longer and longer times.

3.3.2 Earth Acceleration. Figures 3.2 through 3.6 present the replotted records of earth acceleration data obtained on Project 1.4. In these figures, the air-blast arrival time at each

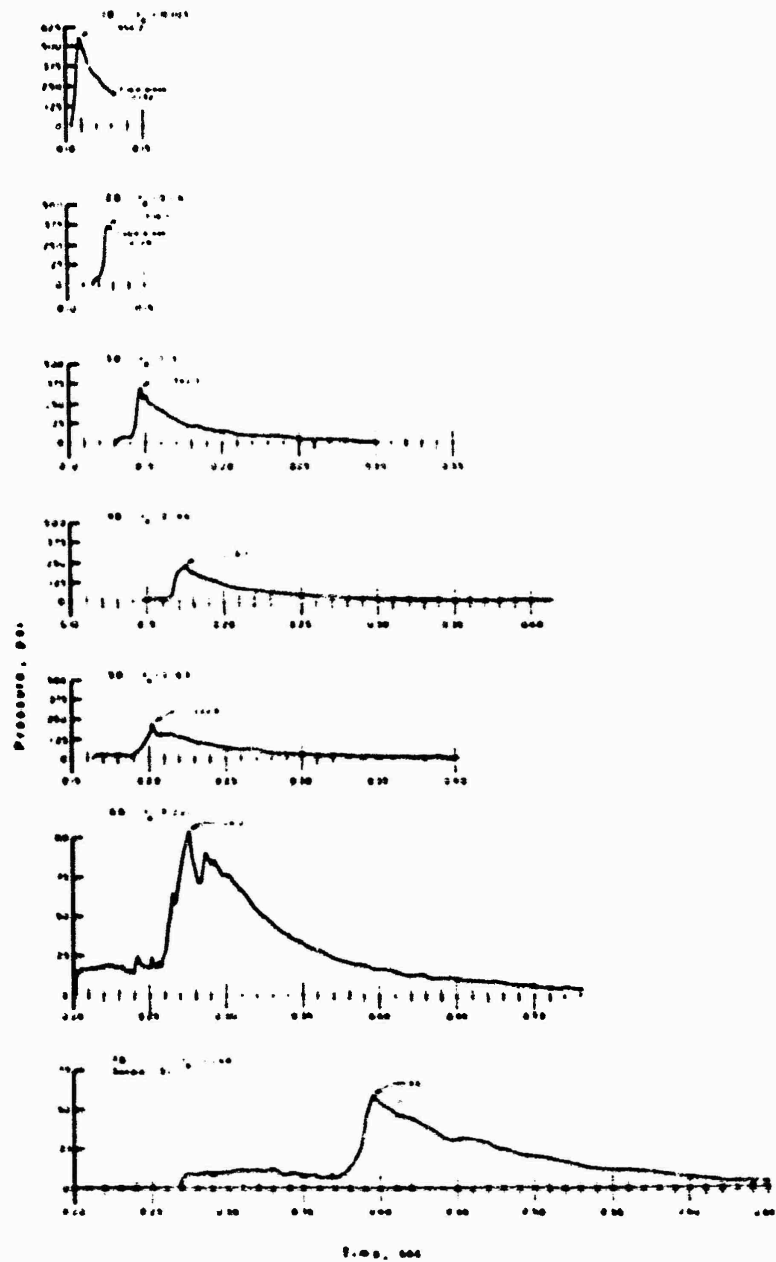


Figure 3.1 Surface overpressure versus time, Stations 1 to 7, Shot Priscilla.

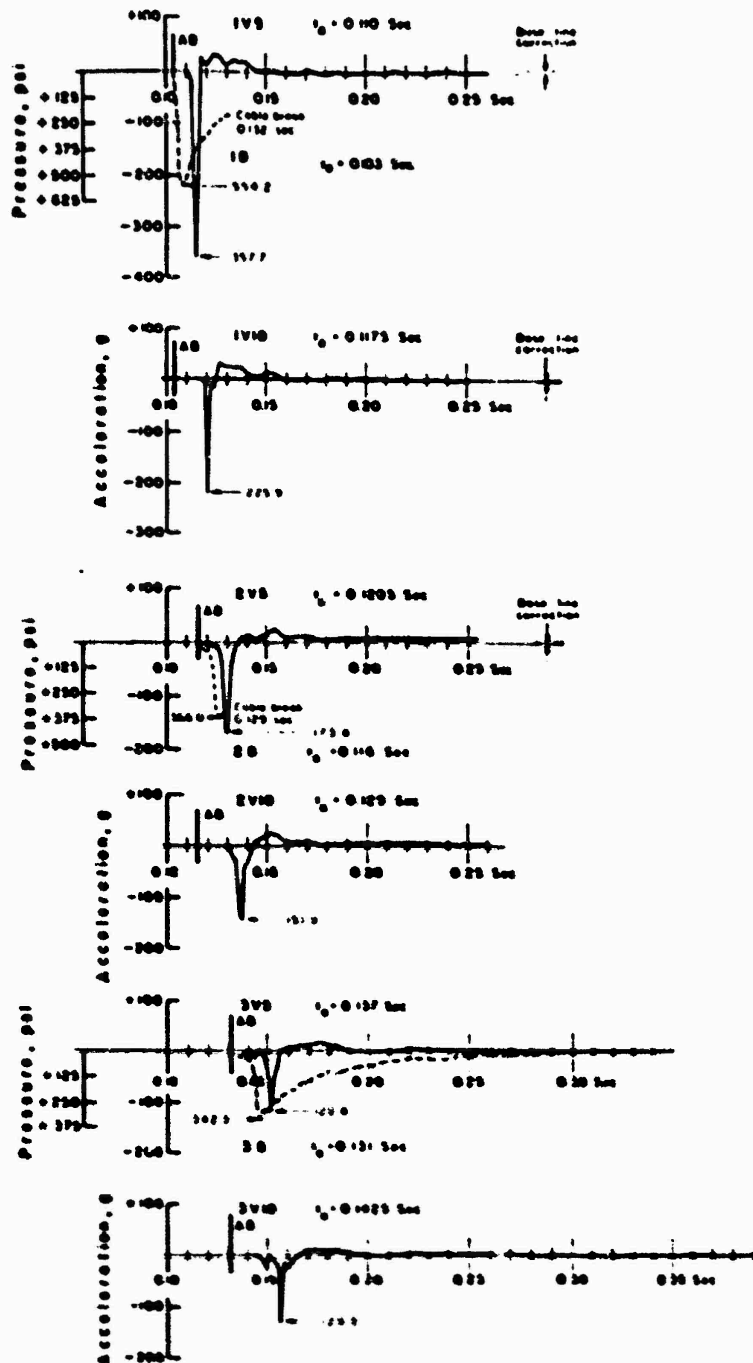


Figure 3.2 Vertical acceleration versus time, Station 1 (GR: 450 feet); Station 2 (GR: 550 feet); Station 3 (GR: 650 feet); Shot Priscilla.

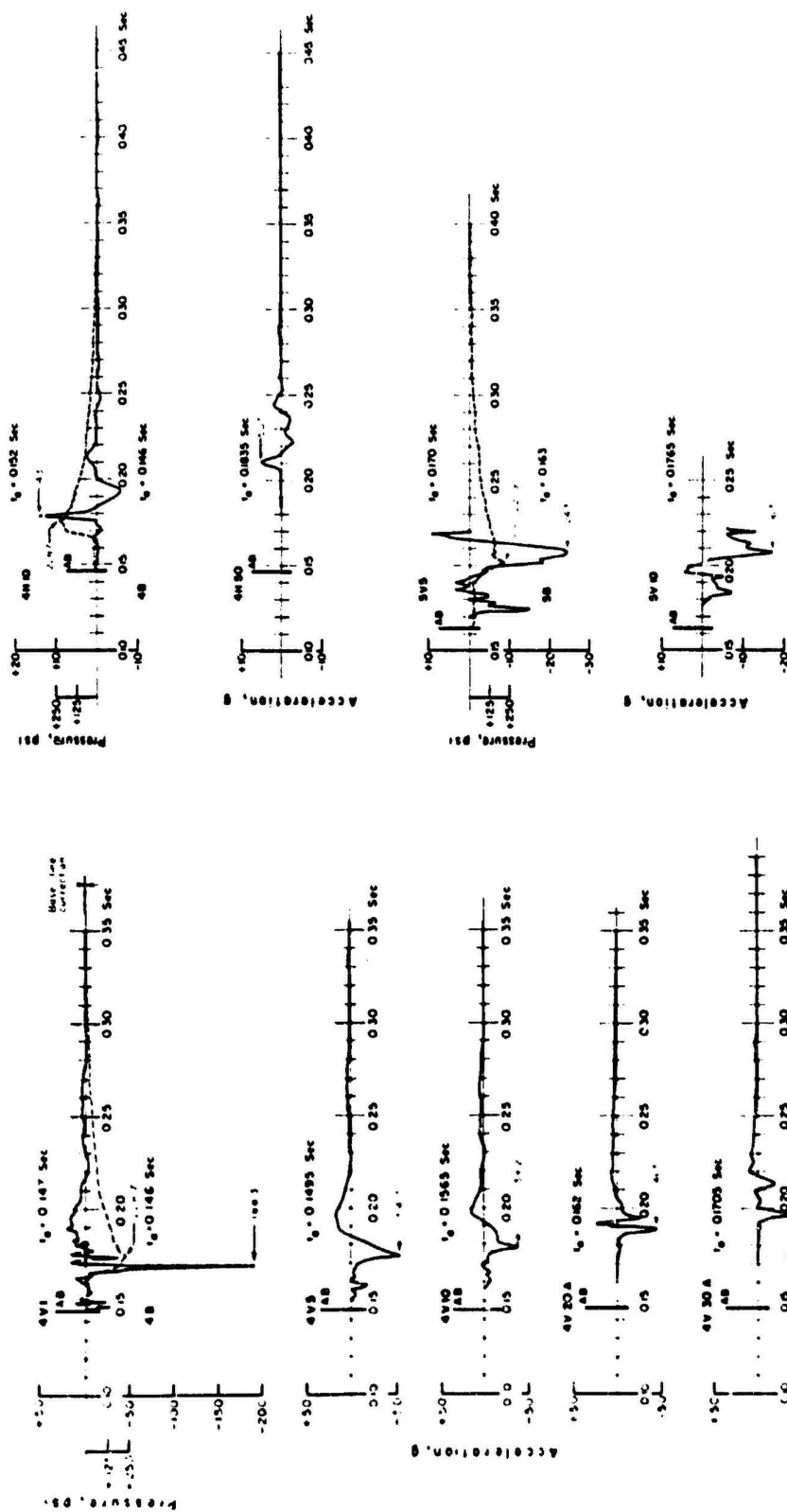


Figure 3.3 Vertical acceleration versus time, Station 4 (GR: 750 feet), Shot Priscilla.

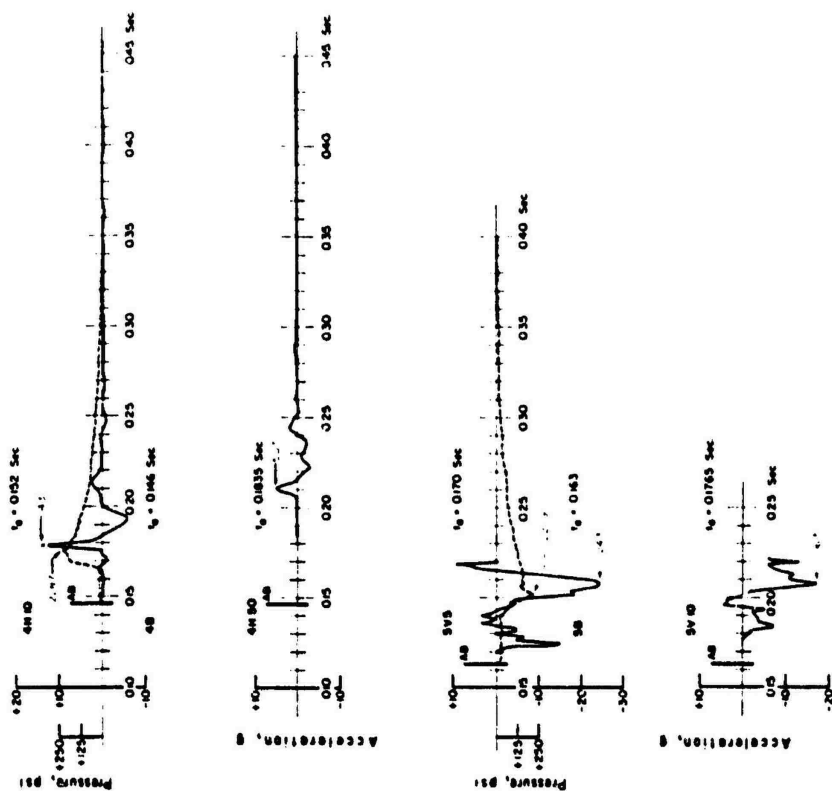
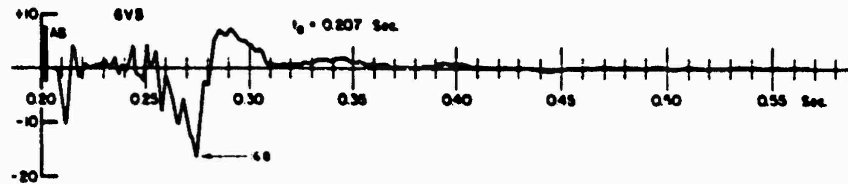
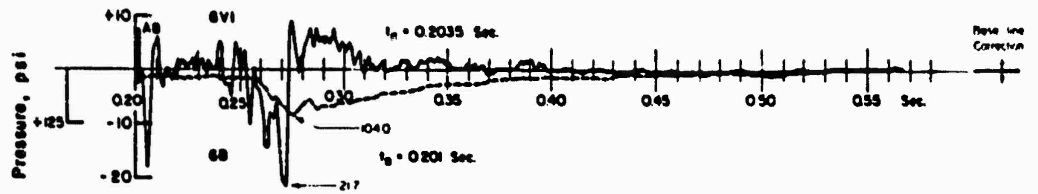


Figure 3.4 Horizontal acceleration versus time, Station 4 (GR: 750 feet); vertical acceleration versus time, Station 5 (GR: 850 feet); Shot Priscilla.



6V10 No Record

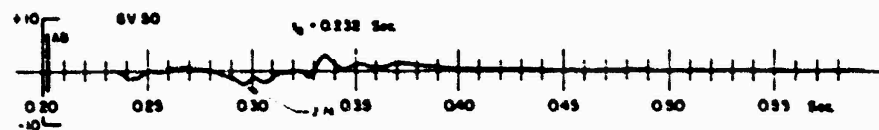
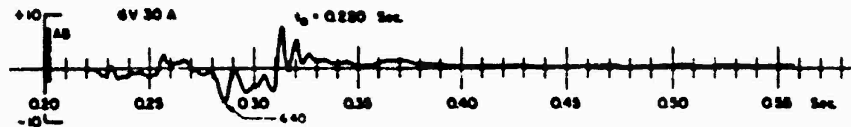
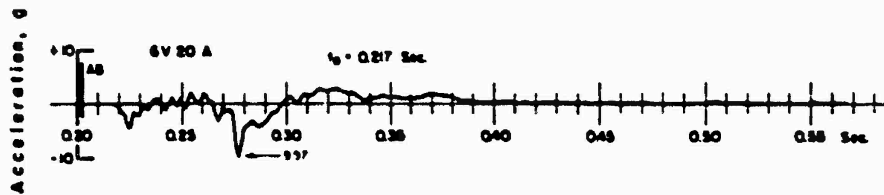


Figure 3.5 Vertical acceleration versus time, Station 6 (GR: 1,050 feet), Shot Priscilla.

station is designated by the vertical line labelled AB on each plot, and the arrival time, time of peak, and peak acceleration are indicated. In addition, the magnitude of the baseline correction applied to each acceleration-time record is indicated by a dashed line which designates the baseline before correction.

The vertical acceleration versus time curves are mainly characterized by a single sharp peak of acceleration in the downward direction, often preceded by minor disturbances. It is obvious that the latter are produced by the precursor and the former by the larger main peak of air blast. The duration of the main sharp peak increased with ground range because of increased rise time

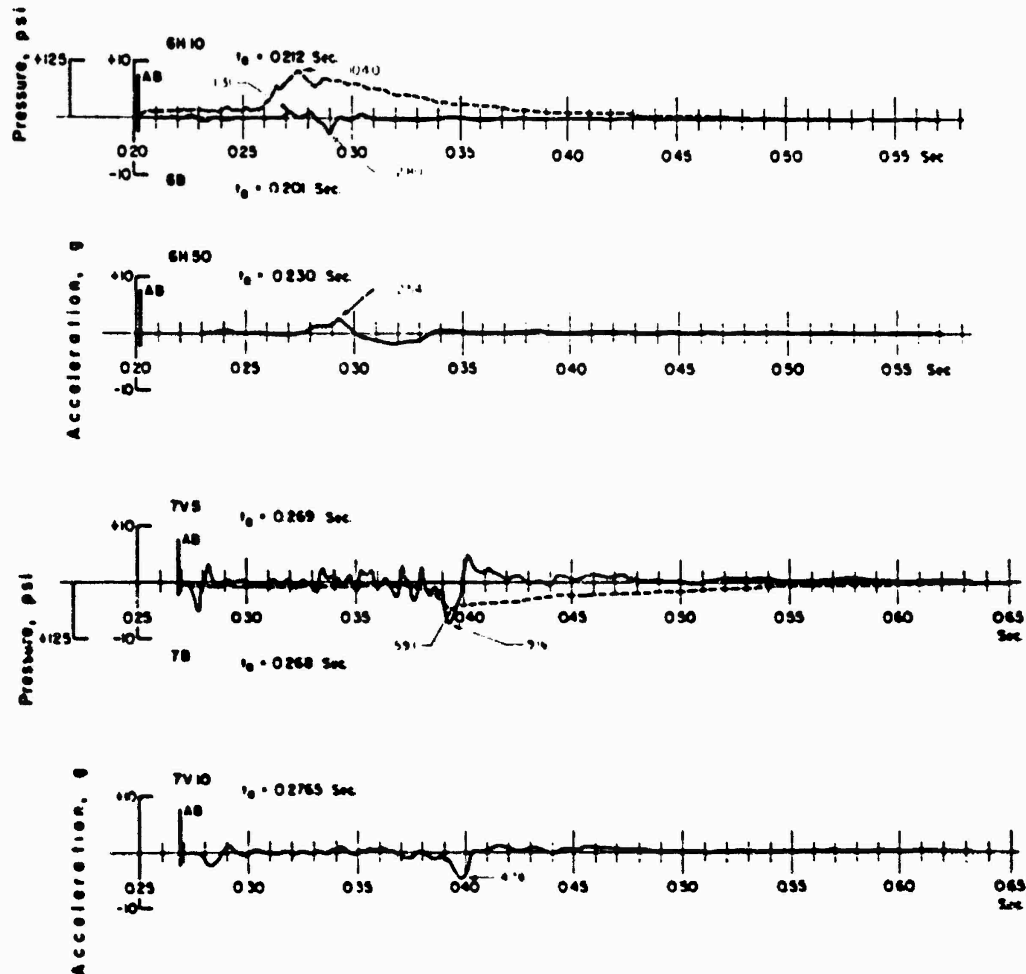


Figure 3.6 Horizontal acceleration versus time, Station 6 (GR: 1,050 feet); vertical acceleration versus time, Station 7 (GR: 1,350 feet); Shot Priscilla.

of the input wave; it increased with depth, because of modification of the wave with travel through the earth. At the deeper gages, particularly at Station 6, the wave form became more complex, without entirely losing these characteristics. The horizontal accelerations showed somewhat similar wave forms, but with the first and major deflections positive (outward from ground zero). They tended to be slightly more oscillatory in character, with rather pronounced negative peaks following the major positive ones.

Table 3.2 presents the corrected acceleration data. In a few cases, the criteria used for making the integration corrections were in some doubt. Therefore, two independent choices were made, and both values are included in the table (see Section 3.3.3 for more details).

TABLE 3.2 SUMMARY OF CORRECTED ACCELERATION, VELOCITY AND DISPLACEMENT DATA, SHOT PRISCILLA
 NR, no record; (1) and (2) indicate alternate baseline choices.

Gage	Ground Range	Gage Depth	Arrival Time	Corrected Acceleration			Corrected Velocity			Corrected Displacement		
				Negative Acceleration g	Time of Peculiar Acceleration sec	Maximum Positive g	Maximum Negative g	Time of Maximum Negative sec	Maximum ft/sec	Maximum ft	Time of Maximum Negative sec	Maximum ft
1V5	450	5	0.110	—	—	37.2	357.7	0.114	25.3	0.116	0.116	0.693
1V10	450	10	0.110	—	—	31.1	225.9	0.120	14.8	0.124	0.124	0.343
2V5	550	5	0.120	—	—	21.1	173.1	0.130	18.0	0.135	0.135	0.586
2V10	550	10	0.129	—	—	22.4	151.9	0.136	20.2	0.143	0.143	0.964
3V5	650	5	0.137	24.2	0.139	15.9	120.8	0.151	16.3	0.156	0.156	0.539
3V10	650	10	0.142	22.5	0.149	13.5	129.3	0.156	13.1	0.164	0.164	0.555
4V1	750	1	0.147	30.8	0.148	25.2	184.3	0.170	15.8	0.180	0.180	0.664
4V5	750	5	0.150	19.2	0.160	16.4	54.7	0.174	15.2	0.185	0.185	0.763
4V10	750	10	0.156	9.19	0.162	14.6	39.2	0.180	10.9	0.193	0.193	0.521
4V20A	750	20	0.162	—	—	14.3	46.5	0.189	7.84	0.206	0.206	0.486
4V30A	750	30	0.170	—	—	9.78	36.1	0.197	7.92	0.218	0.218	0.389
4V50	750	50	0.183	—	—	3.99	13.4	0.212	4.96	0.230	0.230	0.311
4V50A	750	50	0.183	—	—	3.93	12.8	0.241	4.66	0.229	0.229	0.372
4H10	750	10	0.152	—	—	14.3	5.76	0.179	1.42	0.184	0.184	0.078
4H50	750	50	0.186	—	—	5.07	2.88	0.212	0.885	0.216	0.216	0.014
5V5*	850	5	0.170	15.2	0.174	9.17	24.3	0.206	10.5	0.214	0.214	—
5V10*	850	10	0.176	6.88	0.184	4.66	16.7	0.208	6.17	0.220	0.220	—
6V1(1)	1,050	1	0.204	18.0	0.206	7.61	21.5	0.272	6.12	0.274	0.274	0.218
(2)				18.2	0.206	7.42	21.7	0.272	6.55	0.274	0.274	0.299
6V5(1)	1,050	5	0.207	10.4	0.212	7.61	16.7	0.274	6.02	0.282	0.282	0.267
(2)				10.5	0.212	6.94	16.8	0.274	6.18	0.282	0.282	0.307
6V19	1,050	10	NR	—	—	—	—	—	—	—	—	—
6V20(1)	1,050	20	0.217	4.56	0.224	2.52	10.5	0.277	4.07	0.299	0.299	0.306
(2)				4.57	0.224	2.52	10.5	0.277	4.07	0.299	0.299	0.307
6V20A	1,050	20	0.217	4.49	0.225	2.66	9.93	0.278	3.96	0.299	0.299	0.275
(2)				4.52	0.225	2.62	10.0	0.278	4.06	0.300	0.300	0.293
6V30	1,050	30	0.220	1.54	0.228	8.08	6.53	0.286	3.59	0.312	0.312	0.214
6V30A	1,050	30	0.220	1.54	0.229	7.64	6.40	0.286	3.56	0.312	0.312	0.209
6V50(1)	1,050	50	0.232	1.19	0.242	2.71	2.72	0.296	2.30	0.332	0.332	0.169
(2)				1.64	0.242	2.60	2.74	0.296	2.36	0.332	0.332	0.182
6H10	1,050	10	0.212	—	—	1.31	0.293	0.274	0.400	0.286	0.286	0.324
6H50	1,050	50	0.230	—	—	2.54	1.95	0.296	0.920	0.303	0.303	6.022
7V5	1,350	5	0.269	6.03	0.278	4.40	9.16	0.403	2.84	0.400	0.400	0.229
7V10(1)	1,350	10	0.276	2.43	0.283	1.49	4.84	0.406	1.49	0.405	0.405	0.090
(2)	1,350			2.44	0.283	1.65	4.78	0.406	1.67	0.406	0.406	0.154

* Uncorrected values (cable break at 0.2200 sec).

Where dual channels were employed on a single gage, the two results are shown in the table; however, only one of the pair is plotted in the figures.

3.3.3 Earth Velocity. The corrected earth velocity versus time plots are presented in Figures 3.7 through 3.13. The magnitude of the baseline change necessary to obtain zero velocity at a specified time is indicated on each curve; the dashed line designates the baseline of the as-

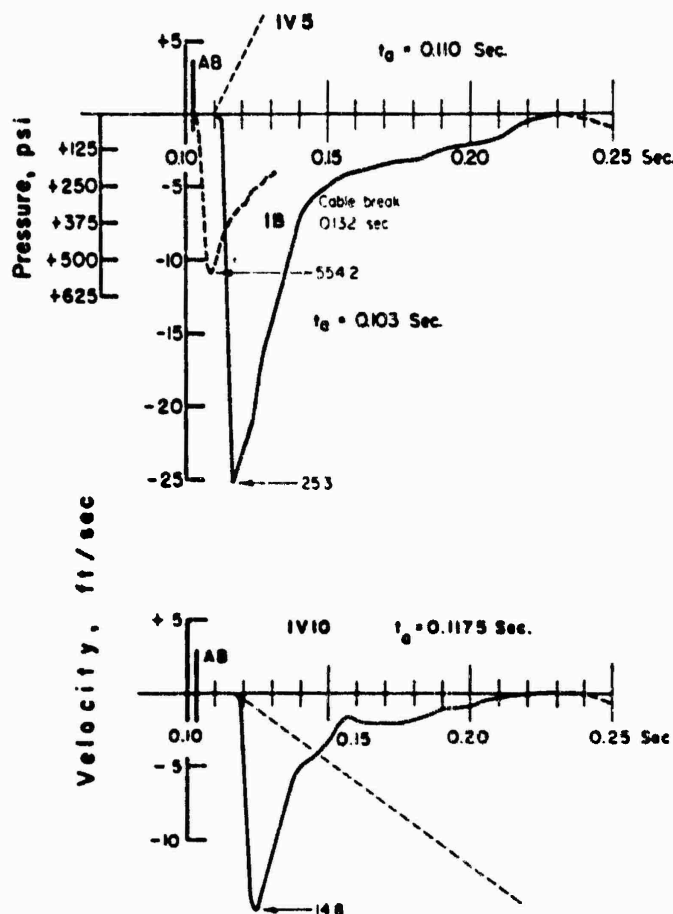


Figure 3.7 Vertical velocity versus time, Station 1 (GR: 450 feet), Shot Priscilla.

read first integration. In general, the wave forms of velocity-time are similar. At the close-in stations, where the precursor is just forming, the curves rapidly rise to maximum velocity. However, as the precursor develops, its influence is evident on the velocity response. Also, the velocity peaks tend to become less sharp with increasing depth of measurement.

The criterion for specification of the time that the velocity is zero was difficult to establish. After considerable study, it was decided that, for local air-blast induced effects only, the end of the overpressure positive phase would constitute a reasonable criterion for velocity equal to zero. Of course, this criterion necessarily was only indicative of the corrections to be made; each choice of time of zero velocity had to be made, taking into account any peculiarities which appeared on individual records.

In a few cases (for example: GV5, Figure 3.12), two different baseline corrections were thought to be equally valid. For these, both values are carried through, and the two displacement values are determined.

The data obtained from the corrected earth velocity plots are tabulated in Table 3.2.

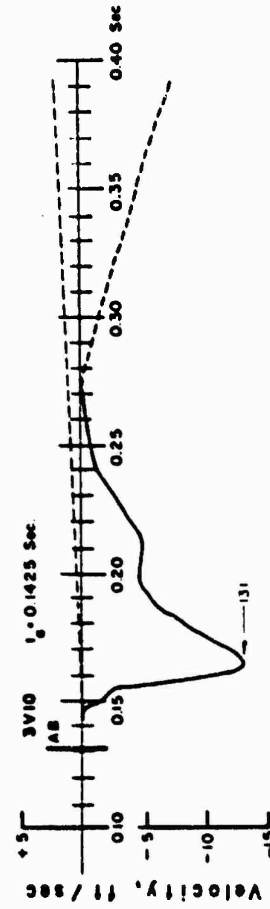
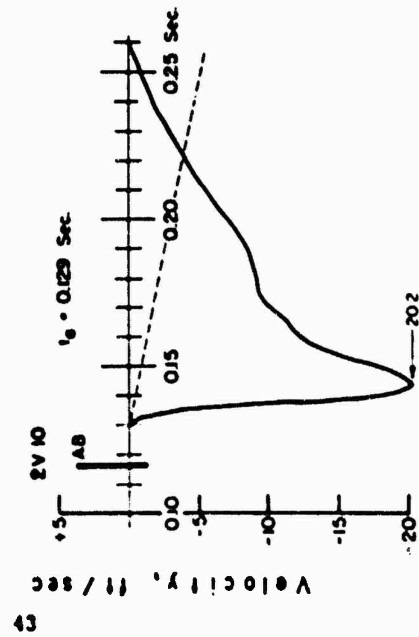
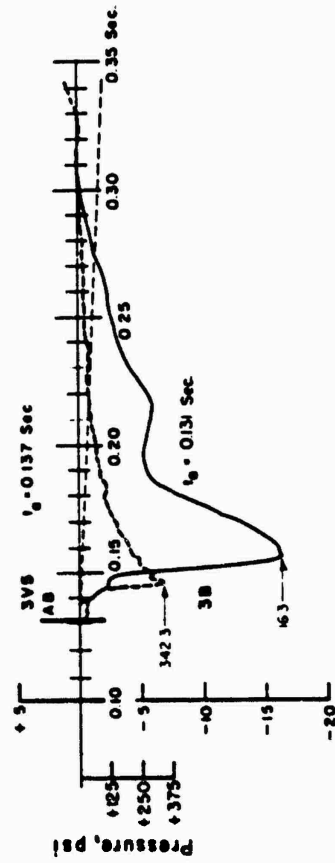
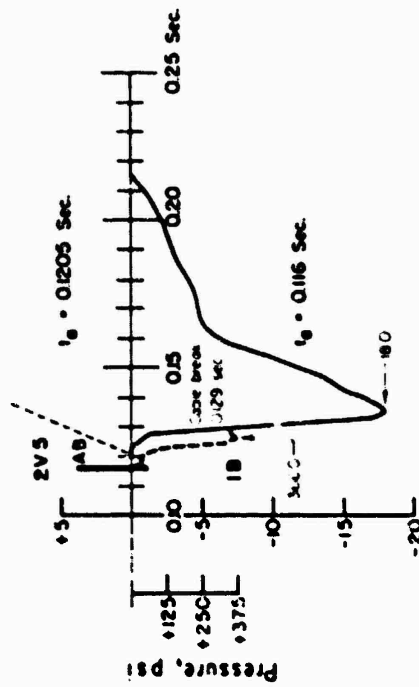


Figure 3.8 Vertical velocity versus time, Station 2 (GR: 550 feet), Shot Priscilla.

Figure 3.9 Vertical velocity versus time, Station 3 (GR: 650 feet), Shot Priscilla.

SECRET

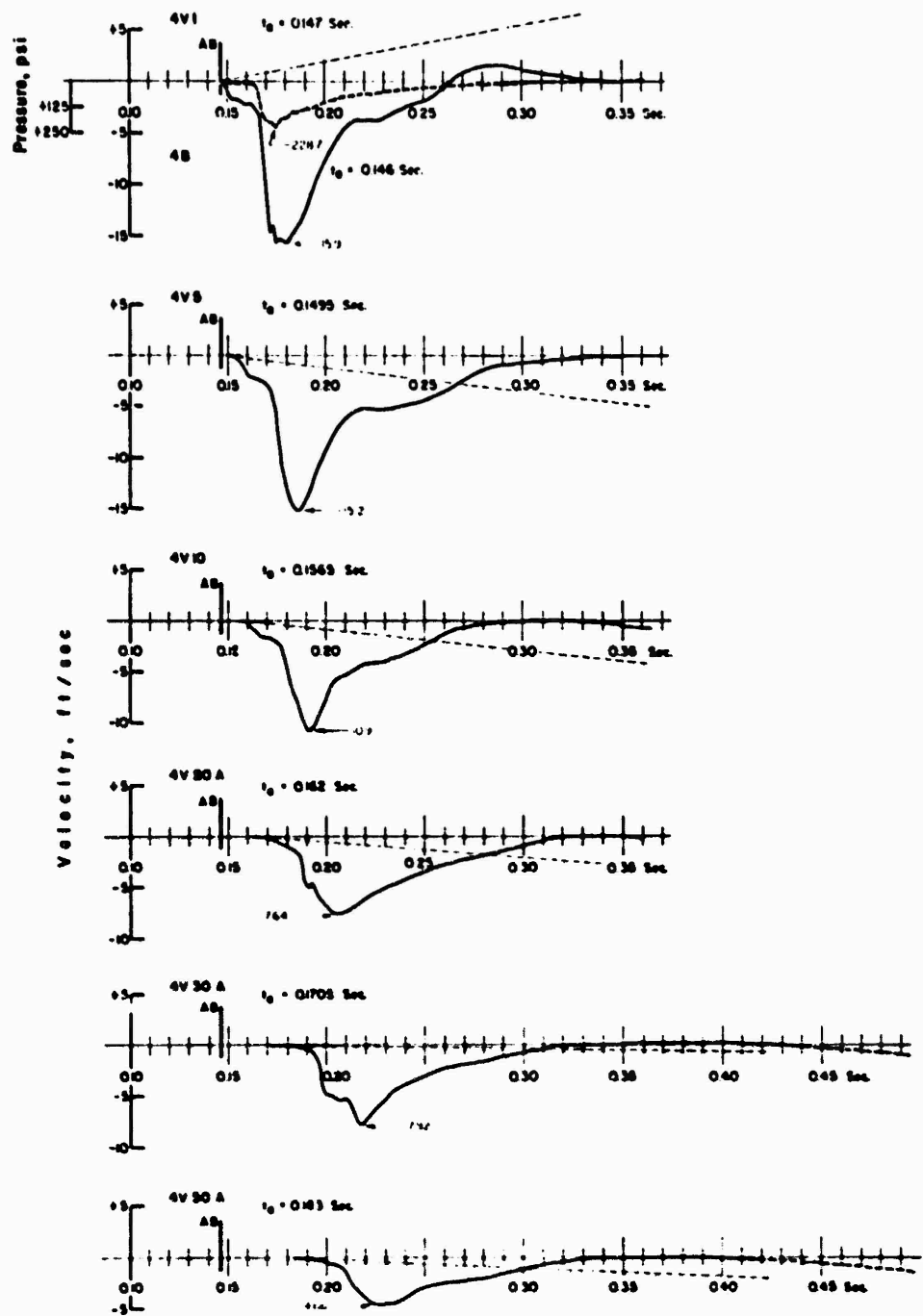


Figure 3.10 Vertical velocity versus time, Station 4 (GR: 750 feet), Shot Priscilla.

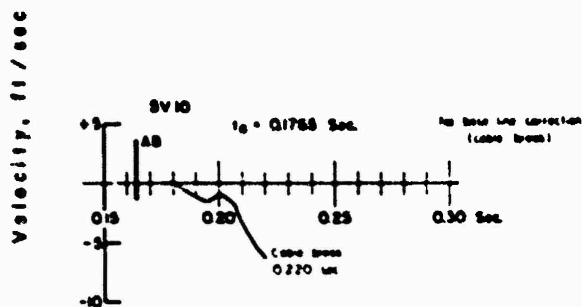
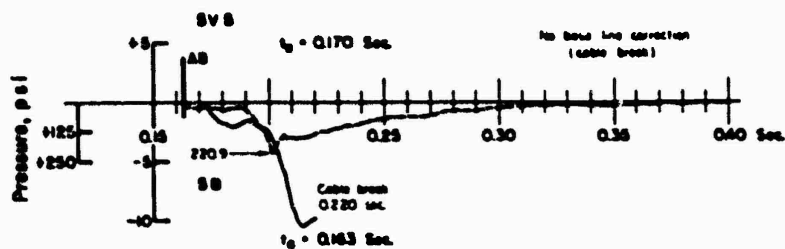
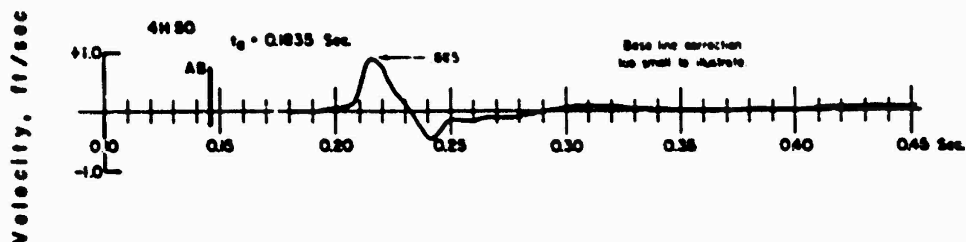
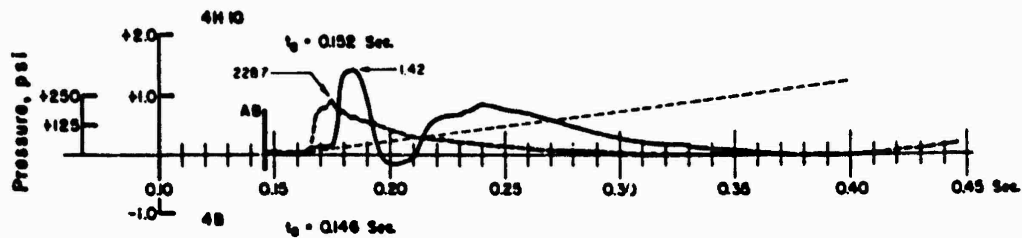


Figure 3.11 Horizontal velocity versus time, Station 4 (GR: 750 feet); vertical velocity versus time, Station 5 (GR: 950 feet); Shot Priscilla.

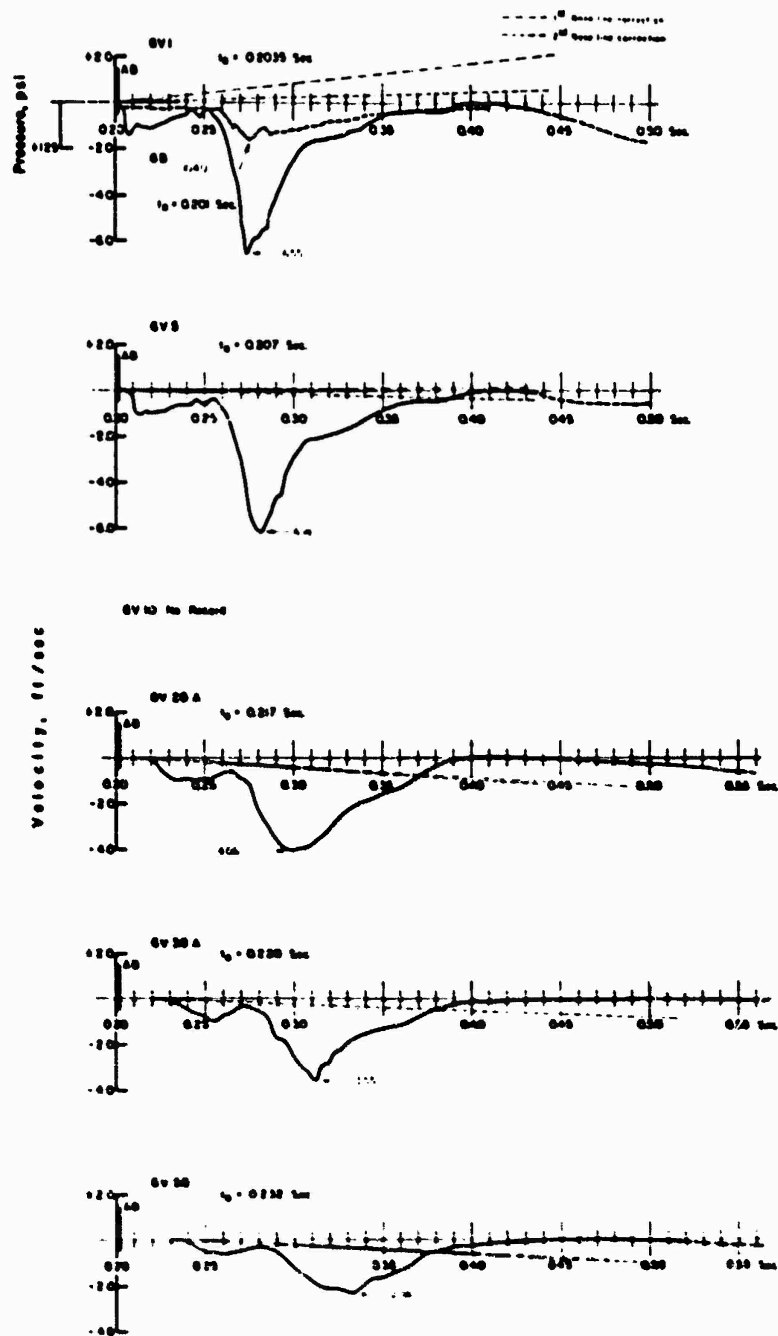


Figure 3.12 Vertical velocity versus time, Station 6 (GR: 1,050 feet), Shot Priscilla.

3.3.4 Earth Displacement. Figures 3.14 through 3.17 present the corrected earth displacement versus time plots, which are obtained from the double integration of the accelerometer records; the pertinent data are tabulated in Table 3.2. Included in Table C.1 (Appendix C) is the approximate uncorrected peak displacement; that is, the displacement obtained by double integration of as-read acceleration-time without correction to zero velocity.

In general, the wave forms of the displacement plots are similar, exhibiting, like the veloc-

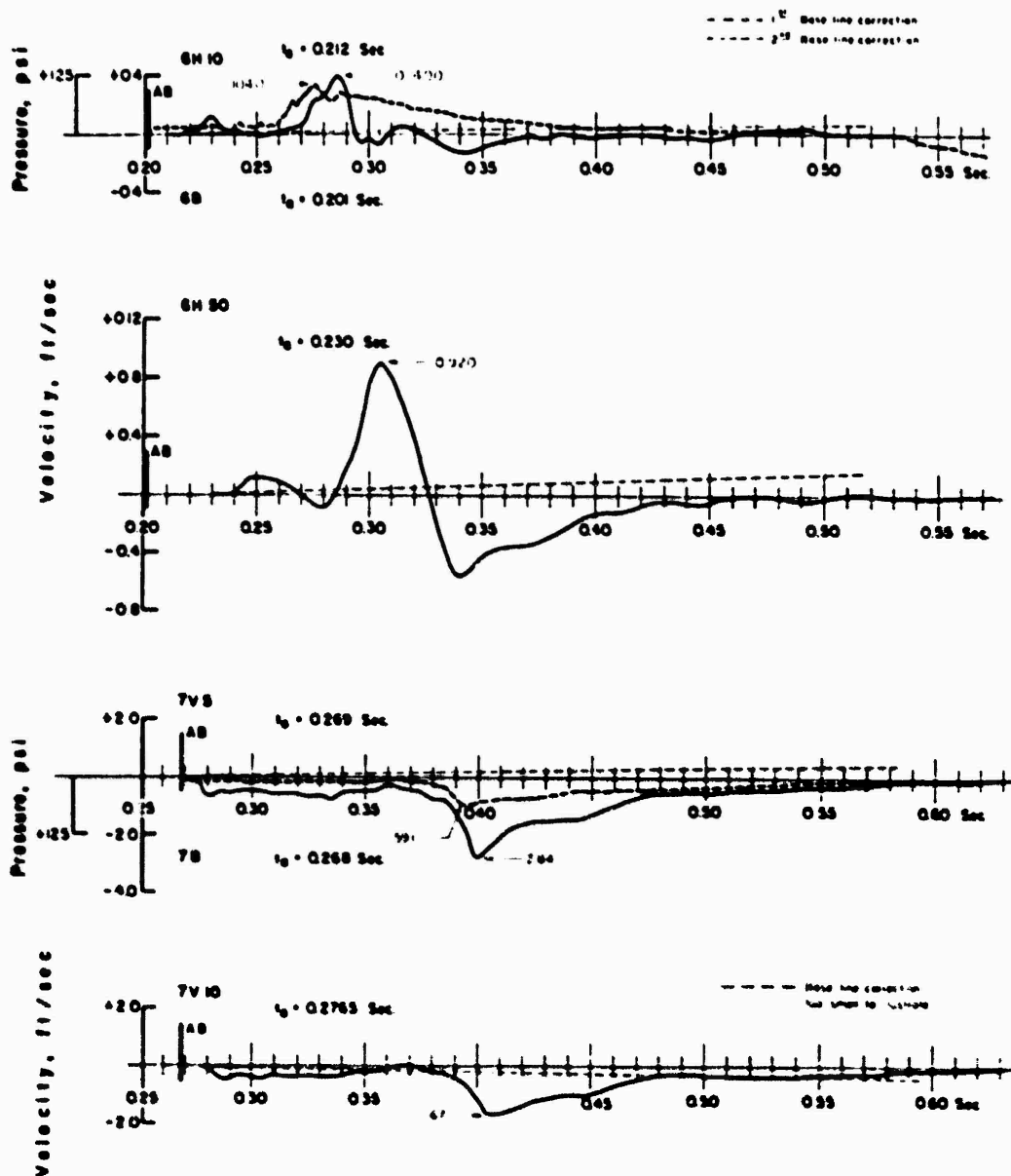


Figure 3.13 Horizontal velocity versus time, Station 6 (GR: 1,050 feet); vertical velocity versus time, Station 7 (GR: 1,350 feet); Shot Priscilla.

ity results, increasing time of rise to peak amplitude for increasing ground range. The effect of the precursor upon displacement is obvious at Station 6 but to a much lesser degree at the closer range stations.

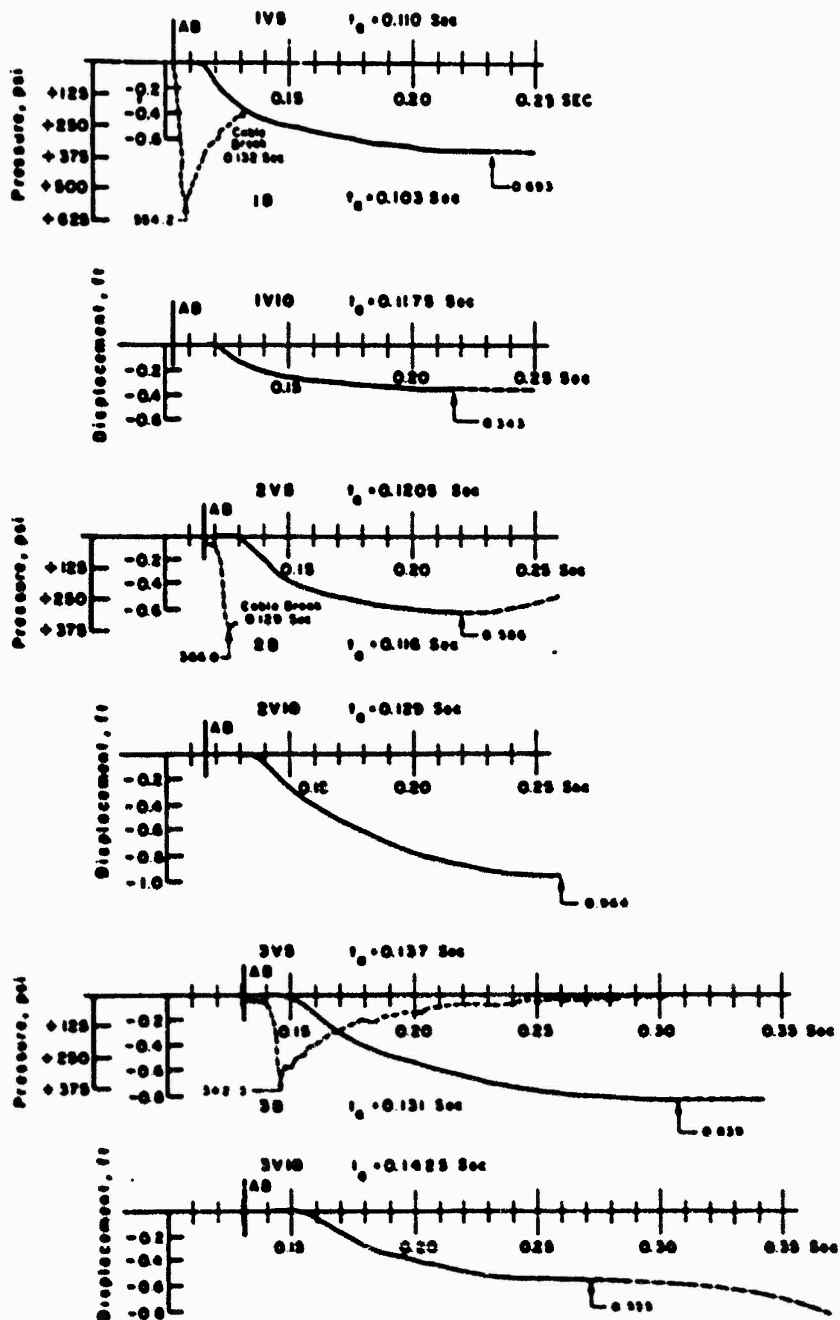
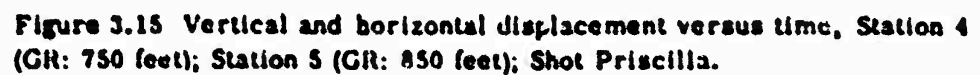


Figure 3.14 Vertical displacement versus time, Station 1 (GR: 450 feet); Station 2 (GR: 550 feet); Station 3 (GR: 650 feet); Shot Priscilla.



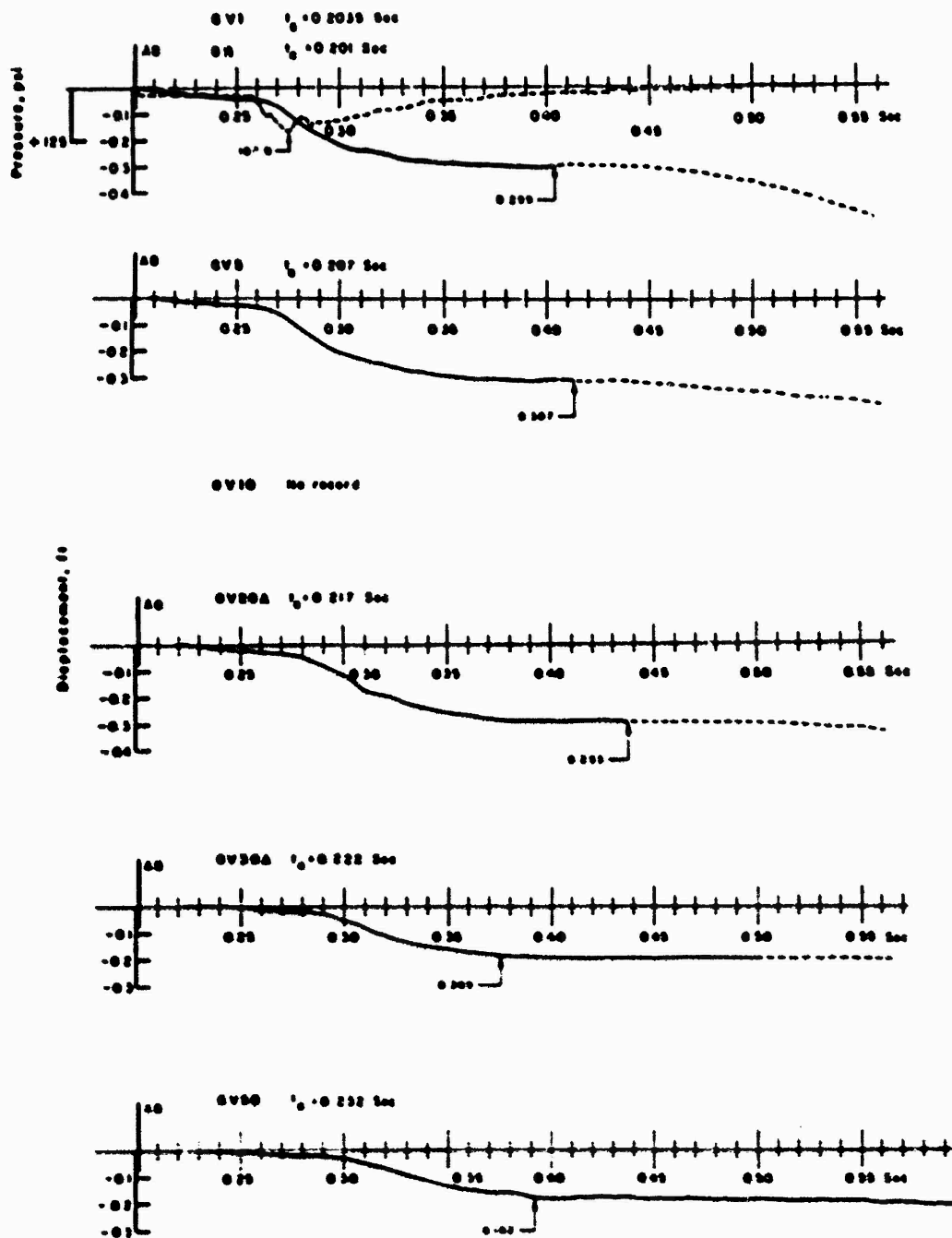


Figure 3.16 Vertical displacement versus time, Station 6 (GR: 1,050 feet), Shot Priscilla.

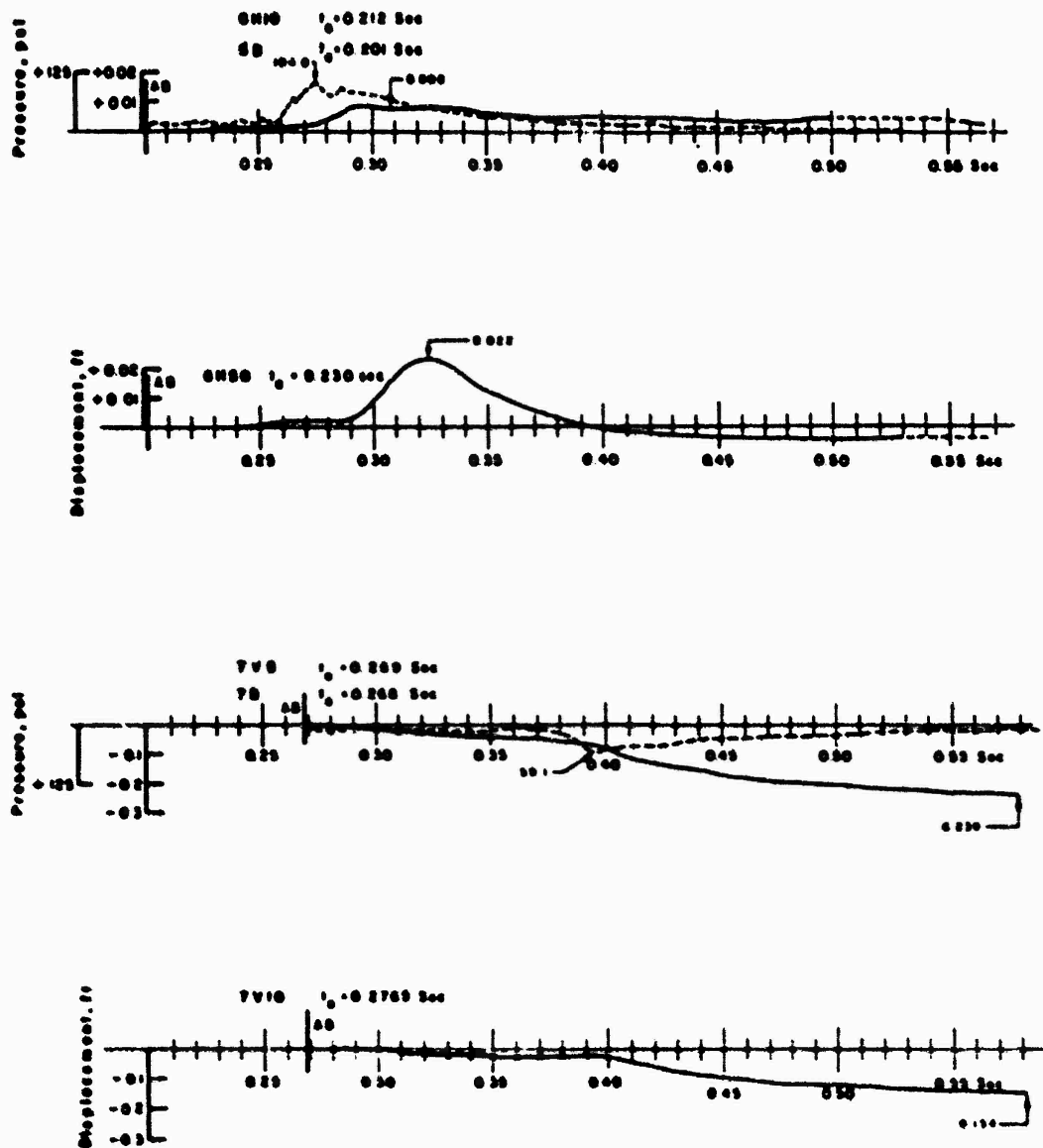


Figure 3.17 Horizontal displacement versus time, station 6 (GR: 1,050 feet); vertical displacement versus time, Station 7 (GR: 1,350 feet); Shot Priscilla.

3.3.5 Earth Stress. The earth stress-time plots from Project 1.4 are shown in Figures 3.18 through 3.23. Included in each figure, for comparison, is a plot of the overpressure-time record obtained at each station.

It is seen that, with few exceptions, the wave forms of these plots, particularly those from shallow gages, are similar to those of applied air-pressure. At the greater depths, the time of

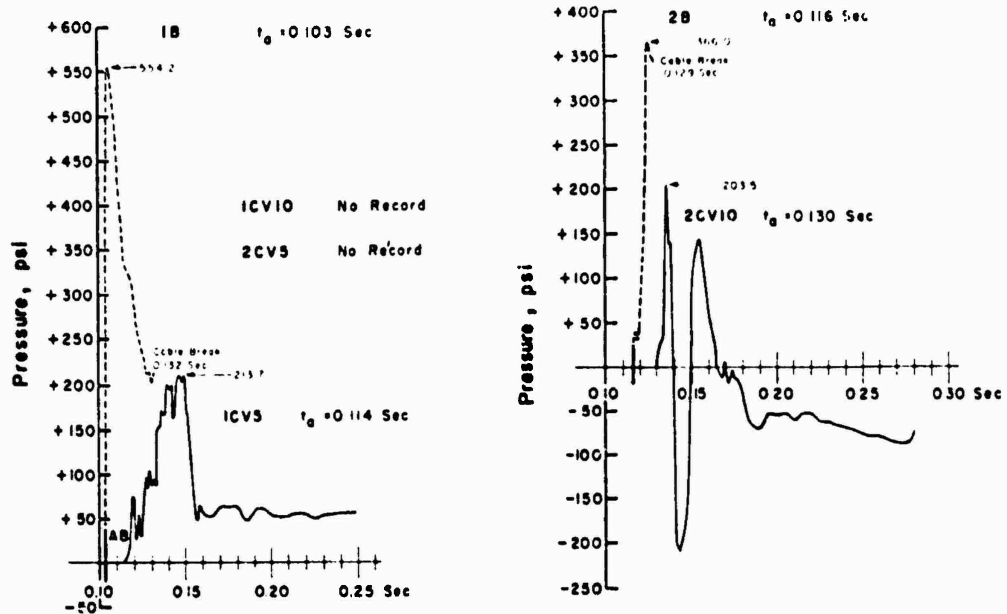


Figure 3.18 Vertical stress versus time, Station 1 (GR: 450 feet); Station 2 (GR: 550 feet); Shot Priscilla.

rise to peak stress is increased, and at Station 6 the effect of the precursor wave is evident. Three records, 6CV5B, 6CV10B, and 6CV20B, obtained from Project 1.7 and buried near Project 1.4, Station 6, (Figure 2.5), are included in Figure 3.22. These records will be considered auxiliary data and will be included in the analysis of results. It is apparent that, whereas at the 5-foot depth the primary and auxiliary stress records are comparable in wave form, the records at 10- and 20-foot depths are not similar in form. Actually, the auxiliary records seem more reasonable; this will be discussed more fully in Chapter 4.

The horizontal stress-time plots appear to exhibit the same general wave form as the vertical component.

Stress data are given in Table 3.3.

3.3.6 Earth Strain. Figure 3.24 presents the plots of the reduced earth strain records obtained, with peak values marked similarly to those of acceleration. It is seen that, while only two of these records are complete, three others give fragmentary information. The intermittent nature of these records is apparently caused by momentary contact of broken cables or connectors caused by earth motions.

The two complete strain records show wave forms which rise to a peak about the time of the peak stress, but decay less rapidly and to a constant value which represents the permanent (residual) strain. This wave form is apparently followed by the fragmentary record of 6SV30, but that of 4SV30 implies a final value of strain which is negative, unless that portion of the record is displaced. The abrupt changes in strain observed on the 4SV10 plot (near 0.180 second) and 6SV30A (near 0.280 second) make these results somewhat suspect. One would not expect the strain in soil to vary in that manner.

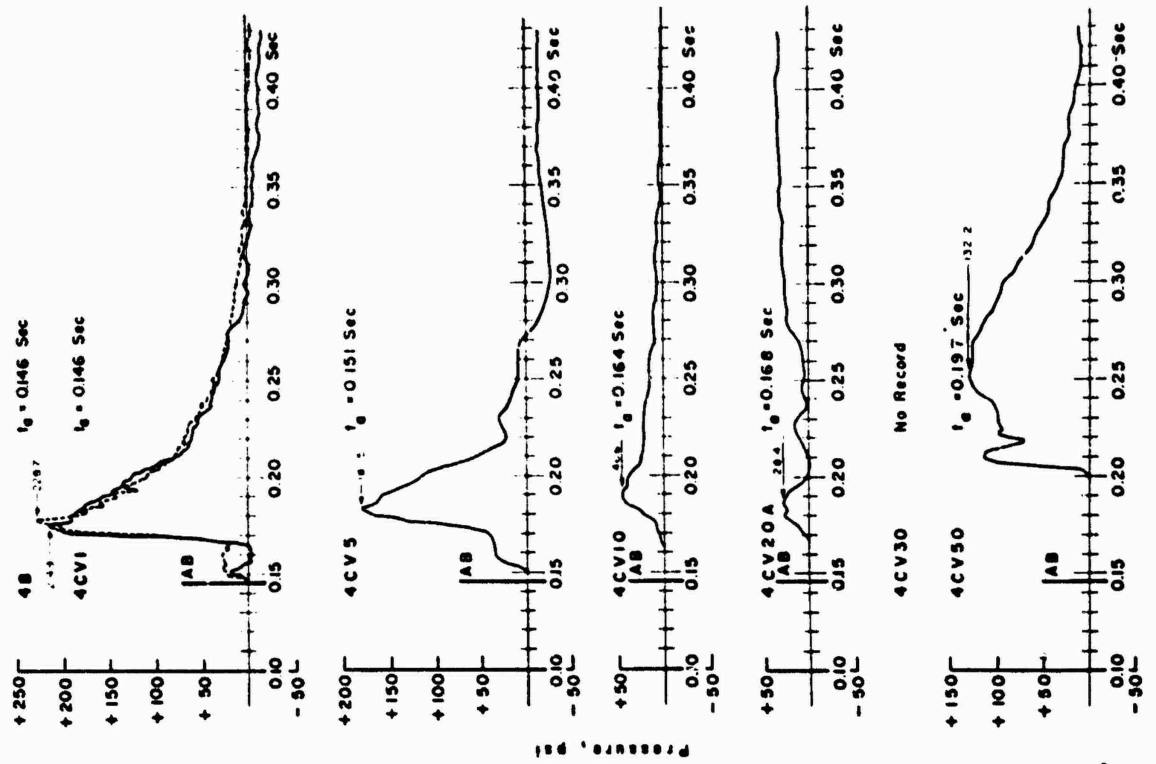


Figure 3.19 Vertical stress versus time,
Station 3 (GR: 650 feet), Shot Priscilla.

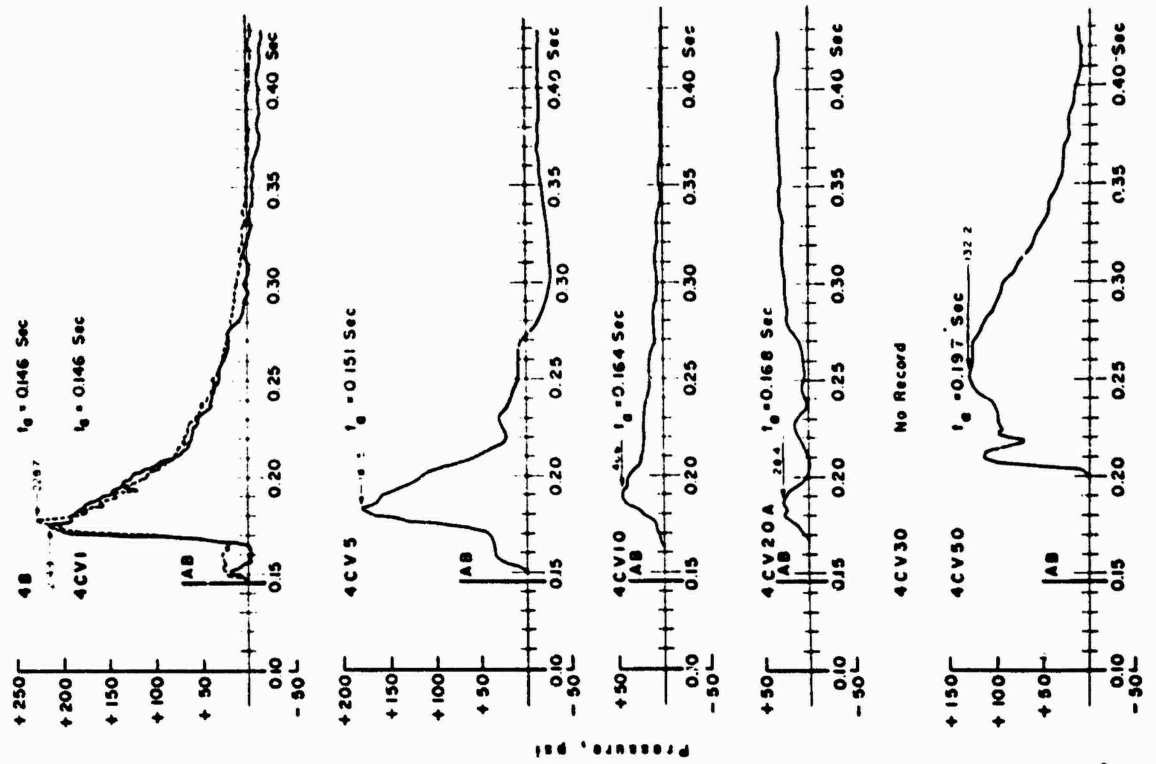


Figure 3.20 Vertical stress versus time,
Station 4 (GR: 750 feet), Shot Priscilla.

TABLE 3.3 SUMMARY OF STRESS DATA, SHOT PRISCILLA

NR, no record; DI, data indeterminate; and CB, cable break.

Gage	Ground Range	Gage Depth	Arrival Time	First Positive Peak	Time of First Positive Peak	Maximum Positive	Time of Maximum Positive	Maximum Negative	Time of Maximum Negative
	ft	ft	sec	psi	sec	psi	sec	psi	sec
1CV5	450	5	0.114	104.1	0.129	213.7	0.147	—	—
1CV10	450	10	NR	NR	NR	NR	NR	NR	NR
2CV5	550	5	NR	NR	NR	NR	NR	NR	NR
2CV10	550	10	0.130	203.5	0.136	203.5	0.136	208.2	0.143
3CV5	650	5	0.138	24.2	0.141	220.5	0.158	—	—
3CV10	650	10	0.149	205.8	0.168	211.8	0.174	7.79	0.285
4CV1	750	1	0.148	18.9	0.150	214.9	0.175	19.3	0.415
4CV5	750	5	0.151	42.3	0.159	181.5	0.183	34.1	0.300
4CV10	750	10	0.164	11.8	0.172	46.6	0.197	—	—
4CV10A	750	10	0.164	7.11	0.167	42.2	0.190	—	—
4CV20	750	20	NR	NR	NR	NR	NR	NR	NR
4CV20A	750	20	0.168	28.4	0.180	28.4	0.180	—	—
4CV30	750	30	NR	NR	NR	NR	NR	NR	NR
4CV30A	750	30	NR	NR	NR	NR	NR	NR	NR
4CV50	750	50	0.197	114.4	0.211	132.2	0.250	—	—
4CV50A	750	50	NR	NR	NR	NR	NR	NR	NR
4CH10	750	10	0.157	20.5	0.165	94.2	0.192	13.0	0.375
4CH50	750	50	0.199	10.0	0.212	14.9	0.247	3.98	0.207
4CH50A	750	50	0.199	10.4	0.220	14.7	0.248	4.36	0.207
5CV5	850	5	NR	NR	NR	NR	NR	NR	NR
5CV10	850	10	0.181	48.6 CB	0.219 CB	48.6 CB	0.219 CB	CB	CB
6CV1	1,050	1	0.204	27.6	0.227	74.5	0.273	8.97	0.515
6CV5	1,050	5	0.207	14.8	0.228	94.4	0.281	8.58	0.530
6CV5B	1,050	5	0.205	13.3	0.221	56.5	0.279	12.2	0.445
6CV10	1,050	10	0.213	DI	DI	54.5	0.283	33.8	0.220
6CV10A	1,050	10	NR	NR	NR	NR	NR	NR	NR
6CV10B	1,050	10	0.208	30.1	0.238	160.1	0.288	—	—
6CV20	1,050	20	NR	NR	NR	NR	NR	NR	NR
6CV20A	1,050	20	0.219	DI	DI	DI	DI	91.9	0.260
6CV20B	1,050	20	0.216	5.38	0.254	19.4	0.323	1.24	0.525
6CV30	1,050	30	0.230	3.40	0.271	7.47	0.301	4.79	0.256
6CV30A	1,050	30	0.230	2.64	0.272	5.93	0.303	5.99	0.255
6CV50	1,050	50	0.256	2.99	0.270	21.7	0.314	2.25	0.500
6CV50A	1,050	50	0.256	DI	DI	23.6	0.316	2.72	0.525
6CH10	1,050	10	0.216	6.44 CB	0.286 CB	6.44 CB	0.286 CB	CB	CB
6CH50	1,050	50	0.281	9.640	0.298	9.64	0.298	0.438	0.485
6CH50A	1,050	50	0.281	9.68	0.297	8.68	0.297	—	—
7CV5	1,350	5	0.270	3.51	0.334	28.3	0.406	0.501	0.362
7CV10	1,350	10	NR	NR	NR	NR	NR	NR	NR

Table 3.4 presents the basic strain data obtained. For convenience, peak air pressure and peak measured stress are included.

3.4 SEISMIC MEASUREMENTS

The seismic measurements were made to obtain data to aid in the interpretation of the below-ground effects on this project. The first phase of the program was the determination of the

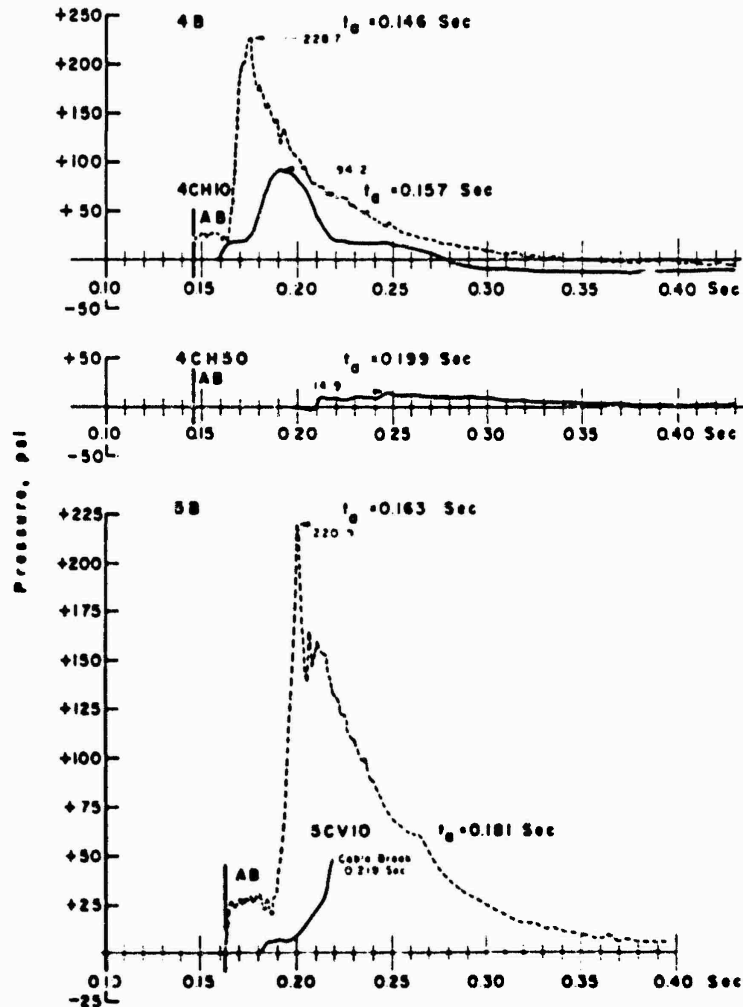


Figure 3.21 Horizontal stress versus time, Station 4 (GR: 750 feet); vertical stress versus time, Station 5 (GR: 850 feet); Shot Priscilla.

variation of velocity (C_L) with depth, particularly in the first 100 feet. Vertically drilled holes were used for this purpose. Small dynamite charges were fired at various depths in these holes, and geophones were placed near the top of the hole and at distances of 50 and 100 feet from the hole. The arrival times were measured and plotted against depth to determine the compressional wave velocities (C_L) in a vertical direction.

The second phase of the seismic program consisted of making a seismic refraction profile to determine the seismic horizontal velocities and their variation with depth. Figure 2.6 shows the location of shot holes and refraction spread used in the seismic program and their relation to the blast line. During this part of the program an effort was also made to generate shear waves and

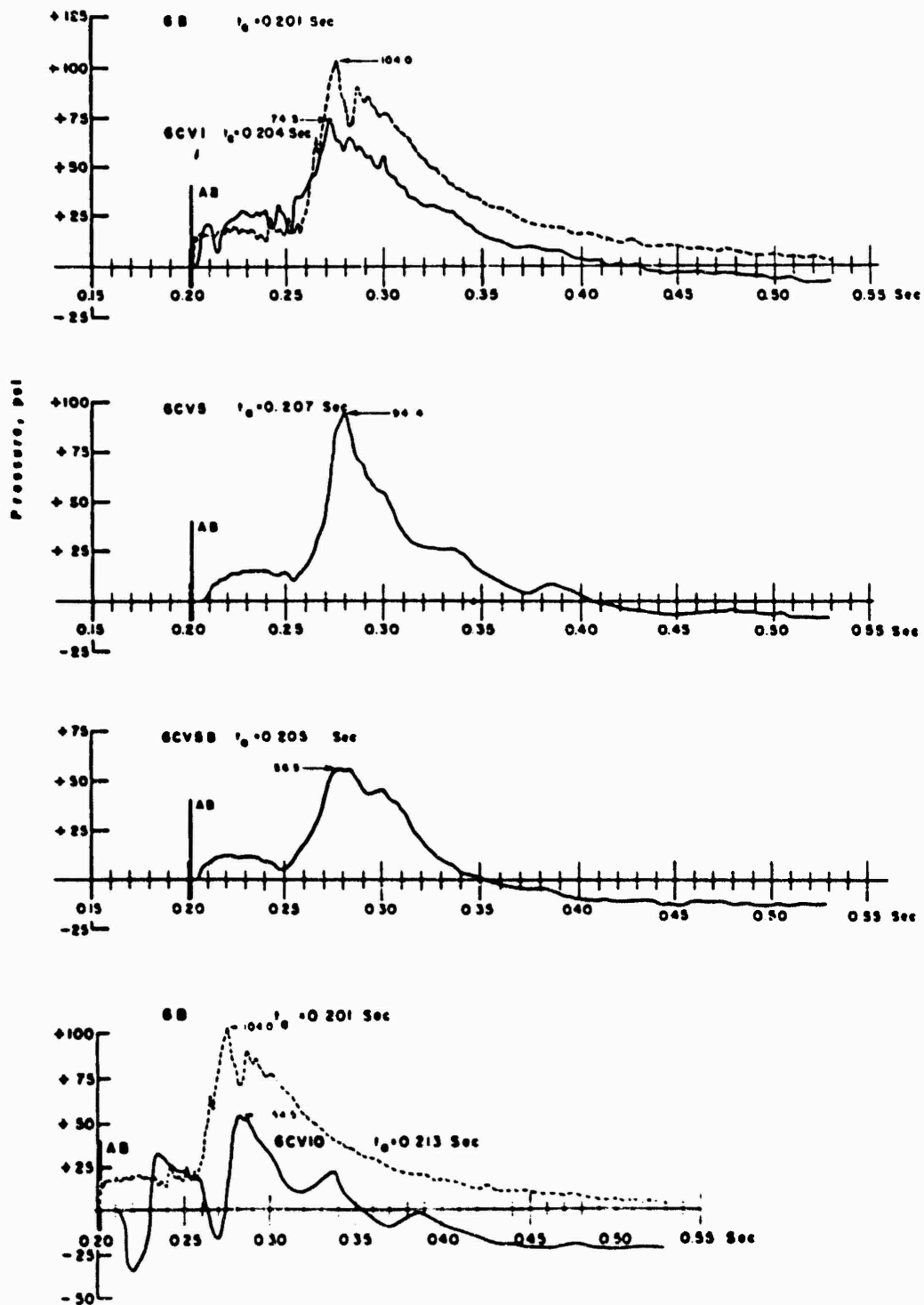


Figure 3.22 Vertical stress versus time, Station 6 (GR: 1,050 feet), Shot Priscilla.

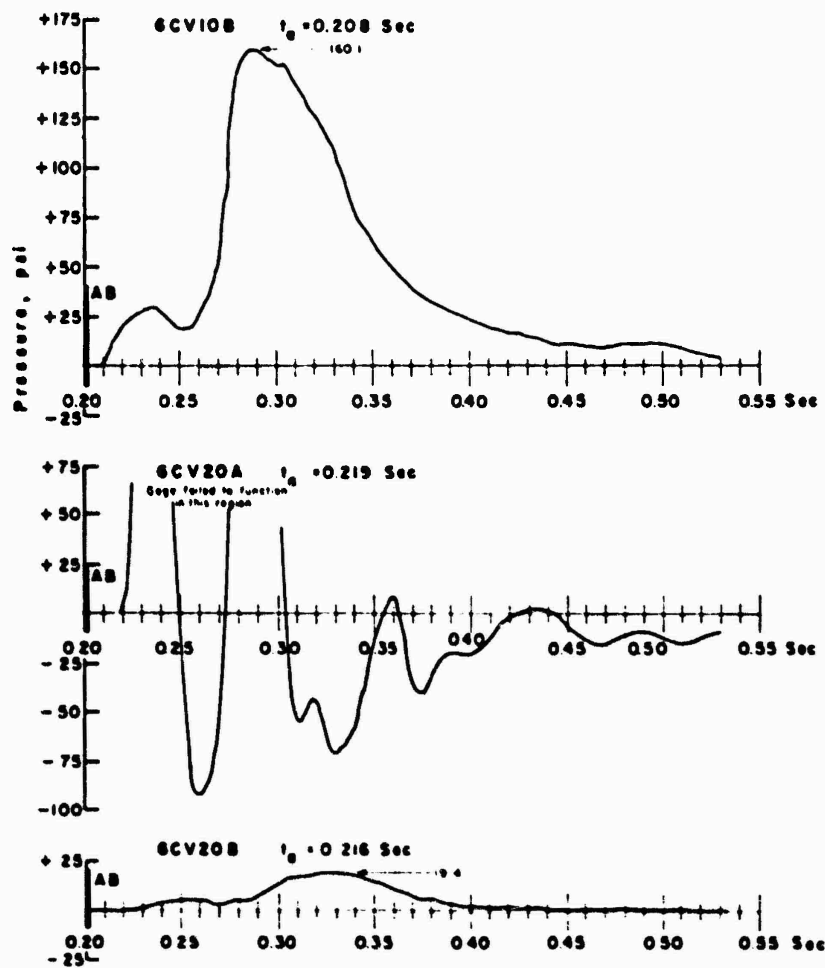


Figure 3.22 Continued.

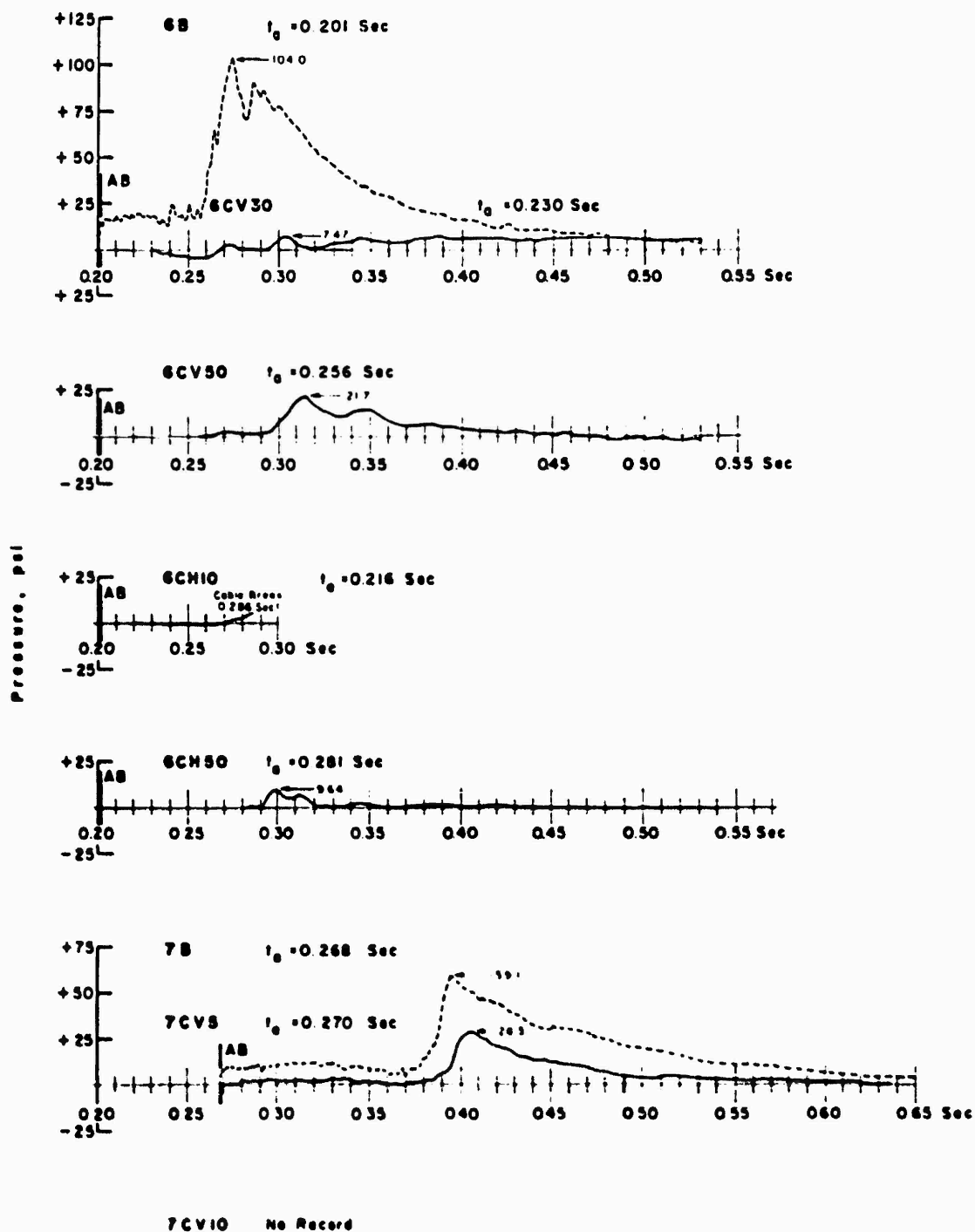
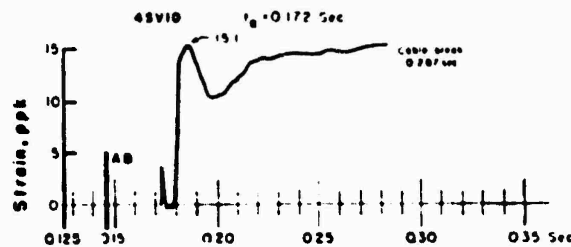
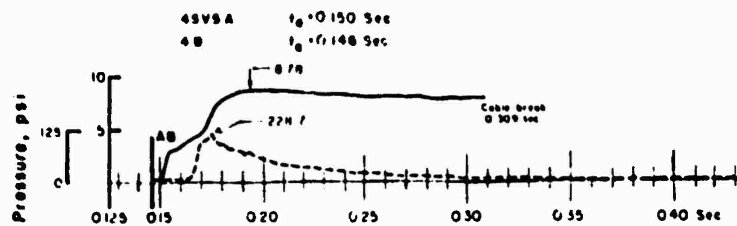
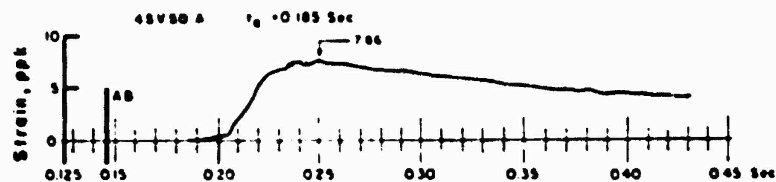


Figure 3.23 Vertical and horizontal stress versus time, Station 6 (GR: 1,050 feet), Shot Priscilla.



4SV20 No Record

4SV30 No Record



6SV5 No Record

6SV10 No Record

6SV20 No Record

6SV30 $t_0 = 0.220$ Sec

6B $t_0 = 0.201$ Sec

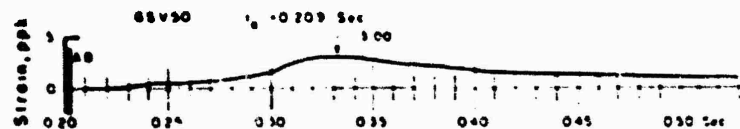


Figure 3.24 Vertical strain versus time, Station 4 (GR: 750 feet); Station 6 (GR: 1,050 feet); Shot Priscilla.

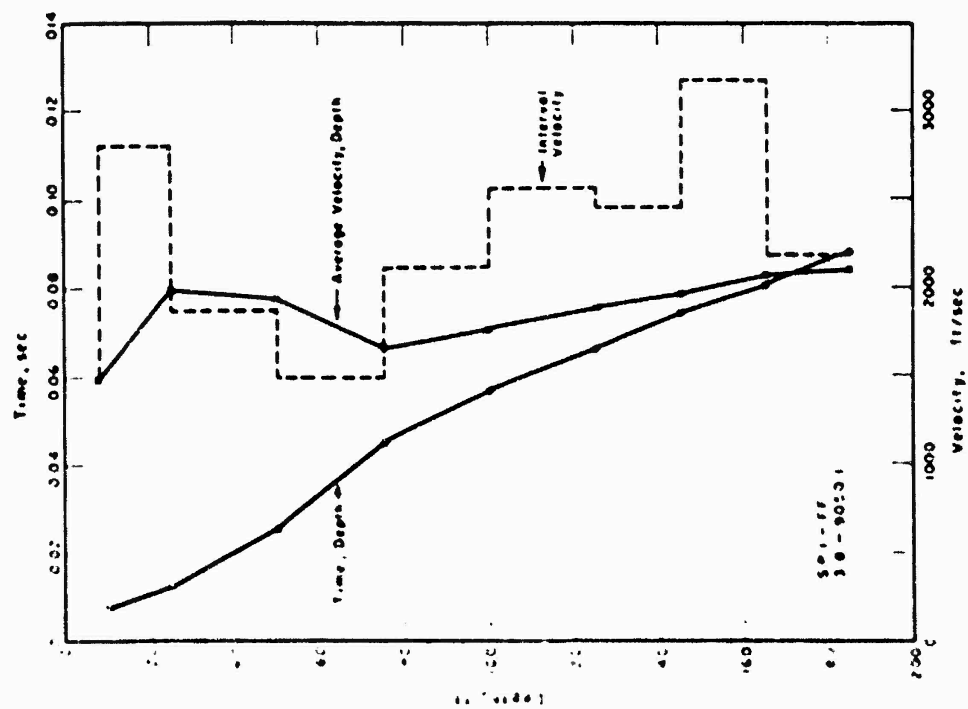


Figure 3.25 Travel-time data, Shot Point 1, Frenchman Flat.

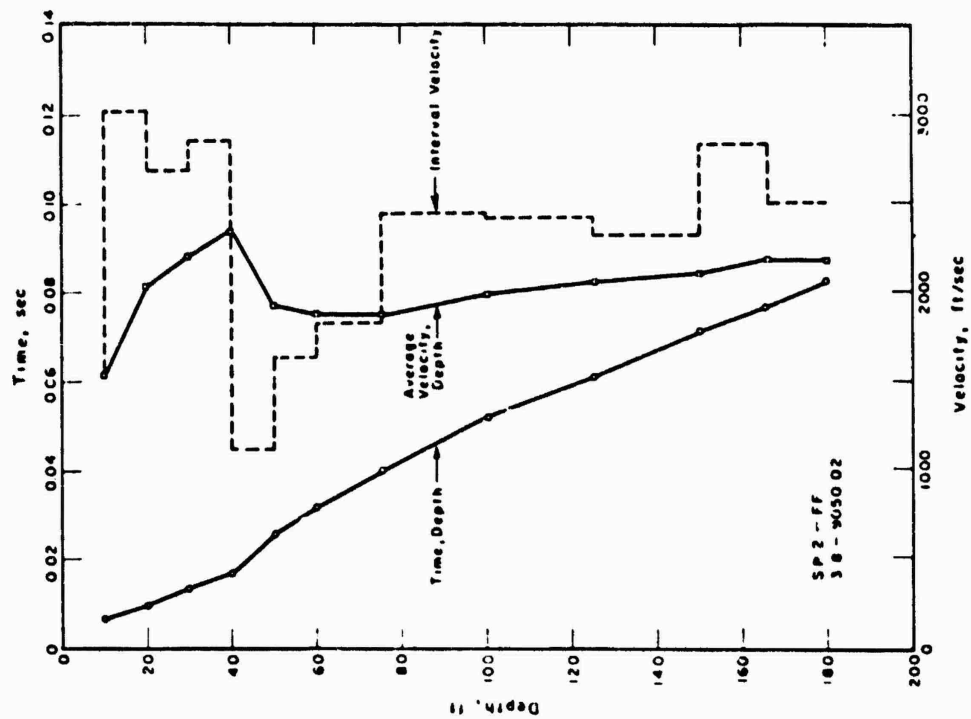


Figure 3.26 Travel-time data, Shot Point 2, Frenchman Flat.

measure shear-wave velocities; however, no success was met in the attempt to measure shear-wave velocity directly. However, some short spreads, using only a blasting cap and hammer blows for energy, were set out and Rayleigh waves were recorded. From these Rayleigh velocities an approximation of the surface shear-wave velocity was made.

3.4.1 In Situ Seismic Velocities. The seismic velocities in a vertical direction were measured by detonating small dynamite charges ($\frac{1}{4}$ to $1\frac{1}{2}$ pounds) at a number of depths in three shot holes (see Section 2.3.4) with detectors placed at the surface. The horizontal velocities were

TABLE 3.4 SUMMARY OF STRAIN DATA, SHOT PRISCILLA

NR, no record; and CB, cable break.

Gage	Ground Range	Gage Depth	Arrival Time	Maximum Positive	Time of Maximum Positive	Maximum Negative	Time of Maximum Negative	Residual Strain	Time of Residual Strain
	ft	ft	sec	ppk *	sec	ppk *	sec	ppk *	sec
4SV5	750	5	0.150	8.81	0.194	—	—	6.60	0.309 CB
4SV5A	750	5	0.150	8.78	0.195	—	—	7.54	0.309 CB
4SV10	750	10	0.172	15.1	0.187	0.233	0.176	15.1	0.287 CB
4SV20	750	20	NR	NR	NR	NR	NR	NR	NR
4SV20A	750	20	NR	NR	NR	NR	NR	NR	NR
4SV30	750	30	NR	NR	NR	NR	NR	NR	NR
4SV50	750	50	0.185	7.58	0.248	—	—	3.65	7.50
4SV50A	750	50	0.185	7.86	0.249	—	—	3.70	4.80
6SV5	1,050	5	NR	NR	NR	NR	NR	NR	NR
6SV10	1,050	10	NR	NR	NR	NR	NR	NR	NR
6SV20	1,050	20	NR	NR	NR	NR	NR	NR	NR
6SV20A	1,050	20	NR	NR	NR	NR	NR	NR	NR
6SV30	1,050	30	0.220	5.79	0.304	—	—	0.758	7.50
6SV30A	1,050	30	0.220	5.99	0.304	—	—	0.730	4.80
6SV50	1,050	50	0.209	2.99	0.330	0.034	0.213	0.457	5.70
6SV50A	1,050	50	NR	NR	NR	NR	NR	NR	NR

* Parts per thousand.

determined from the refraction profile by setting out a line of geophones and shooting small charges in shallow holes at various distances in line with the geophone spread.

The results of the vertical seismic profiles shot at the three different positions show the variations of the velocities with depth. Figures 3.25 through 3.27 are plots of the time-depth curves at the three hole positions. While there is some 20 percent lateral variation, all the time-depth curves are similar. (No effects of water intrusion on the vertical velocities was apparent in the third hole.) The average-velocity depth and the interval velocities, determined by the increments of the time-depth curves, are also shown in these figures. It is not implied that the interval velocities are as abrupt as shown, but this presentation is conventional, and attempts to smooth the curve are not justified by data of this type.

The results of the seismic survey do not show the gradual increase of velocity with depth that was expected. The low-velocity layer in the vicinity of 40- to 50-foot depth was not indicated from previous data taken by earlier refraction surveys (Reference 10). The refraction-survey method has the inherent limitation that it cannot detect a low-velocity layer which underlies a high-velocity layer. When the 50-foot instrument hole was examined, there was no visual indication that the plays in the 40- to 50-foot low-velocity region was any different than the upper high-velocity material. One explanation for this low-velocity material would be that rate of deposition for this region was faster than for the rest of the overlaying material. This higher rate would produce material that was not as compact and of a lower modulus and would thus have a lower velocity.

The unexpected results of the vertical seismic-velocity surveys were sufficiently different from those assumed in the original predictions to cause some concern as to the validity of the

predictions. There was insufficient background as to the effects that the velocity inversion would have on the stress and acceleration to justify their modification. The strain, however, was considered to be more directly affected by the local modulus, and these predictions were modified to take the seismic results into account. The revised values are shown in Table 2.1.

The results of the refraction profile show four layers having different horizontal velocities to a depth of 200 feet. The surface layer to a depth of 20 feet showed an average velocity of $1,050 \pm 100$ ft/sec, the second layer, which was 42 feet thick, had an average velocity of 2,260 ft/sec and the third layer, 106 feet thick, had an average velocity of 2,665 ft/sec. The fourth layer was penetrated only a few feet and showed a velocity of 3,340 ft/sec. If the seismic profile had been extended beyond 900 feet along the surface, the depth and velocity of deeper layers could have been determined.

Figure 3.28 shows the travel curve of the refraction profile and a wave-front diagram indicating the depths and velocities of the various refraction horizons. The horizontal velocities shown by the seismic-refraction work are somewhat greater than the vertical velocities. This

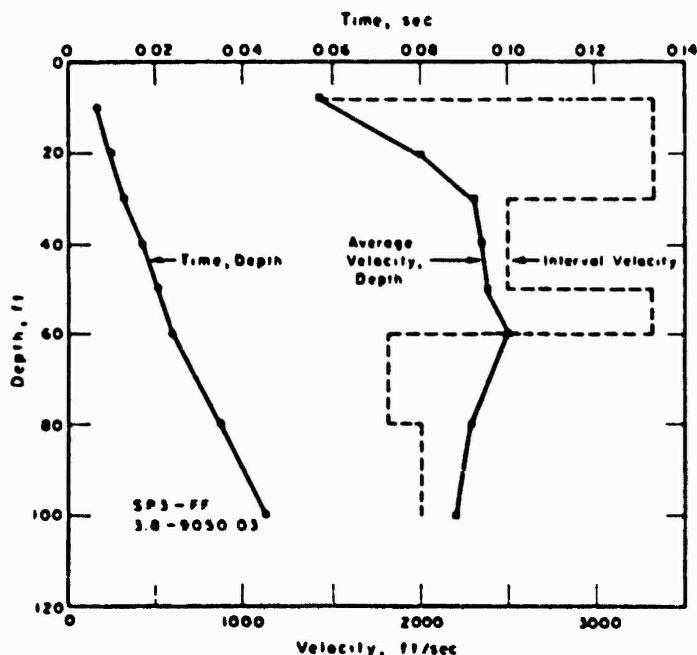


Figure 3.27 Travel-time data, Shot Point 3, Frenchman Flat.

is normal and to be expected in multilayered formations. As stated before, a break in the time-travel curve occurs only when a higher velocity layer is below a layer of low velocity. The vertical velocities probably give better overall velocity data than the refraction velocities which only indicate velocities in specific layers.

A close examination was made of the refraction records to see if any shear waves were recorded. No definite arrivals were observed that could be identified as shear waves. However, two short spreads were recorded using geophone intervals of only 20 feet and hammer blows and a blasting cap as a source of energy, and Rayleigh waves were observed on these short refraction profiles. The results of this survey are shown in Figure 3.29, which shows a Rayleigh wave velocity of 575 ft/sec \pm 15 percent and a C_L of 1,520 ft/sec \pm 15 percent. This gave a ratio of $C_p/C_L = 0.378$ (Figure 3.29) which gives a Poisson's ratio (σ) of 0.40 for the surface material to a depth of approximately 15 feet; using the extreme values of velocity, one obtains $0.22 \leq \sigma \leq 0.44$.

3.4.2 Velocities in Backfill. During the backfilling of the deep gage holes at Stations 4 and 6, a geophone was planted in each hole near the wall at a depth of 50 feet. Late in the preshot

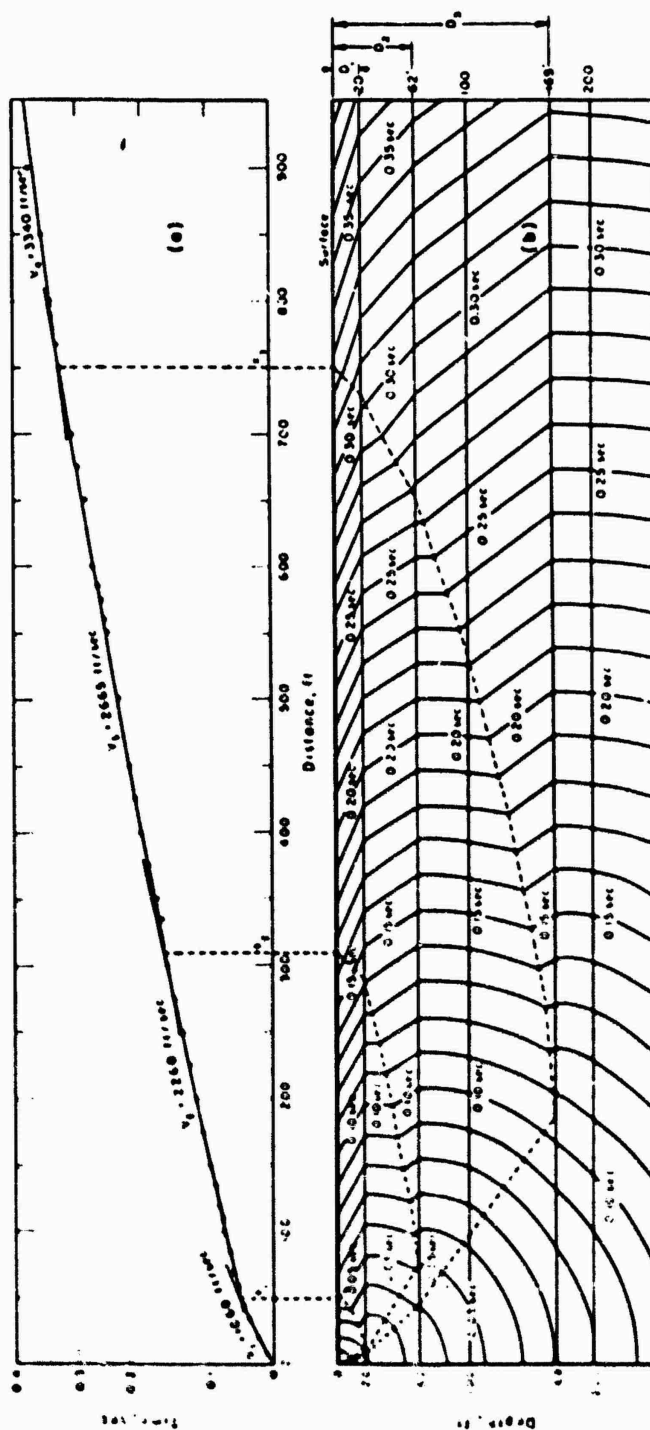


Figure 3.28 Refraction survey, travel-time data, and wave-front diagram, Frenchman Flat.

operation after backfilling was completed, measurements were made of the travel time of the seismic impulse from the geophone to the surface.

Small charges consisting of only a blasting cap were fired on the surface. One charge was shot on the opposite side of the hole from that where the geophone was planted and the other charge 5 feet away from the edge of the hole above the geophone (also 5 feet off vertical). The

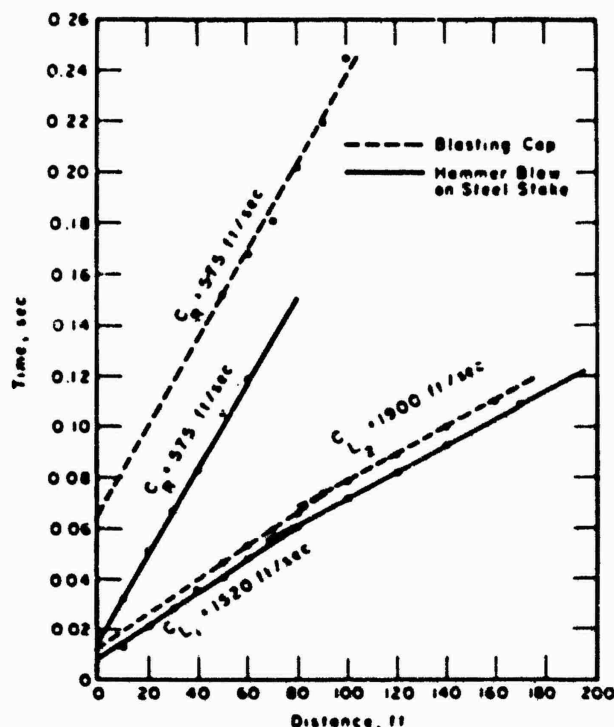


Figure 3.29 Refraction survey, short-span instrument array, Frenchman Flat.

travel times through the undisturbed material were 33 and 36 msec and through the backfilled material they were 36 and 37 msec. These travel times correspond to average velocities of $1,390 \pm 40 \text{ ft/sec}$ and $1,450 \pm 60 \text{ ft/sec}$. The average travel time for the first 50 feet from Shot Points 1, 2, and 3 showed a time of 24.2 msec which corresponded to an average velocity of 2,060 ft/sec. These data imply that the backfill failed to reach the original modulus and that the effect of backfilling and moisture content also reached somewhat beyond the edge of the hole.

Chapter 4 DISCUSSION

After a brief description of acceleration and velocity wave form types, the Shot Priscilla ground shock data will be discussed. Where applicable, the results of the Tumbler, Upshot-Knothole, and Jangle shots (Appendix B) will be compared with those from Shot Priscilla. The main topics to be discussed are attenuation of ground shock with depth, earth response as affected by the character of air-blast pressure input, local effects versus effects from remote sources, and response spectra. Also included will be a brief analysis of deduced stress-strain relations for soil.

4.1 ACCELERATION AND VELOCITY WAVE FORMS

The most typical characteristic of ground accelerations induced by the air blast is that there is no single ideal wave form. In the elastic model, the accelerations caused by the direct wave appear proportional to the time rate of change of overpressure; hence, one would expect the character of the accelerations to change with overpressure wave form. The integral of vertical acceleration, vertical particle velocity, is perhaps the most familiar of all ground-motion parameters since it bears a direct relationship to the overpressure. Six of the more predominant acceleration and velocity wave form types characteristic of the NTS are shown schematically in Figure 4.1. Examples of these wave form types taken from various tests are listed in Table 4.1. When the wave form is ideal and traveling superseismically, the downward acceleration is large compared with the following upward accelerations (Figure 4.1a), examples: Records 1V5, 1V10, and 2V5 (Figure 3.2). The resulting velocity is similar to the air pressure, falling off somewhat more rapidly than the pressure and becoming zero before the end of the positive phase of the air pressure. At lower peak overpressures, the first downward acceleration is followed by an upward peak acceleration of nearly equal or sometimes greater magnitude (Figure 4.1b). This type of wave form is common in small high-explosives charge work even at high overpressures.

The resulting velocity decreases more rapidly than in Type a and becomes positive prior to the end of the positive phase. The peak upward velocity is always much smaller than the peak downward velocity, however. The first indication that the air blast is traveling transseismically is an outrunning of the downward acceleration (Figure 4.1c) compared with the sharp onset of acceleration illustrated previously, example: Record 4V20A (Figure 3.3). This type of outrunning, although infrequently observed during nuclear tests, is common on small high-explosives shots.

The character of the ground acceleration in the precursor region changes markedly as the precursor develops and decays. Figure 4.1d illustrates a wave form typical of the early stages of precursor development, examples: 4V1, 4V5, and 5V5 (Figures 3.3 and 3.4). The precursor induces accelerations similar to those of Figure 4.1b. The main pressure wave induces larger (since the pressure is much greater) downward accelerations. The peak upward accelerations are low since the pressures are large in this region. As the precursor transgresses its various stages of development, the air pressure wave form becomes violent, producing the high frequency acceleration record of Figure 4.1e, examples: 6V1, 6V5 (Figure 3.5). As the blast wave cleans up, these accelerations may become small in magnitude.

When the refracted ground wave outruns the local wave, the first peak vertical acceleration is positive or upward as in Figure 4.1f. The frequencies associated with the remote source accelerations are much lower than those of the local effect; onset of acceleration is gradual and in many cases hardly perceptible; and successive peaks grow in magnitude and then decay. The

signals often last for two or three times the positive phase duration of the air blast wave. Although the accelerations from remote sources are generally small compared with those of the local wave, their low frequency results in velocities and displacements which are comparable with those of the local wave.

The arrival of the local effect is identified by a sudden increase in velocity (Figure 4.2), the velocity jump, as it is called in British weapons effects reports. Since the velocity jump may

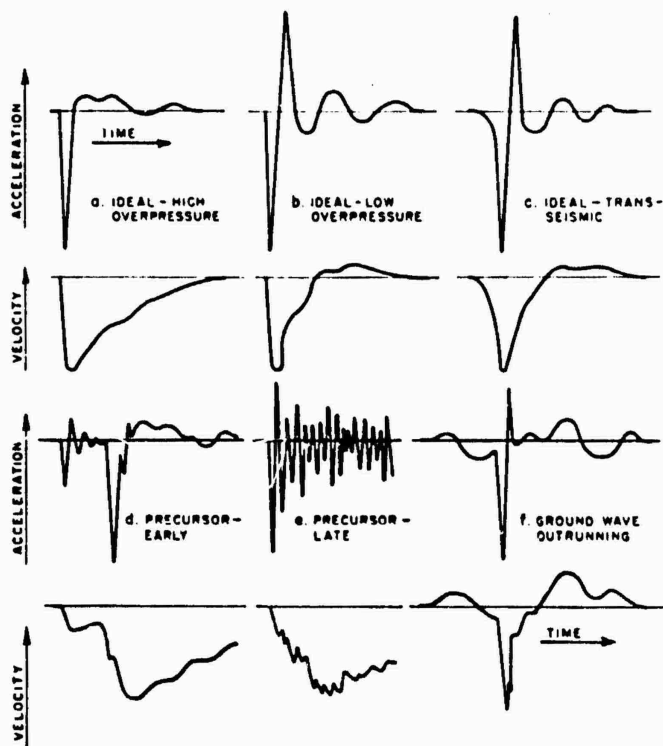


Figure 4.1 Schematic diagrams of vertical acceleration and velocity wave forms.

be superimposed on ascending or descending portions of the remote effect, it represents the most probable peak downward value of the velocity. Furthermore, it bears a direct relationship to the overpressure in the same manner as the peak downward velocity in the supersismic case. The influence of the refracted wave not only appears ahead of but also behind the arrival of the local wave. Because of this, the peak upward velocities become comparable with the velocity jump, Figure 4.3.

Even though the blast wave may be supersismic, i.e., outrunning is not observed, the signal produced by the refracted wave may be sufficient to modify the velocities in the later portions of the acceleration pulse. Thus, the remote source wave can have marked effects on the peak displacements, effects which are not observed in the peak velocity.

At depth, outrunning occurs earlier than at the surface, and the accelerations of the direct wave are attenuated. In such cases, the acceleration wave type becomes extremely confused, particularly in the precursor region where types d, f, and possibly c emerge. This combination may occur at depths as small as 20 feet, cf., Shot Priscilla gages 4V20A and 6V30A (Figures 3.3 and 3.5).

4.2 SIGNALS FROM REMOTE SOURCES

The origin of signals from sources other than the local air-blast slap has been discussed

for the general case in Section 1.3. Figure 4.4 shows the air pressure time of arrival plot for the Priscilla event; also plotted on the figure are the data from the refraction survey taken at Frenchman Flat as a part of Project 1.4. Sliding the seismic curve up the air-blast curve, one finds that the surface level outrunning ground range for Priscilla was about 2,500 feet, due to a signal originating approximately 600 feet closer to ground zero. However, the plot of Figure 4.4 does not tell the whole story; it is possible for: (1) outrunning to occur at closer ranges for measurements taken underground; and (2) refracted signals to be manifest on records after the arrival of the first signal.

Therefore, although the Priscilla acceleration results (measurements out to 1,350-foot ground range) show no outrunning in the strict sense of the term, they show that refracted signals from remote sources were present, particularly from the deeper gages. Notable examples are found

TABLE 4.1 EXAMPLES OF VERTICAL ACCELERATION WAVE FORM TYPES SHOWN IN FIGURE 4.1

Wave Form	Example *	Shot	Overpressure psi
a	1V5	Plumbbob, Priscilla	554
	14V1	Upshot-Knothole 9	21.5
b	17V1	Upshot-Knothole 9	11.5
	5V	Mole Round 104	78
c	4V	Mole Round 208	> 160
d	4V1	Plumbbob, Priscilla	104
	7V5	Plumbbob, Priscilla	59
	15V1	Upshot-Knothole 10	300
	1V	Tumbler 4	45
e	17V1	Upshot-Knothole 10	14.5
	0V1	Upshot-Knothole 10	8.1
f	8V	Tumbler 1	5.2
	5V	Tumbler 2	3.4
	9V2	Mole Round 308	13.8

* Gage designation corresponds to that given in reports of these shots.

at Stations 6 and 7 (Figures 3.5 and 3.6). Record 6V30A exhibits the type of behavior expected when the signals from remote sources arrive after the local precursor slap and the main wave slap; however, when this occurs, it is almost impossible to identify the effect of the refracted wave. Similar behavior is evident on the 7V5 and 7V10 records (Figure 3.6); it is likely that the low frequency, small amplitude acceleration oscillations beyond about 0.5 second on these records are due to remote source signals.

It is readily apparent that the remote source disturbances are extremely bothersome when one is integrating acceleration-time records to obtain velocity and displacement versus time. Any criteria which are ordinarily useful for determining the time of zero velocity (Appendix C), may be rendered void by the presence of signals from a remote source.

4.3 ATTENUATION OF GROUND SHOCK WITH DEPTH

By far the major portion of data which may be used to determine the attenuation of ground motion with depth are the measurements on Shot Priscilla. For this reason, observations made on other shots are discussed concurrently with the Shot Priscilla data.

4.3.1 Acceleration (Attenuation with Depth). The attenuation with depth of maximum downward acceleration measured on Priscilla is summarized in Figure 4.5. Both the Stanford Re-

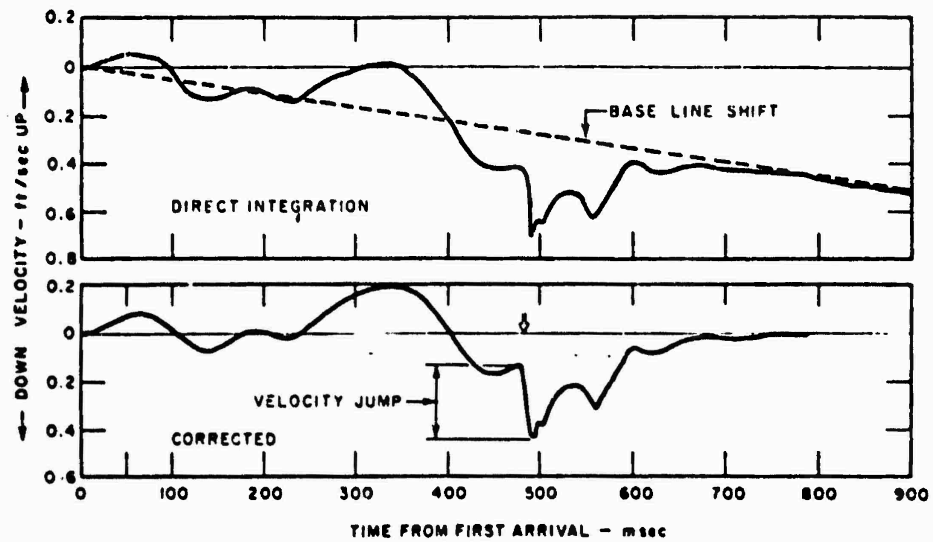


Figure 4.2 Uncorrected and corrected vertical velocities, 5-psi overpressure, Tumbler Shot 1 (arrow shows air-blast arrival).

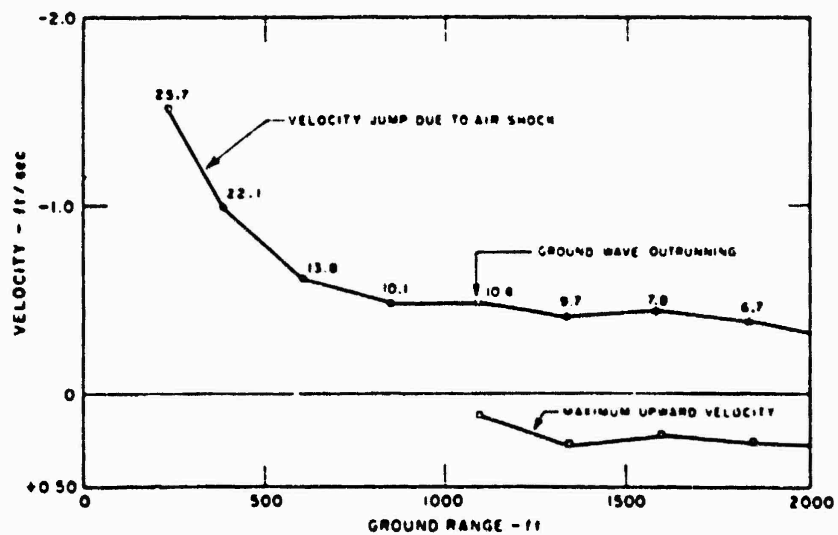


Figure 4.3 Vertical velocity versus ground range, Tumbler Shot 1, 5-foot depth (numbers adjacent to data are overpressures in psi).

search Institute (Project 1.4) and the Sandia (Project 1.5; Reference 15) data are plotted on the figure. Reference to Figure 4.5 shows that between 5- and 10-foot depths the attenuation varies between about 30 to 45 percent, except at the 550- and 650-foot ground ranges where the change in peak acceleration with depth is negligible. There is no apparent explanation for this behavior; it is significant that the Sandia data indicated rather sharp attenuation at greater depths at a range of 650 feet.

Taking the Stanford Research Institute (SRI) and Sandia data together at 750- and 850-foot

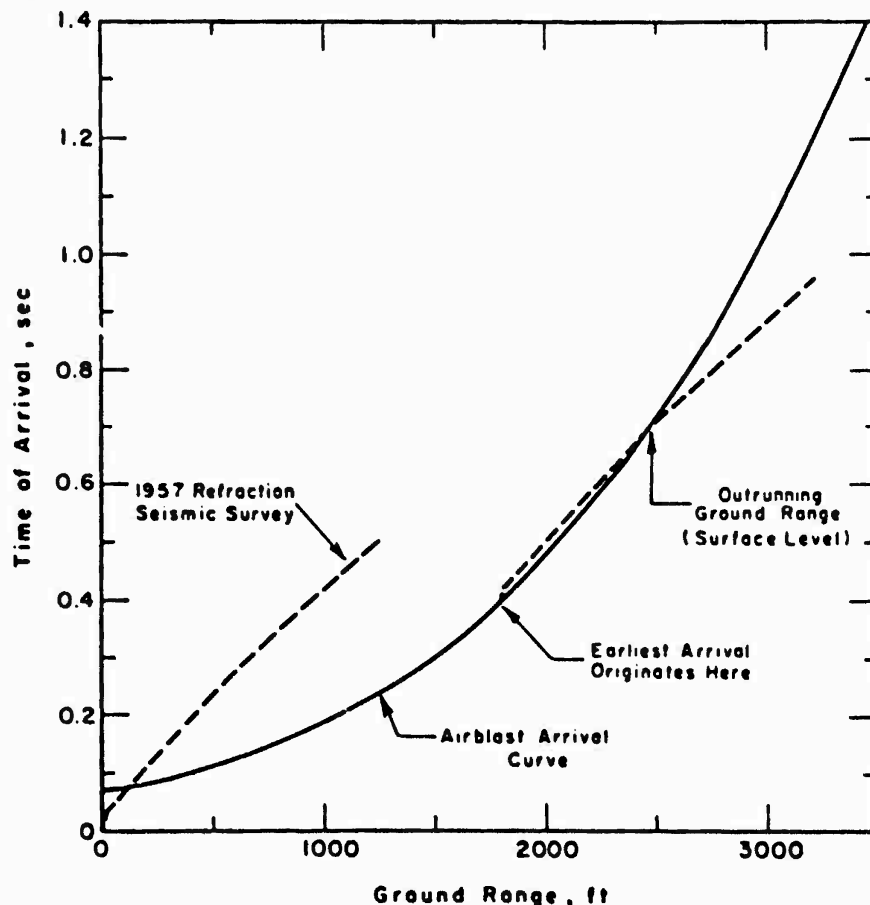


Figure 4.4 Air-blast time of arrival, Shot Priscilla, and seismic soil survey, Frenchman Flat.

ranges, it is evident that the tendency is toward a decided decrease in acceleration attenuation between 10- and 30-foot depths. Wave theory gives the following formula for the particle velocity at the interface between two materials after passage of a step pulse:

$$V = \frac{\sigma}{\rho_1 C_1} \frac{2}{1 + \frac{\rho_2 C_2}{\rho_1 C_1}} \quad (\text{Equation 4.1})$$

Where σ is the stress change across the approaching wave front; $\rho_1 C_1$ is the impedance of the material in front of the interface; and $\rho_2 C_2$ is the impedance beyond the interface. The step velocity across the approaching front is $V = \sigma / \rho_1 C_1$. Therefore, the theory suggests the following: (1) If an accelerometer is located at or near the transition from a hard to a soft mate-

rial, the peak acceleration is increased. (2) If an accelerometer is located at or near the transition from a soft to a hard material, the peak acceleration is decreased.

Reference to the seismic profile measured at Frenchman Flat prior to Priscilla (Section 3.4) indicates that the presence of an underlying soft (lower seismic velocity) layer may explain the behavior at the 750- and 850-foot ranges on Priscilla.

Because the 10-foot deep gage at 1,050-foot ground range was lost, there are no data between 5 and 20 feet at this station. At 1,350-foot range, the SRI and Sandia data agree well and indi-

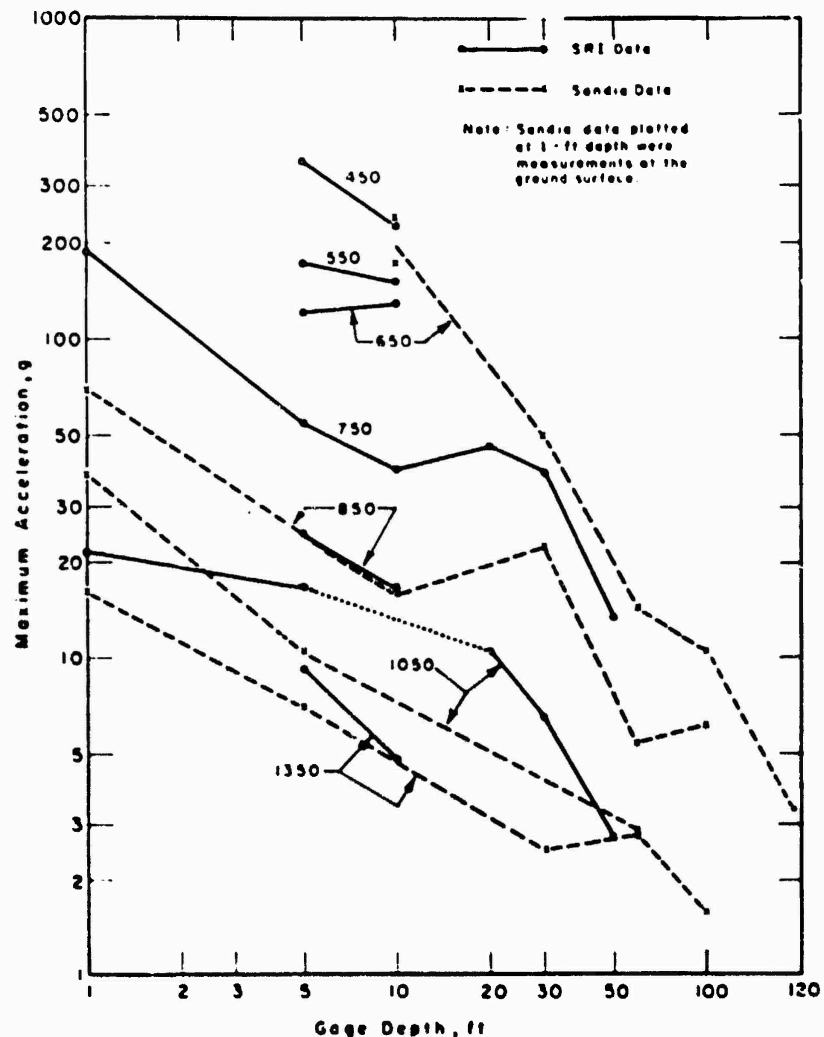


Figure 4.5 Earth acceleration versus depth, Shot Priscilla.

cate no pronounced change in logarithmic attenuation with depth for peak downward acceleration.

To summarize the attenuation of peak outward horizontal acceleration between 10- and 50-foot depths, it is apparent that at the two stations instrumented (750 and 1,050 feet) the attenuation is less than for the corresponding peak downward component; numerically, it is about 40 percent for the outward acceleration and about 80 percent for the downward.

Peak negative accelerations on Priscilla and Jangle S, normalized against the peak acceleration at 10-foot depth, are shown in Figure 4.6. The 10-foot depth was chosen as a basis of comparison since the 5-foot depth was not common to these observations. The dashed lines shown

In the figure are estimates of the confidence limits of the correlation. The identical data are also shown in Figure 4.7 on an exponential plot. The power law plot of Figure 4.6 appears most satisfactory.

The accelerations at 5-foot depth are 1.3 ± 0.2 times those at 10-foot depth. Using this figure, the Jangle S and Sandia Priscilla measurements were adjusted to conform to a normalization against the acceleration at 5-foot depth, Figure 4.8. To complete the acceleration data summary, the Tumbler observations have also been plotted. The same confidence limits are shown as in

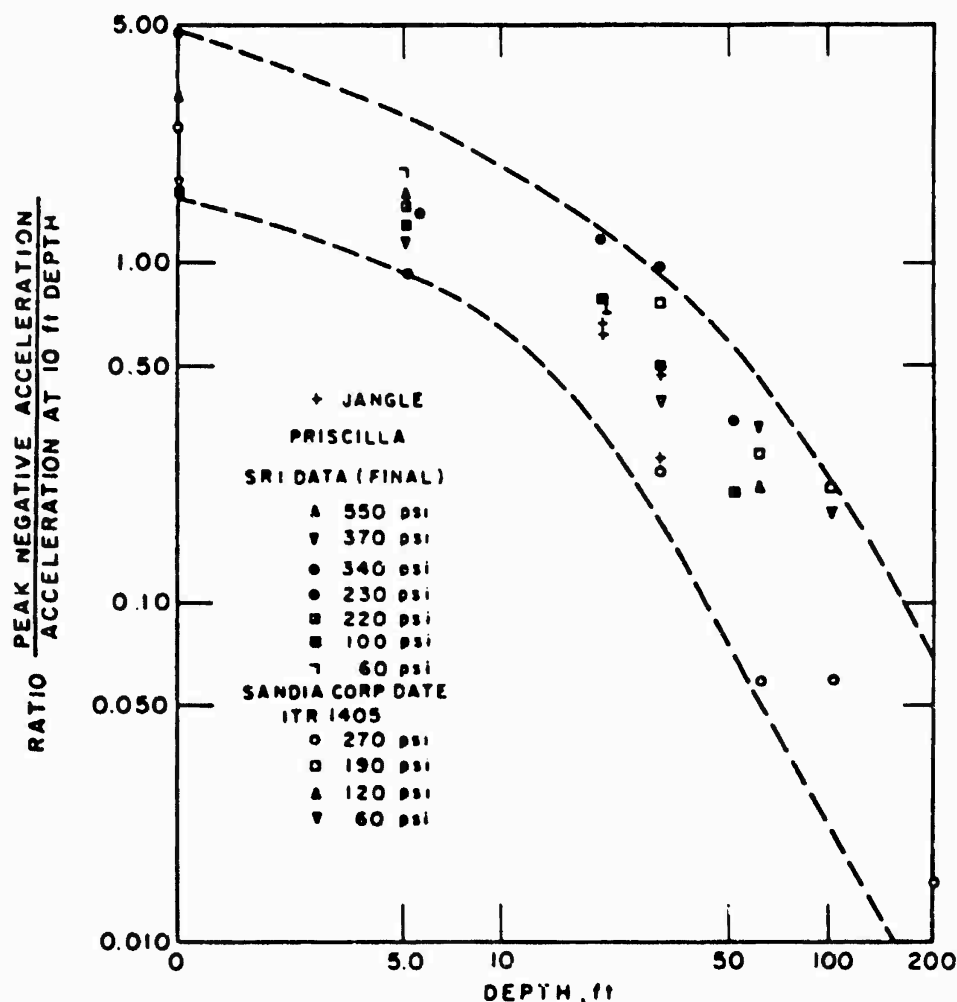


Figure 4.6 Attenuation of vertical acceleration with depth, Nevada Test Site (power law attenuation).

Figure 4.6 and are seen to include 93 percent of all acceleration measurements at the NTS.

Because of the wide variation in acceleration-time wave forms, it is well known that analysis of peak accelerations alone has only limited value. Changes of response with depth will now be discussed using the velocity and displacement data.

4.3.2 Velocity (Attenuation with Depth). In Figure 4.9 are shown the vertical velocity jump at depth referred to the velocity jump at 5-foot depth. This manner of presentation has been chosen to tie into the correlation of Figure 4.27. An exponential decay law appears to represent the data better than a power law decay. There is nothing fundamental about this choice of cor-

dinates; the choice was simply a matter of convenience in providing a straight line extrapolation to greater depths.

Also shown in Figure 4.9 are five datum points from Tumbler. Three of these observations are in excellent agreement with Priscilla data; two are 50 percent larger.

On Priscilla, at the two stations (peak overpressures of 275 and 100 psi) where measurements were obtained down to 50-foot depth, attenuation of peak downward velocity is similar for these overpressure inputs. There is some indication on the figure that the underlying soft layer affected the peak downward velocity at the 100-psi station; however, at 275 psi, the effect observed on the peak acceleration (Figure 4.5) is almost completely eliminated.

The peak outward velocity data from Priscilla shows somewhat less attenuation with depth

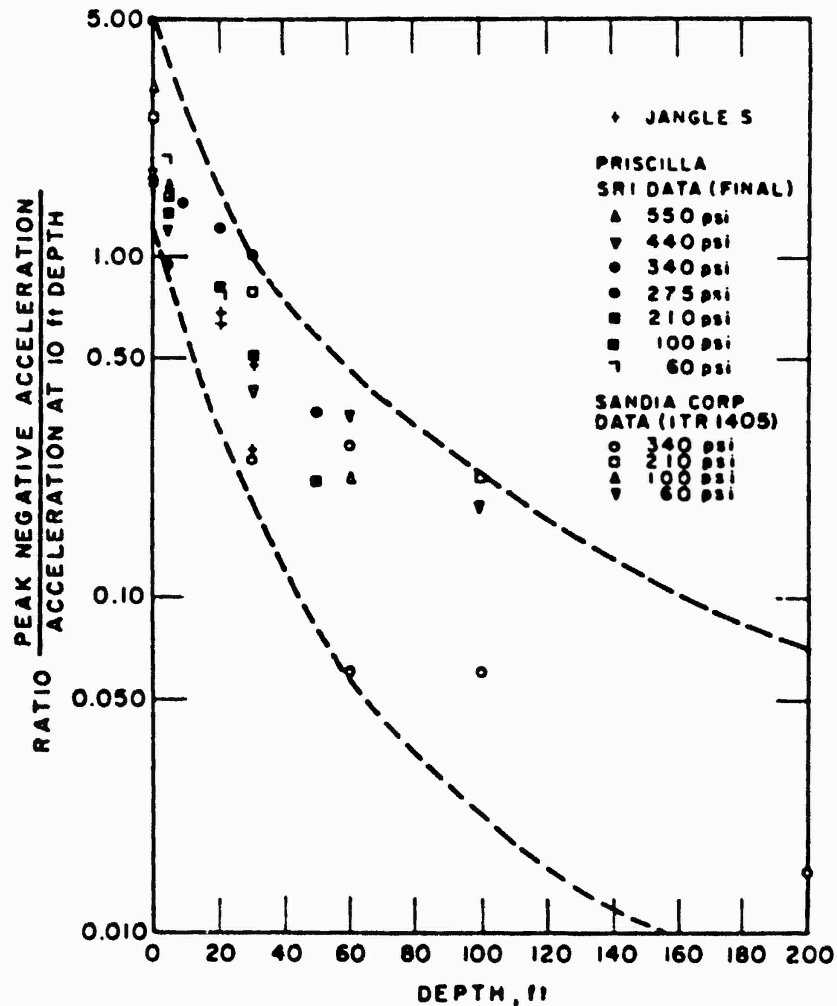


Figure 4.7 Attenuation of vertical acceleration with depth, Nevada Test Site (exponential law attenuation).

than the downward component at 275-psi overpressure; at the larger ground range (100-psi overpressure), the outward velocity at 50-foot depth is actually more than double that measured at 10 feet. This latter effect can be explained on the basis of the influence of ground motion signals from remote sources closer to ground zero.

The vertical velocity-time curve is similar to the overpressure-time curve when the air-blast wave is supersonic. The velocity peak is, however, more rounded and progressively

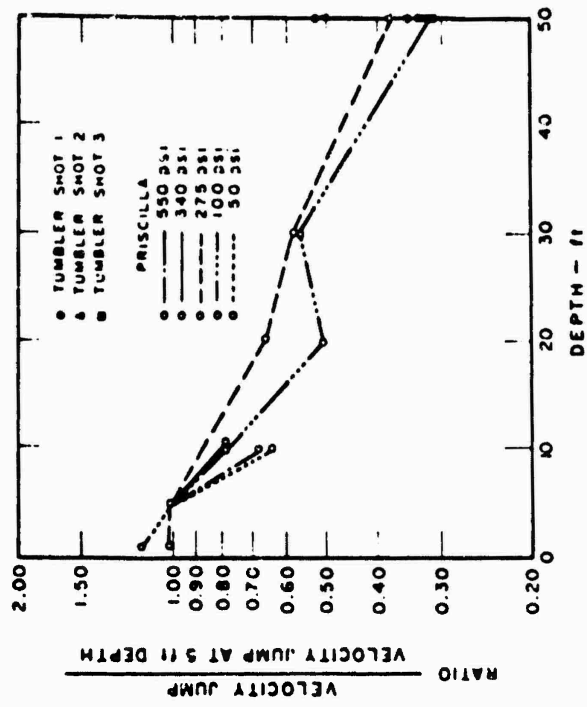


Figure 4.9 Attenuation of downward velocity with depth, Nevada Test Site.

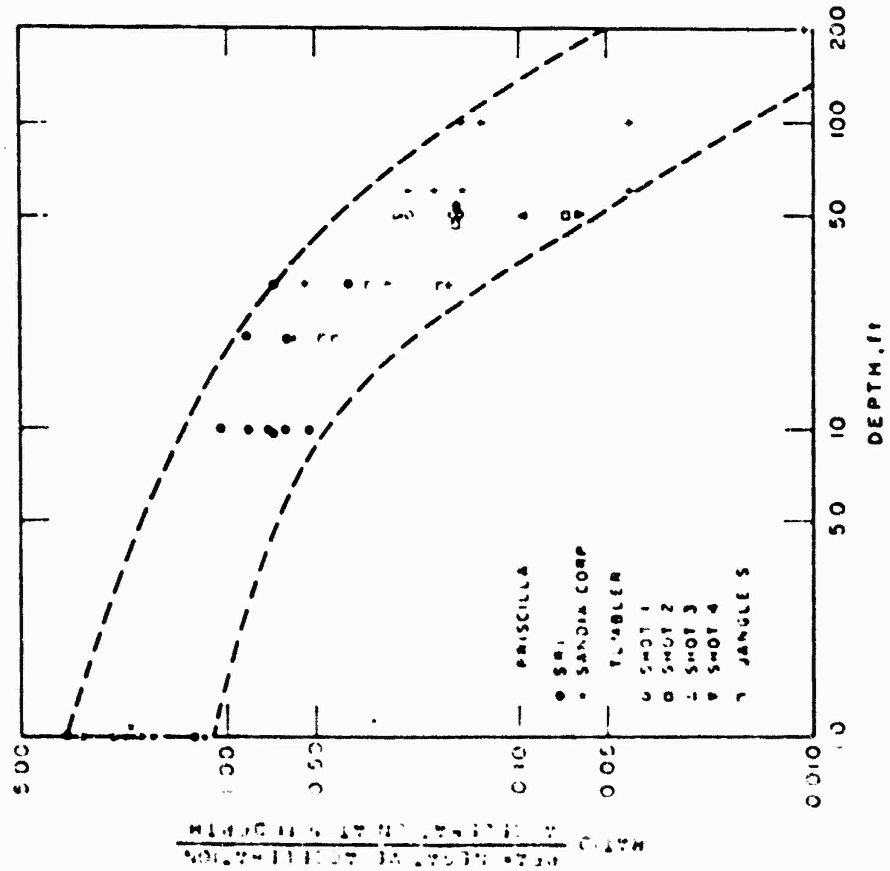


Figure 4.8 Attenuation of vertical acceleration with depth, data normalized against acceleration at 5-foot depth, Nevada Test Site.

lags the wave front by an increasing amount as the depth increases. This lag is the sum of the overpressure rise time plus a time lag due to spreading of the acceleration pulse with depth. For an ideal overpressure wave form (no precursor), the latter time difference would correspond to the rise time of the vertical velocity pulse. The rise time (corresponding to an ideal overpressure wave form) has been deduced from the Stanford Research Institute Priscilla acceleration and velocity data (corrected for transmission time) and is shown in Figure 4.10. The single satisfactory observation on Tumbler is also shown and compares surprisingly well with the Priscilla data.

Still another method has been employed to show how velocity-time traces change with depth. The overpressure-time records and the velocity-time curves were normalized to their peak values; that is, each parameter magnitude was divided by the peak value and the ratio plotted versus time. Figures 4.11 through 4.15 present the results of these normalizations. Also in-

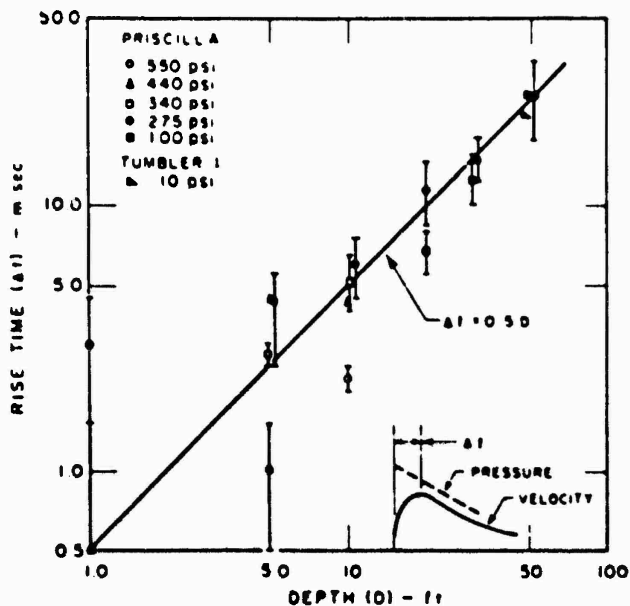


Figure 4.10 Increase in vertical velocity rise time with depth, Frenchman Flat.

cluded in the figures are the normalized earth stress records, which will be discussed in Section 4.3.4. The records are aligned so that the peaks coincide and velocity curves are inverted; in this way easy visual comparisons can be made of rise times and decay times.

Due to the many overpressure gage cable breaks, Figure 4.11 indicates only limited conclusions. It appears that at Stations 1 and 2 (550-psi and 365-psi peak overpressure) the particle velocities at 5-foot depths attain a peak value in approximately the same time as the surface overpressure; however, at 10-foot depth the velocity rise time is about 5 msec longer. At Station 3 (Figure 4.12) the increased rise time for velocity is evident at both 5- and 10-foot depths and the decrease following the peak is close to that displayed by the surface overpressure. Similar behavior is observed at Station 4 (Figures 4.12 and 4.13) down to depths of 10 feet. But below 10 feet the velocity rise time increases significantly. Also the record appears to decay more slowly than does the surface overpressure. At Station 6 (Figures 4.14 and 4.15), where the precursor is well-developed, the rise to peak velocity follows the surface overpressure down to 30-foot depth, but deviates markedly at 50 feet. Also, at this station, one observes the first definite tendency for the velocity to decay more rapidly than the surface overpressure-time measurement. At a depth of 50 feet (Figure 4.15), the velocity rise time is about 20 msec longer than for the overpressure, which represents the only significant departure from following the input at Station 6; here again, however, the velocity decay is more severe than the over-

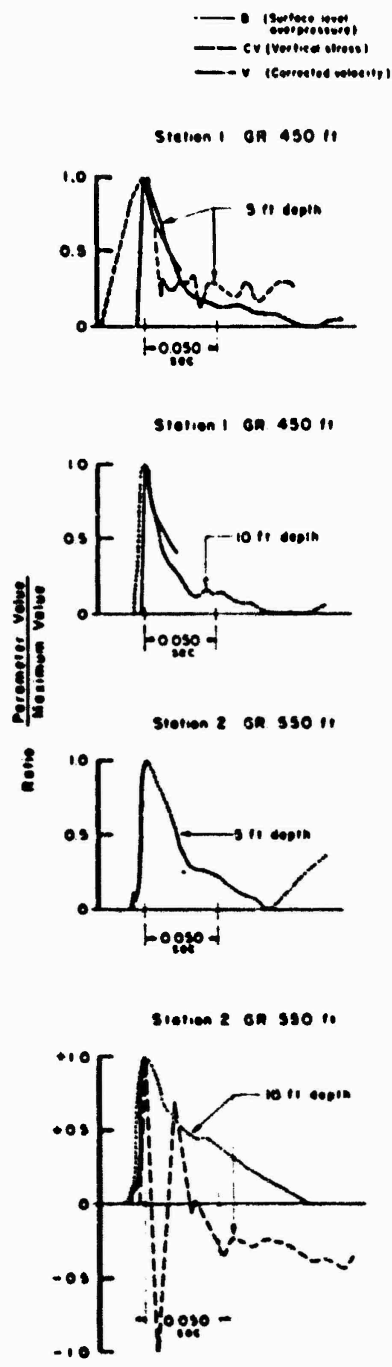


Figure 4.11 Overpressure, particle velocity, earth stress, normalized to maximum value, Stations 1 through 3, Shot Priscilla.

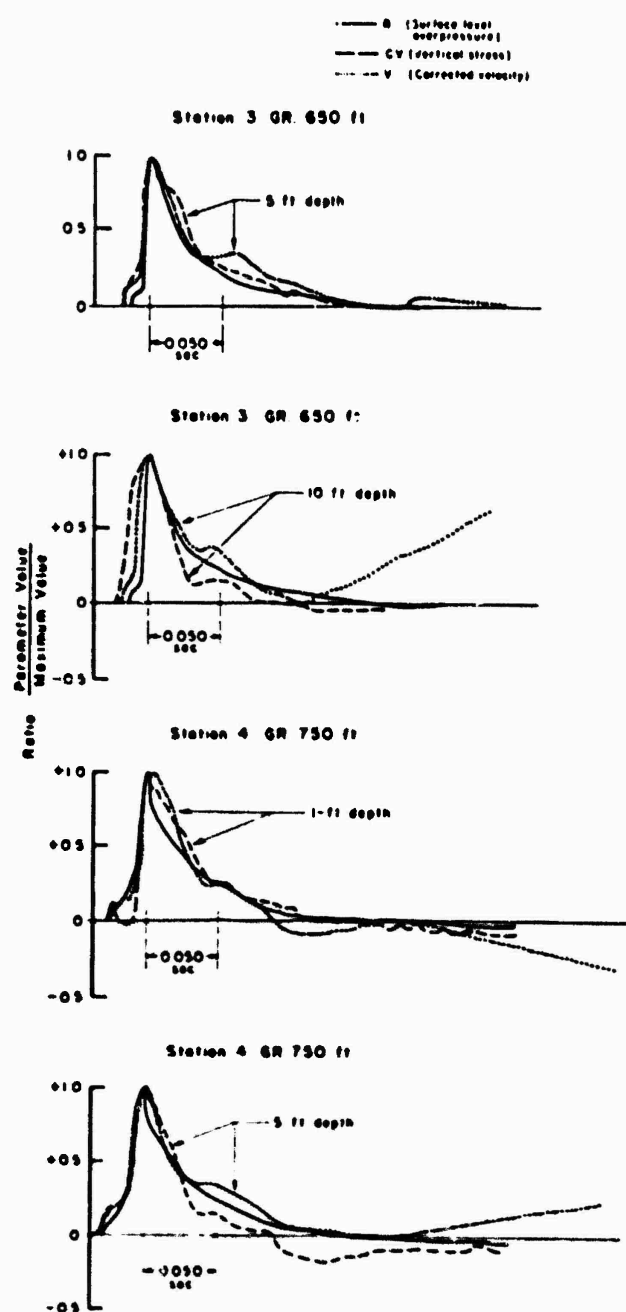


Figure 4.12 Overpressure, particle velocity, earth stress, normalized to maximum value, Stations 3 and 4, Shot Priscilla.

pressure decay. Station 7 (Figure 4.15) shows similar behavior to Station 6, there is only a small increase in velocity rise time at 10-foot depth.

4.3.3 Displacement (Attenuation with Depth). The integrations of the Stanford Research Institute acceleration data are at present the only displacement data available for Priscilla. These data are shown in Figure 4.16, normalized against the peak displacement at 5-foot depth. Additional data will be available for correlation when Sandia Corporation acceleration and long-span displacement gage data have been reduced (Reference 15).

The attenuation of displacement for all ground ranges except the 100-psi station approximates the attenuation of velocity. Figure 4.9. At the 100-psi station the displacements below 5-foot depth are larger than would be expected from observations at the other stations. From the character of the acceleration records, it is suspected that a refracted ground wave was superimposed on the direct motion induced by the main air-blast wave. Due to the direct motion induced by the precursor, it is difficult to clarify this point since outrunning cannot be definitely established. Since outrunning occurs at depth prior to outrunning at the surface, ground wave interference is not unlikely and would explain the greater displacements, cf., Figure 4.33, Tumbler 1. The Project 1.5 displacement data expected on Priscilla may clarify this point.

It should be noted that the displacement-time plots are probably not reliable beyond the time of peak value. The truth of this statement was demonstrated when, for the Project 3.5 data analysis (Reference 16) it was necessary to attempt correlation between the integrated displacements and scratch gages attached to a buried structure. Reading the acceleration-time records out to much later times and using the scratch gage data as a guide to proper corrections to be applied, it was found that the vertical displacements behaved differently from those shown in Figures 3.14 through 3.17. The primary difference was that, after reaching about the same peak value, the Project 3.5 integrations decreased steadily to almost zero displacement beyond 1.0 second. The procedure used for Project 3.5 illustrates the distinct advantage of having an independent measurement with which to guide the corrections.

4.3.4 Stress (Attenuation with Depth). The maximum vertical earth stress is plotted versus gage depth in Figure 4.17. For each gage station the curve has been joined to the maximum surface overpressure datum point (plotted on the figure at 1-foot depth). Maximum stress, as determined by Carlson-type gages on Project 1.7, is also plotted for the 1,050-foot ground range. There is some doubt about the validity of comparing Project 1.4 stress measurements with those from Project 1.7. The latter gages were immersed in a large back-filled hole and the 20-foot deep gage was positioned on the bottom of the excavation.

The attenuation of maximum vertical stress between the surface and 5 feet is not severe and is greatest at the first and last station instrumented; the attenuation at these shallow depths is probably strongly a function of the duration of the overpressure input pulse.

The marked increase in stress at 50 feet for both the 750- and 1,050-foot stations is unexpected; however, there is little reason to expect these larger values of stress to be caused by over-registration of the gage. On the contrary there are many more situations which could cause under-registration of the Carlson stress gage than could cause serious over-registration.

The pattern of attenuation of vertical stress with depth between 0 and 30 feet is in general agreement with the attenuation equation proposed on the basis of Upshot-Knothole data (Reference 1), which predicts a halving of stress for each 10-foot increase in depth. Point by point, the data of Figure 4.17 depart severely from this attenuation equation. However, the fit of data is only slightly poorer than the original data on which the equation is based. The 50-foot stresses, however, tend to deny the validity of this attenuation equation.

Referring to Project 1.4 and Project 1.7 results plotted on Figure 4.17, the large discrepancy between the maximum stress at 5 and 10 feet, measured at the two adjacent locations, is readily apparent. Since no systematic behavior is observed at the two locations, it is difficult to reason that the differences are due only to the different planting procedures used by the two projects (also see wave forms of Figure 3.23). Since these locations represent wide variations in stress

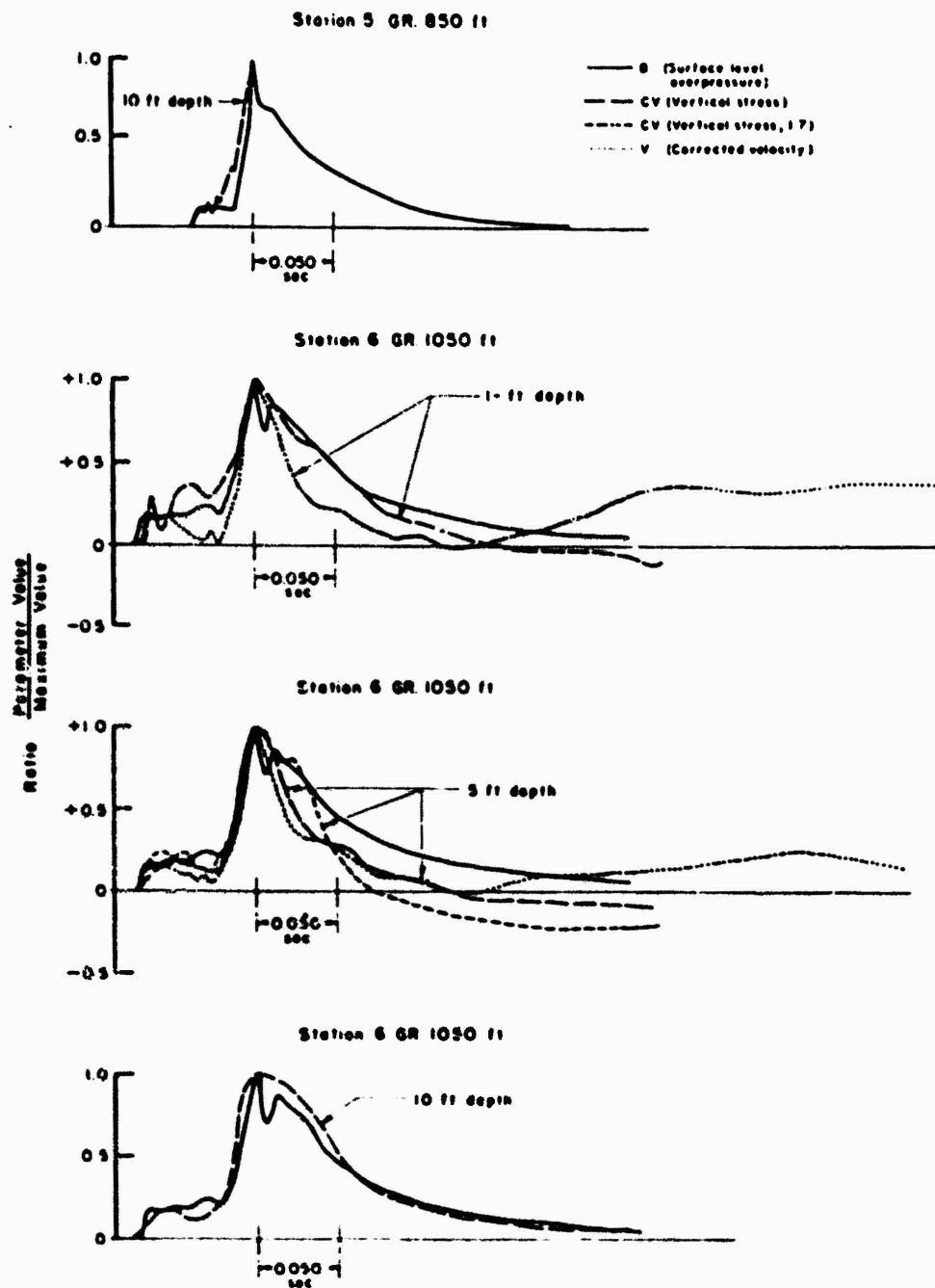


Figure 4.14 Overpressure, particle velocity, earth stress, normalized to maximum value, Stations 5 and 6, Shot Priscilla.

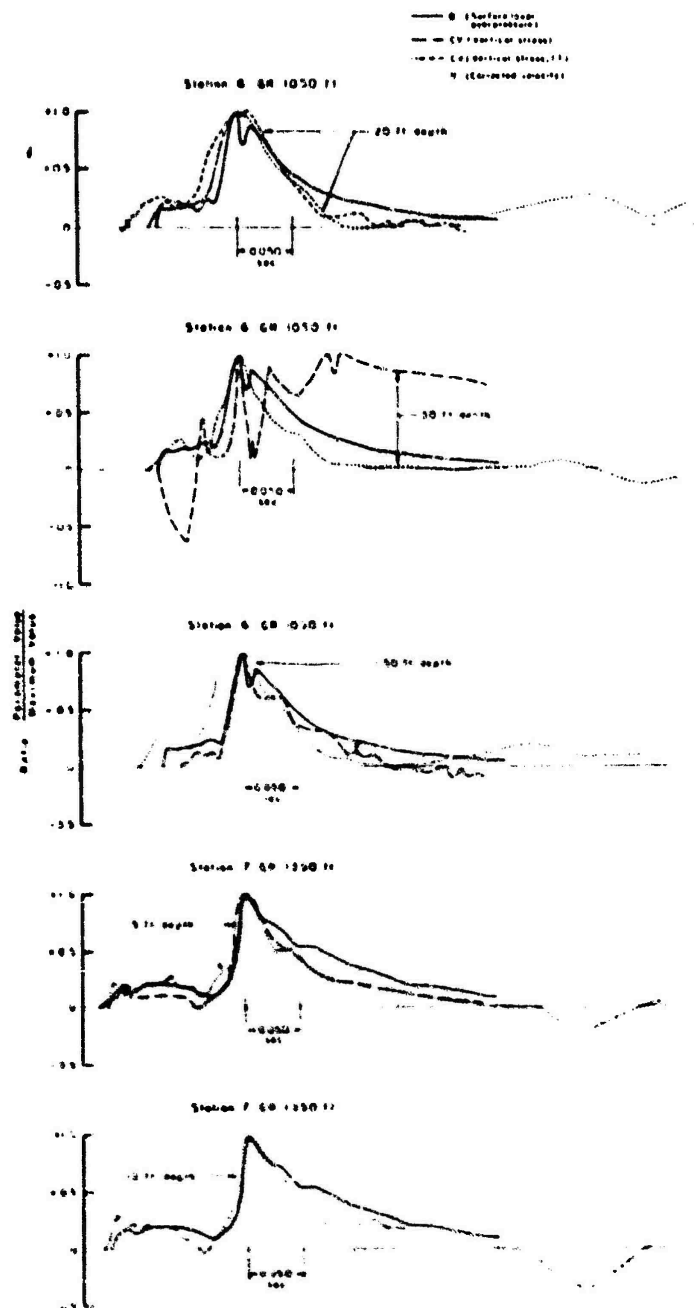


Figure 4.15 Overpressure, particle velocity, earth stress, normalized to maximum value, Stations 6 and 7, Shot Priscilla.

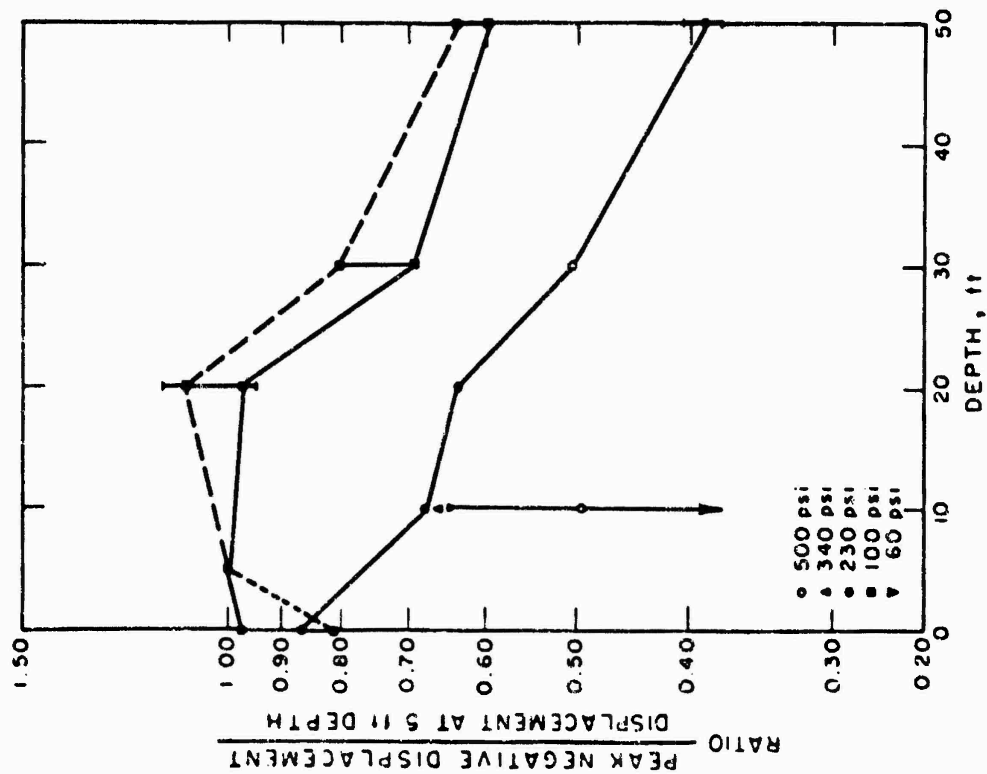


Figure 4.16 Attenuation of vertical displacement, Frenchman Flat.

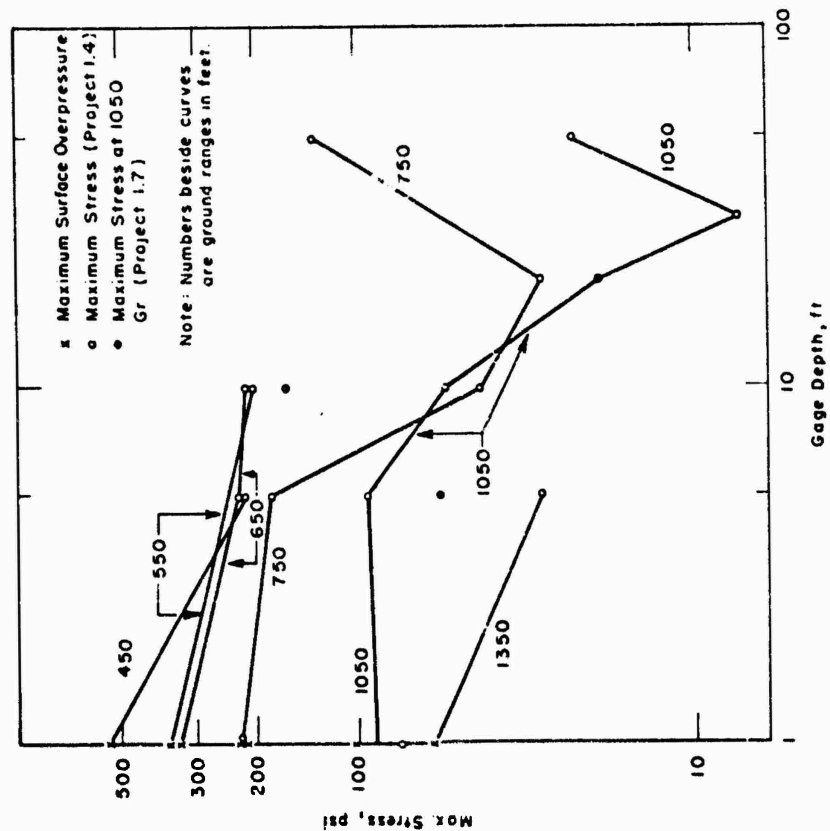


Figure 4.17 Maximum earth stress versus gage depth, Shot Priscilla.

response, one is not very encouraged about the usefulness of a limited number of Carlson gage results in predicting ground motion and/or structure response.

One cause of decay of peak stress with depth is the finite duration of the blast wave on Shot Priscilla. An inspection of the air-blast wave forms shows that the duration of the main peak of the blast wave was relatively short. Measuring between points of arrival and one half the peak pressure, this was about 28 msec at 750 feet and 55 msec at 1,050 feet. By rough calculations of trace velocity, these correspond to a wave length of half-peak pressure of only about 100 to 125 feet. This is certainly not long enough to be considered infinite compared with gage depths of 50 or even of 20 feet. There is reason to believe that, had the duration been much longer, the stresses measured at 20 and 30 feet would have more nearly approached the peak air-blast pressure.

There are several ways of looking at the effect of changing soil characteristics upon the attenuation with depth of maximum vertical earth stress.

One is to assume initially that the gages record true free-field phenomena and then look at the effect of the hard and soft layers upon wave reflection patterns. By so doing, one can give a possible explanation for an increase (i.e., negative attenuation) in response with depth. However, this argument applies only if the duration of the peak overpressure is short compared with the time required for the wave to be reflected once again at the earth's surface. Moreover, it is improbable that the high measured stresses recorded at 50 feet could be explained on this basis; the stress-time curves are relatively flat in the region of maximum stress and give no indication of reflections. Furthermore, the Project 1.7 20-foot gage was at the bottom of the backfill and did not exhibit an increase in stress.

Another way to approach the problem is to consider it statically and to surmise how the load at the surface was carried down through the soil. During the backfilling of the deep holes at Stations 4 and 6, a geophone was planted in each hole near the wall at a depth of 50 feet, and measurements were made of the travel time from the surface to each geophone. These travel times correspond to average velocities from 0 to 50 feet of $1,390 \pm 40$ ft/sec and $1,450 \pm 60$ ft/sec, compared with 2,060 ft/sec from Shot Points 1, 2, and 3, (Figure 2.6). These data imply that the backfill failed to reach the original modulus and that the effect of this condition reached somewhat beyond the edge of the hole.

On the assumption that the stress gages were placed in a medium of uniformly low elastic modulus, one would expect the measured stresses to be lower than those of the free field, with the stress differences largest where differences in elastic modulus (or seismic velocity) are largest. This conclusion is based on the premise that the boundary between lower and higher elastic modulus media can carry vertical shear. This assumption is good for the undisturbed medium and probably satisfactory even at the backfill-hole wall boundary. Under loading, the two media will undergo much the same strain; hence, the stress will be lower in the media of lesser modulus.

Note, however, that the local seismic velocity at 40- to 50-foot depths in the free field (Figures 3.25 and 3.27) is only slightly higher than that which appears characteristic of the average at the 750- and 1,050-foot stations. This fact may offer a possible explanation, in the light of the above discussion, of the higher measured stresses at both 50-foot depths. It can be concluded that the 50-foot stresses are more indicative of the free-field stresses and that those measured at intermediate depths were depressed due to the lowered modulus.

Still a third way to view the problem of explaining the stress results is to take a somewhat cynical approach. One can say that the backfill in the niche around the stress gages at 20- and 30-foot depths was not well compressed, and hence these gages saw only a minute stress.

To summarize, it is probable that all these effects are present in varying degrees of severity. Suffice it to say that it is difficult to determine the validity of the free-field earth stress results obtained by Project 1.4 on Priscilla. The control of backfill operations during Priscilla was considered optimum and extraordinary care was taken in placement of Carlson gages; still the stress measurements appear inconsistent internally and hence leave much to be desired. It is believed at this time that the present concept and method of earth stress measurement may be inadequate and misleading. Alternative methods cannot as yet be offered, except that probably

stress must be derived from other primary measurements such as strain and acceleration, which are more independent of hole size and the character of the backfill.

Reference to the normalized records of Figures 4.11 through 4.15, reveals some interesting facts about the stress-time wave form changes with depth. At Station 3 (Figure 4.12), the rise time to peak stress increases noticeably from 5- to 10-foot depths; however, the decay of stress at both depths, is comparable with the decay of the overpressure input. Figures 4.12 and 4.13 include the results at Station 4; here no significant increase in stress rise time is noted at 1-, 5-, and 10-foot depths. The stress records at 20- and 50-foot depths deviate markedly from the input overpressure-time wave form; also, they do not resemble each other.

At Station 6 (Figures 4.14 and 4.15), the stress rise time and decay follows the overpressure input quite closely to depths of 10 feet. At 20 feet, the rise time is noticeably longer for the stress, whereas at 30 feet the stress record is strange, and at 50 feet the stress response to the precursor portion of the input wave is depressed relative to the peak. The one comparison possible at Station 7 reveals that at 5-foot depth the stress record followed the overpressure input quite faithfully.

4.3.5 Strain (Attenuation with Depth). Due to the full or partial failure of eight of the ten short-span strain gages, the strain-time data of Project 1.4 were rather meager. On some of the partial records it was possible to identify the maximum vertical strain recorded at the gage station; thus, the measurements yielded a total of five peak strain values, three at 750-foot ground range and two at 1,050 feet.

In addition to the strain gage measurements, it was possible to compute the average vertical strain from the integrated accelerations (i.e., displacement-time plots). Using the strain-time results as a guide to give the time of maximum strain; these computations were carried out and are listed in Table 4.2. The results are plotted in Figure 4.14 and show that the calculated maximum average strains are not inconsistent with the few strain-time measurements obtained. This takes the form of an independent check and leads to more confidence in the manner in which the acceleration-time records were integrated.

The data of Figure 4.18 indicate that at the 750-foot station (275 psi maximum overpressure) the peak earth strain had a decided attenuation with depth, with a pronounced decrease between 1 and 30 feet below the ground surface; at larger depths (to 50 feet), the maximum vertical strain appeared to level off at about 5 parts per thousand. On the other hand, the data obtained at 1,050 feet (100-psi overpressure level) showed practically no change in maximum vertical strain with increasing depth; in fact, there was even a slight indication of larger (negative attenuation) strain near the 30-foot depth. The reason for this difference in behavior was probably traceable to the character of the input overpressure-time at the two stations; this is discussed in more detail in Section 4.4.4.

It is noted that the Station 4 strain measurement at 5-foot depth (4SV5A) had a much smaller peak magnitude than indicated by the computations using integrated accelerations. Also, the 5-foot measurement was even smaller at maxima than was the 10-foot strain at the same station (4SV10). Another pertinent point can be made upon inspection of the 4SV5 gage record (Figure 3.24). The record indicates that although the overpressure input increased from a precursor pressure of about 25 psi to a peak pressure exceeding 225 psi, a nine-fold increase, the strain merely doubled. The 4SV50A and 6SV50 strain records are examples of characteristic behavior in this regard.

It must be concluded, therefore, that the 4SV5 strain measurement was, for some reason, erroneous; the true peak strain at this position was significantly larger than was recorded.

4.4 GROUND SHOCK AND OVERPRESSURE

4.4.1 Acceleration (and Overpressure). To compare accelerations on the basis of air-blast input, the ratio of peak acceleration to peak overpressure versus overpressure was plotted.

Figure 4.19 summarizes all 5-foot depth vertical acceleration observations in Frenchman

Flat. Also plotted are the acceleration-overpressure ratios for the Priscilla and Upshot-Knothole Shot 10 precursor. The measured overpressures at Priscilla Stations 2 and 4 appeared low when compared with pressure data of previous shots. At Station 2, a cable break occurred prior to recording of the peak overpressure. The source of the apparently low pressure at Station 4 has not been found. Both the as-read and smoothed data points are indicated. The accelerations induced by the main air-blast wave decayed rapidly on Priscilla due to the formation of the precursor and also due to the distance effect (Tumbler data discussed below). Taking this into account, the Upshot-Knothole Shot 10 Type 1 overpressure wave form accelerations were in agreement with those of Priscilla. The single Upshot-Knothole Shot 9 observation appeared

TABLE 4.2 MAXIMUM STRAIN, SHOT PRISCILLA

Gage Code	Computations				Measurements		
	Depth	Time, t_s	Displ at t_s	Aver Max Strain	Gage Code	Peak Strain	Time of Peak
	ft	sec	ft	ppk*		ppk*	sec
4V1	1	0.193	0.390	23.8	—	—	—
4V5	5	—	0.295	—	—	—	—
4V1	1	0.195	0.411	26.6	—	—	—
4V10	10	—	0.171	—	4SV5	8.8	0.195
4V5	5	0.205	0.409	30.0	—	—	—
4V10	10	—	0.259	—	4SV10	13.7	0.215
4V10	10	0.225	0.365	11.2	—	—	—
4V20	20	—	0.253	—	—	—	—
4V20	20	0.235	0.304	7.0	—	—	—
4V30	30	—	0.234	—	—	—	—
4V30	30	0.240	0.254	6.3	—	—	—
4V50	50	—	0.127	—	4SV50	7.8	0.249
6V1	1	0.284	0.147	5.8	—	—	—
6V5	5	—	0.124	—	—	—	—
6V5	5	0.290	0.156	5.1	—	—	—
6V20	20	—	0.080	—	—	—	—
6V20	20	0.300	0.122	6.5	—	—	—
6V30	30	—	0.037	—	6SV30	5.9	0.304
6V30	30	0.317	0.110	2.5	—	—	—
6V50	50	—	0.061	—	6SV50	3.0	0.330

* Parts per thousand.

lower than would be expected from Tumbler Shot 1, and the Priscilla precursor accelerations were larger by about the same amount. In general, the accelerations appeared to be larger in the Frenchman Flat area than in the Yucca area, not however by an amount which was significant compared with the scatter of data.

Of some interest were the peak acceleration-overpressure ratios obtained from the horizontal (positive outward) acceleration observations at 10- and 50-foot depths. At Station 4, the ratios were about one third those corresponding to the vertical accelerations and at Station 6, although the 10-foot depth vertical gage was lost, the 50-foot data indicated that the horizontal and vertical components were approximately equal.

The ratio of peak negative acceleration to peak overpressure versus overpressure is plotted in Figure 4.20 for Tumbler Shots 1 and 2 (References 2, 17 and 18). The ratio appears to be fairly independent of overpressure. The heights of burst of both Shot 1 and Shot 2 were sufficiently high that no precursor formed and all overpressure wave forms were nearly ideal. Since the yields were nearly identical, it must be concluded that the two to one difference in acceleration-pressure ratio must result from differences in soil properties between the Frenchman Flat and Yucca test areas.

Figure 4.21 compares the three Tumbler shots detonated over the same portion of the Yucca

test area. One first notes the marked reduction in the Shot 4 acceleration-pressure ratio at 10 psi. The smaller than expected accelerations were the result of the nonideal precursor wave forms. The Type 4 overpressure wave form has the largest rise time and hence induces the least ground acceleration. As soon as the wave forms return to near ideal (Type 7), the acceleration assumes its normal value. Taking the effect of overpressure wave form into consideration, the effect of device yield if any, does not appear to be discernible within the scatter of data.

In Figures 4.20 and 4.21 there is an obvious tendency for the acceleration-pressure ratio to increase at both ends of the pressure scale. When the data of Figure 4.21 are plotted against ground range as in Figure 4.22, there appears to be a fair correlation with distance. This characteristic may be due to changes in soil properties or due to shock wave parameters not

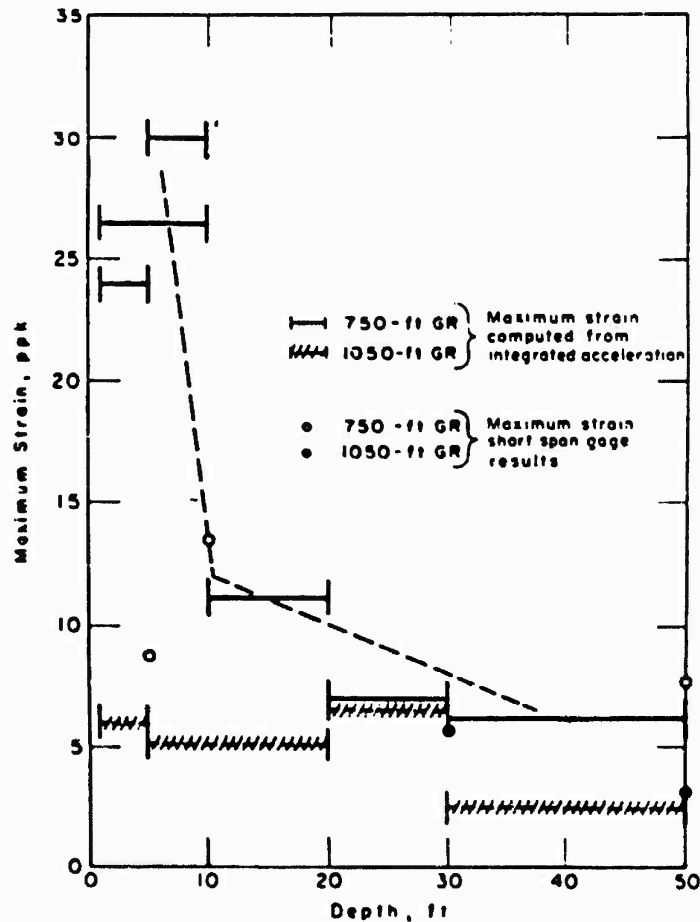


Figure 4.18 Earth strain versus depth, Shot Priscilla.

considered, e.g., shock velocity and/or wave front curvature. The increase in acceleration ratio at close-in stations may possibly be connected with the latter since the same tendency is observed on Tumbler Shot 1 (Figure 4.20) and on the two near ideal wave forms on Priscilla (Figure 4.19). This point cannot be clarified at the present time due to insufficient theoretical investigation and without more detailed study of soil properties in the Yucca area.

The remaining set of observations at 5-foot depth are the vertical acceleration data of Jangle HE-4 (Reference 4), 2,560 pounds of TNT detonated at the ground surface. The acceleration-overpressure ratios are plotted in Figure 4.23 and are consistent with previous observations.

Jangle (Reference 19) vertical acceleration data are shown in Figure 4.24. The scatter of

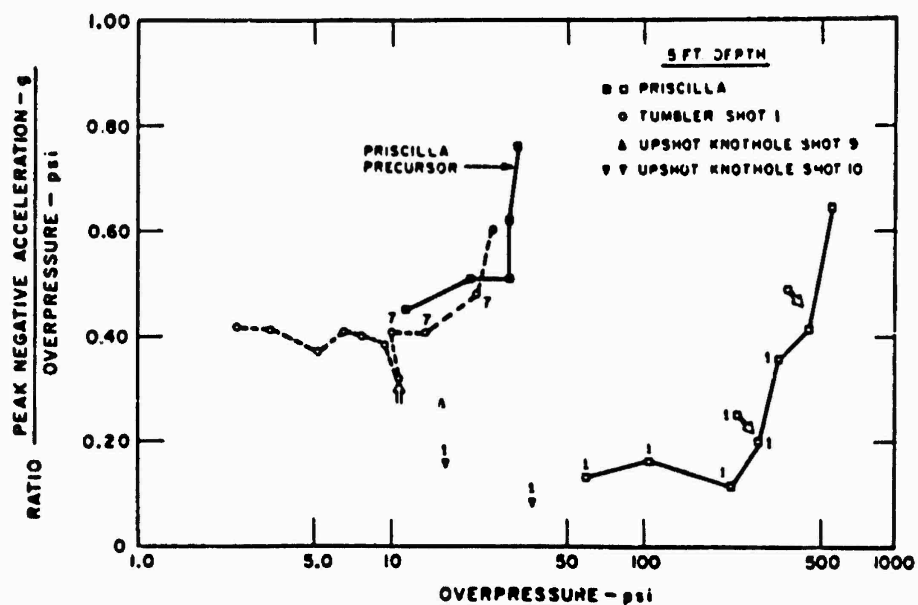


Figure 4.19 Vertical acceleration, Frenchman Flat, 5-foot depth (numbers indicate overpressure wave form).

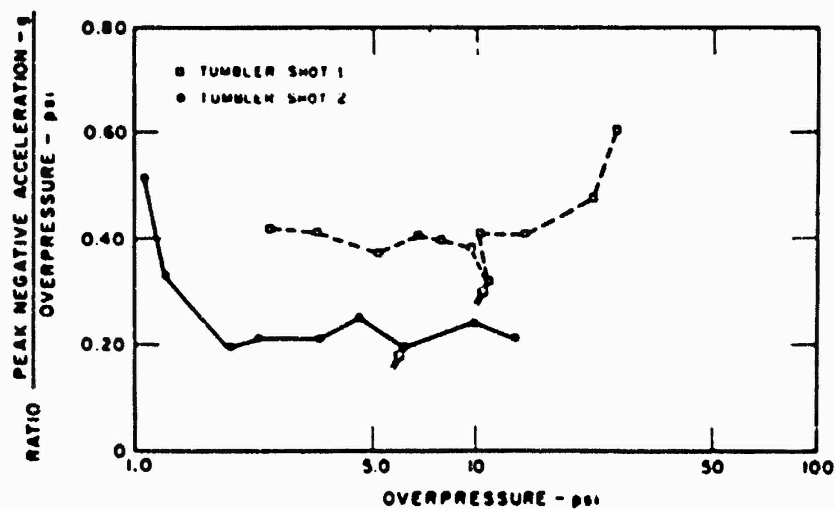


Figure 4.20 Vertical acceleration, Tumbler Shots 1 and 2, 5-foot depth (arrow points to first ground wave outrunning wave form).

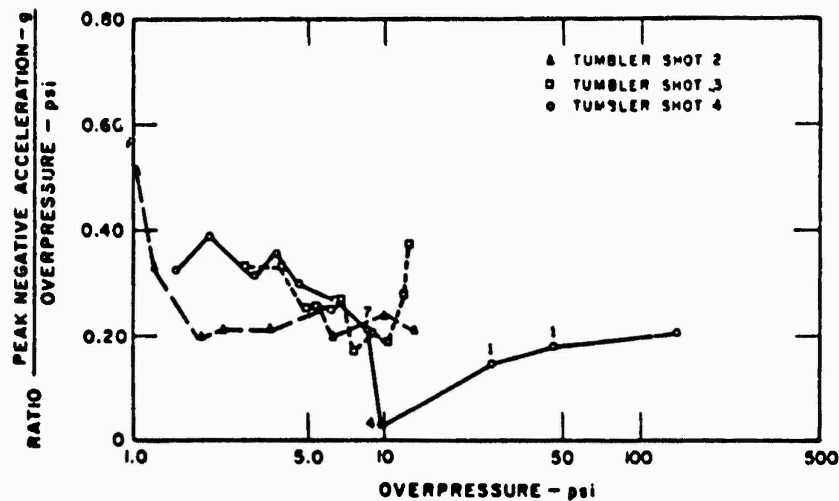


Figure 4.21 Vertical acceleration, Tumbler Shots 2, 3, and 4, 5-foot depth (numbers adjacent to data indicate overpressure wave form).

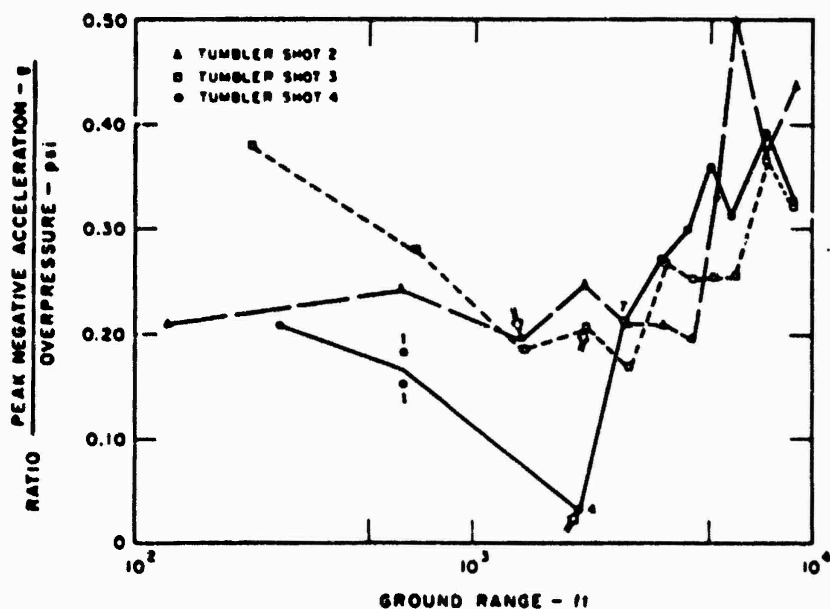


Figure 4.22 Vertical acceleration at 5-foot depth versus ground range, Tumbler (arrows point to first ground wave outrunning wave form; numbers indicate overpressure wave form).

these data is much greater than on any of the previous experiments discussed, which makes analysis of these data rather tenuous. The attenuation indicated by the Jangle S 10-foot data appears to be greater than that observed on Tumbler or Priscilla, as was discussed earlier.

The vertical acceleration data of Project Mole (Reference 3) aboveground detonations are shown in Figures 4.25 and 4.26. Nevada sand and gravel mix corresponds to the soil in the Jangle S, HE-4 test area. The Utah dry clay site was located at Dugway Proving Ground, Utah.

In Figure 4.25, although the scatter of data is large, (note that acceleration-pressure ratios are plotted on logarithmic scales), no systematic variation with height of burst is to be found. Secondly, the range over which the acceleration-overpressure ratio extends is an order of magnitude large, i. e., the ratio is more dependent on overpressure (or ground range) than that of the large HE (Jangle HE-4) or nuclear (Jangle S) detonations in the same area. This trend toward higher ratios at the extreme ground ranges is observed however in Tumbler Shots 2, 3, and 4 and may be connected with outrunning of the ground wave.

In Figure 4.26 the dependence on overpressure is not as pronounced, and the accelerations appear to be a factor of two larger than those of Figure 4.25 for pressures greater than 30 psi.

4.4.2 Velocity (and Overpressure). Subsequent to outrunning of the ground wave, the velocity-jump overpressure ratio increases with decreasing overpressure (or increasing ground range). This observation is in conformity with elastic theory (private communication with J. K. Wright, AWRE). Prior to outrunning, the ratio should be independent of pressure. All 5-foot depth peak velocity data, where the air blast was superseismic, are shown in Figure 4.27; 80 percent of the data fall within a velocity-pressure ratio range of 0.04 to 0.06. There appears to be no systematic variation with either yield, overpressure level or wave form, or test area. The last conclusion is at variance with the behavior of the acceleration data.

The data shown in Figure 4.27 may be compared with the theoretical result,

$$\frac{U_V}{P} = \frac{1}{\rho C_L} = \frac{32.2 \times 144}{90 \times 1,600} = 0.032 \frac{\text{ft/sec}}{\text{psi}}$$

Where the soil density is taken at 90 pcf, and from Figure 3.30, C_L at 5-foot depth is 1,600 ft/sec. The agreement between theory and experiment appears extremely good, especially if one recognizes the approximate nature of the theoretical result. Secondly, the true seismic velocity in the first 5 feet is difficult to measure accurately: the estimated error is of the order of 30 percent. The large seismic velocity gradient also presents both a theoretical and practical problem.

The velocity of propagation of ground motion may be determined directly during an experiment from the arrival time of ground motion and the air blast arrival over the gage location. This calculation was made for Priscilla using arrival times at 10-foot depth. These calculations, Table 4.3, lead to the conclusion that the average propagation velocity of ground motion between the surface and 10-foot depth is less than 1,000 ft/sec. If the average velocity of Table 4.3 is used in the previous calculation one arrives at the result,

$$\frac{U_V}{P} = 0.060$$

The fact that the high amplitude stress wave propagates slower than the seismic wave is not unexpected in view of the theoretical treatment of von Karman and Duwez (Reference 20) of wave propagation in plastic solids. However, additional treatment of this observation is required before definite conclusions can be derived.

Velocity-jump-overpressure ratios for Tumbler Shots 1 through 4 are shown in Figures 4.28 through 4.31. All data displayed in Figure 4.28 have been reintegrated as outlined in Appendix C. Data in Figures 4.25 through 4.31 have been reintegrated only for those stations where the blast wave is superseismic (the first station at which the ground wave outruns is also included).

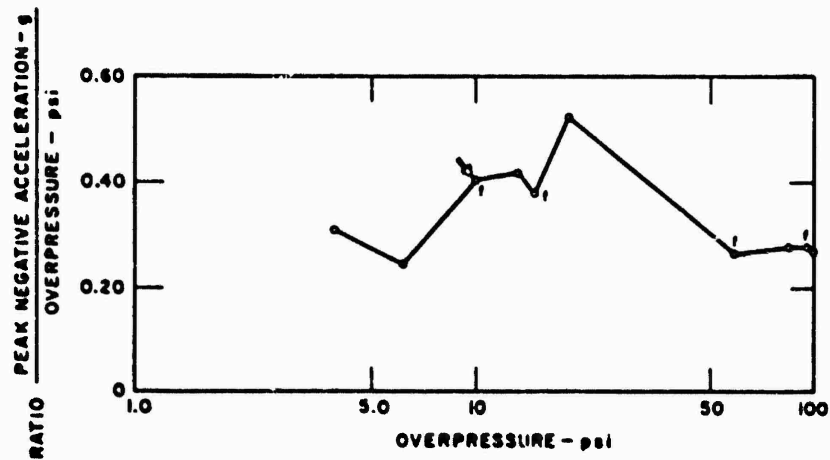


Figure 4.23 Vertical acceleration, Jangle HE-4, 5-foot depth (f indicates interpolated overpressure data).

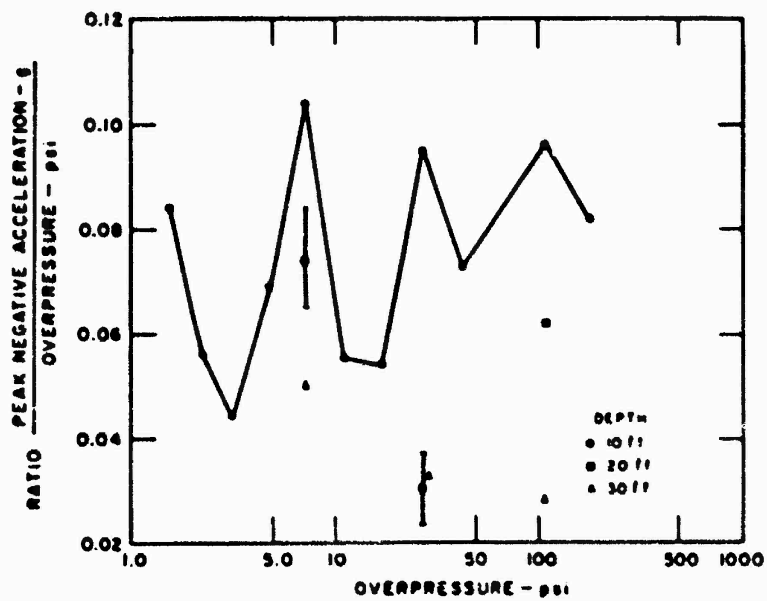


Figure 4.24 Vertical acceleration, Jangle S.

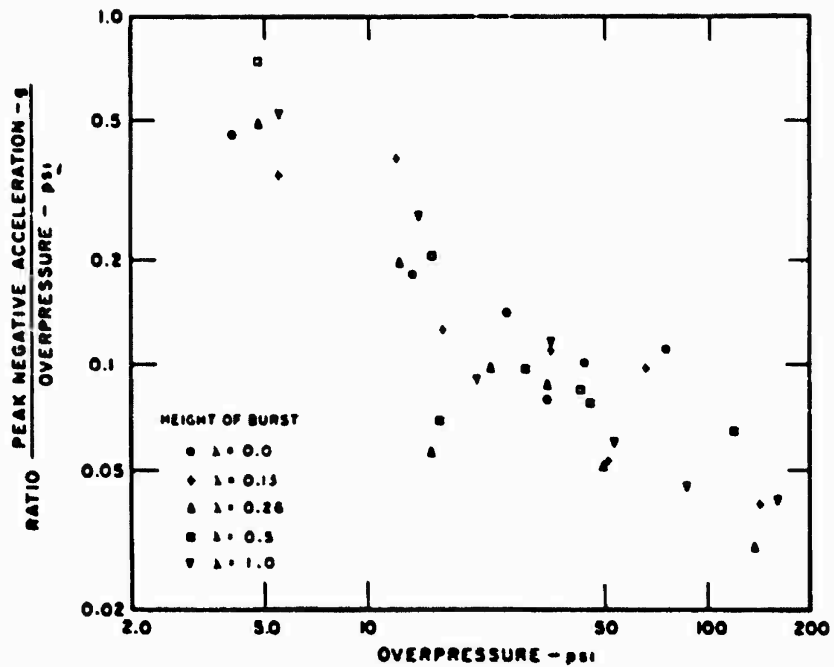


Figure 4.25 Vertical acceleration, Project Mole, Nevada sand and gravel mix, 5-foot depth.

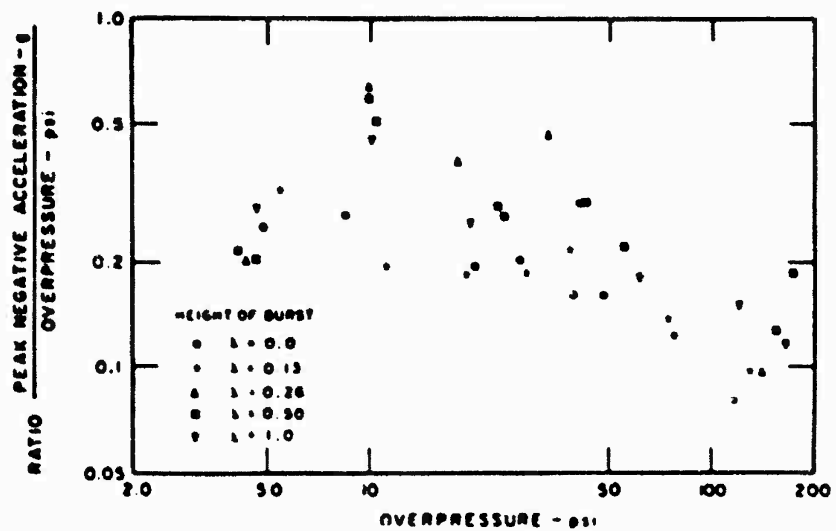


Figure 4.26 Vertical acceleration, Project Mole, Utah dry clay, 5-foot depth.

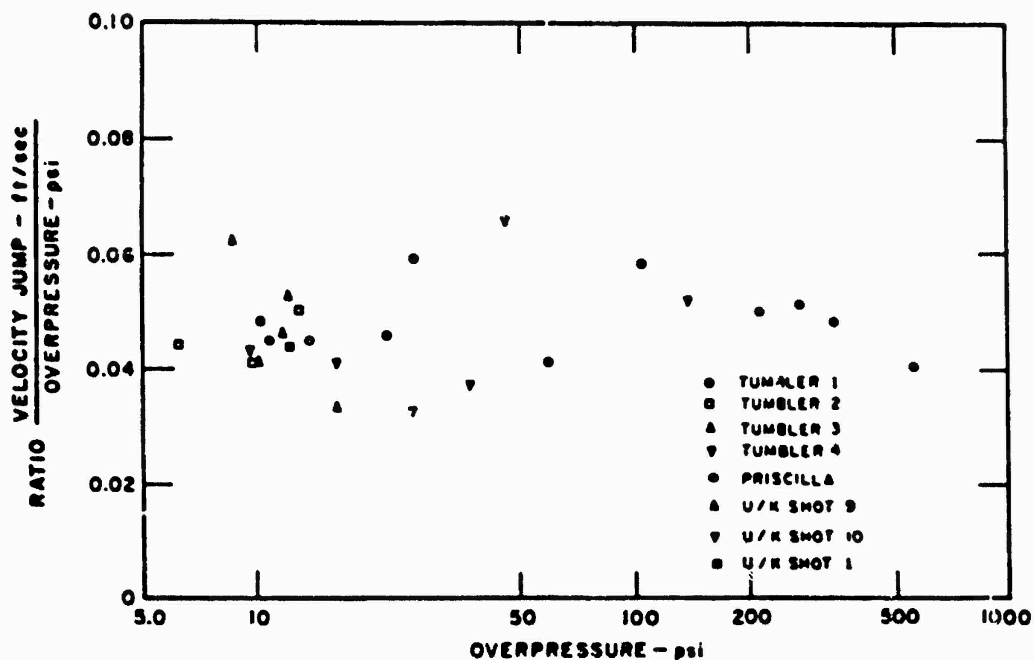


Figure 4.27 Vertical velocity, 5-foot depth, summary of superseismic data.

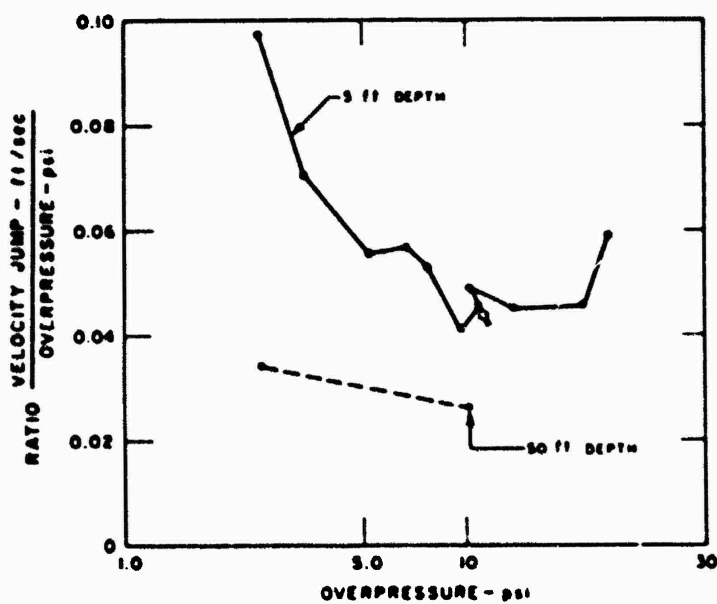


Figure 4.28 Vertical velocity, Tumbler Shot 1, 5-foot depth.

The remaining data are the original reported results. In Figure 4.32 are shown all 5-foot vertical velocity observations in Frenchman Flat.

The horizontal outward velocity at Station 4 on Shot Priscilla gave a peak value at 10- and 50-foot depths which is about one sixth the maximum downward velocity at the same locations. Although the 10-foot vertical accelerometer record at Station 6 was lost, the comparison at 50 feet reveals that the maximum outward velocity was less than one half the peak downward velocity. The apparent relative increase in the outward component as one goes to increasing depths and ground ranges is due to the greater influence of signals from remote sources upon the ground motion.

4.4.3 Displacement (and Overpressure). The peak vertical displacement-positive overpressure impulse ratios at 5-foot depth for all records analyzed to date are shown in Figure 4.33. Some remarks on the Priscilla results are pertinent. First, the 5-foot depth displacement at

TABLE 4.3 AVERAGE PROPAGATION VELOCITY OF DIRECT WAVE, 0 TO 10 FEET, SHOT PRISCILLA

Overpressure	C _L
psi	ft/sec
550	695
440	660
340	980
275	1,080
210	755
100	830
60	980
Average value	960

Station 2 has been estimated from the displacement at 10-foot depth, Point c of Figure 4.33, and the attenuation of displacement with depth (Figure 4.11). Second, the overpressure and impulse at Station 2 have been estimated by a reasonable interpolation between Stations 1 and 3.

The smaller-than-expected displacement at Station 1 on Priscilla has been checked and is further verified by the 10-foot depth displacement.

Considerable variation exists between the Tumbler displacement impulse ratios. No further correlation appears evident through consideration of device yield since the variation of displacement impulse ratio is not systematic. The agreement between Tumbler 4 and Priscilla is encouraging but possibly fortuitous.

Figure 4.34 displays reed-gage displacement data for a number of Plumbbob detonations in the Yucca test area (Reference 21). Positive impulse values have been estimated from measured overpressures and device yield using the correlation presented in Appendix D. The vertical lines adjacent to each datum point indicate the possible error involved in this estimate. Corresponding displacements have been computed from Priscilla accelerograms (Section 4.5). The same degree of variation is evident between these data as was found in Figure 4.33.

The reasons for the wide scatter of displacement data are not known. The only conclusions which appear valid at the present time are that approximately the same degree of variation exists in Frenchman Flat as between the Frenchman Flat and Yucca test areas, and that displacements twice those observed on Priscilla are possible for similar geological conditions.

The variation of displacement-impulse ratio with peak overpressure is not surprising phenomenologically; however, from an empirical prediction standpoint it would be desirable to eliminate such a dependency. Several inquiries have been made along these lines, and it appears possible that displacement may be proportional to that fraction of overpressure impulse above a certain pressure or to that fraction of overpressure impulse delivered prior to a cer-

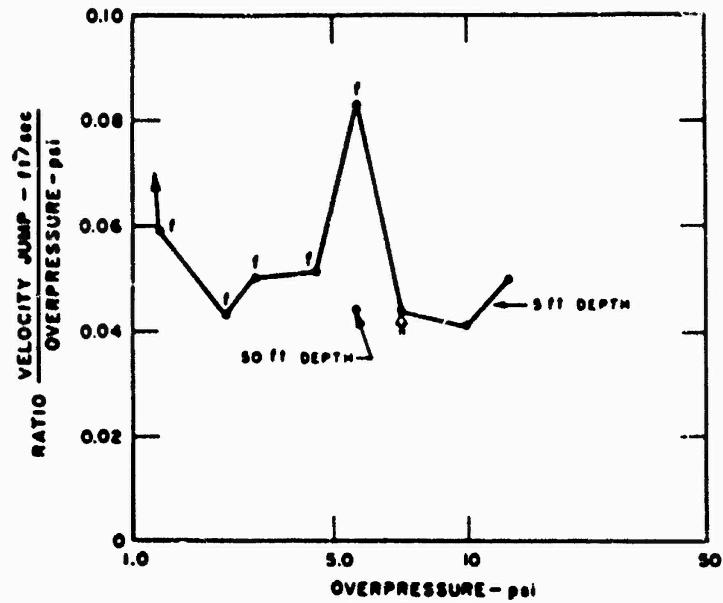


Figure 4.29 Vertical velocity, Tumbler Shot 2, 5-foot depth (f indicates as-reported data).

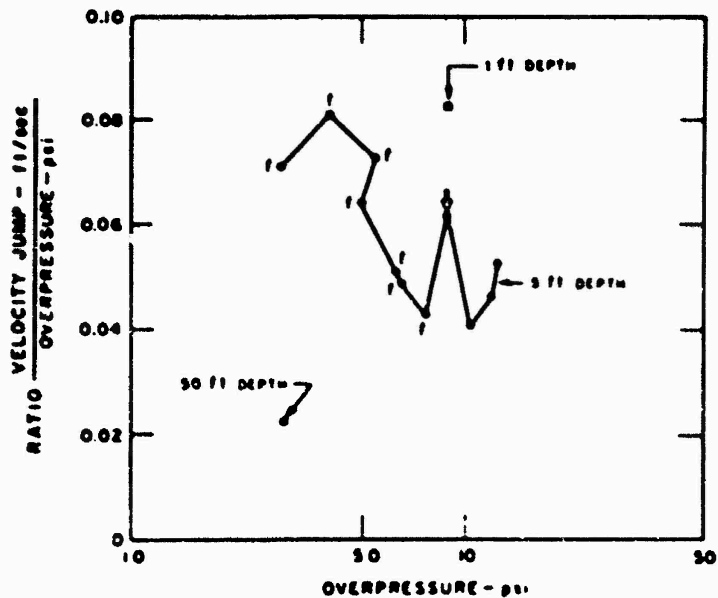


Figure 4.30 Vertical velocity, Tumbler Shot 3, 5-foot depth (f indicates as-reported data).

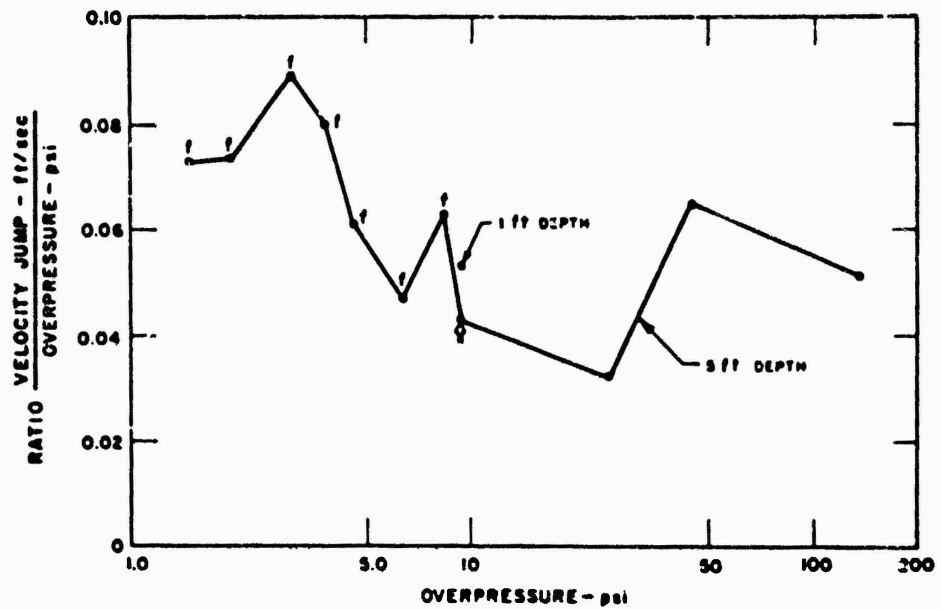


Figure 4.31 Vertical velocity, Tumbler Shot 4, 5-foot depth (f indicates as-reported data).

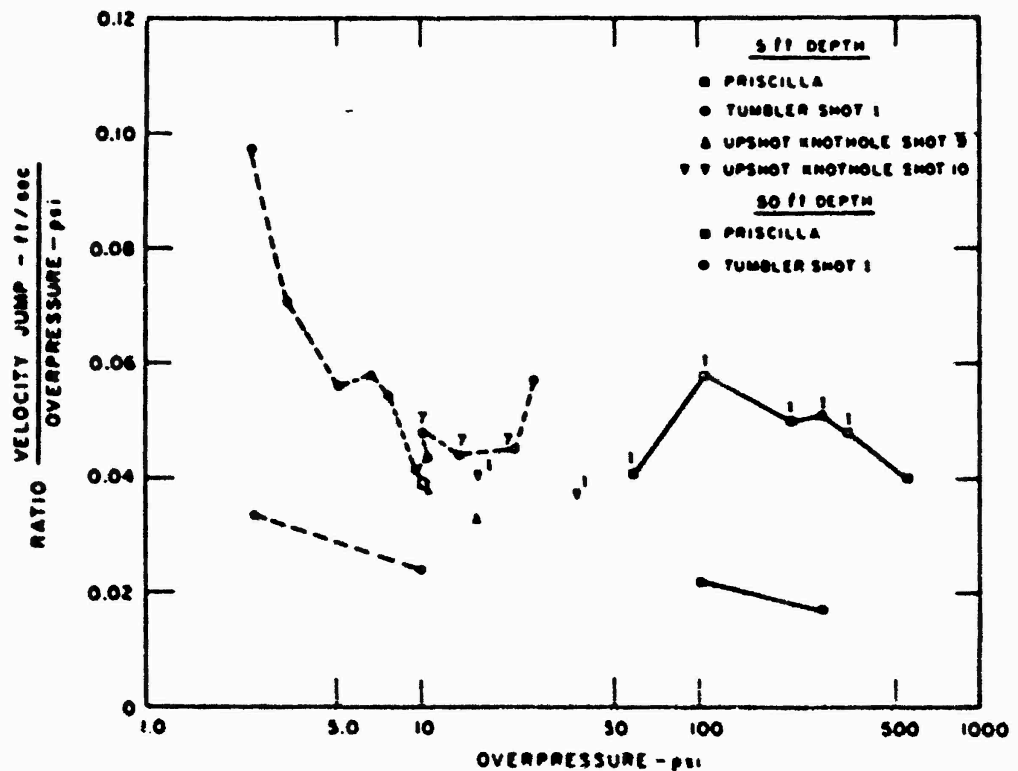


Figure 4.32 Vertical velocity, Frenchman Flat, 5-foot depth (numbers adjacent to data indicate overpressure wave form).

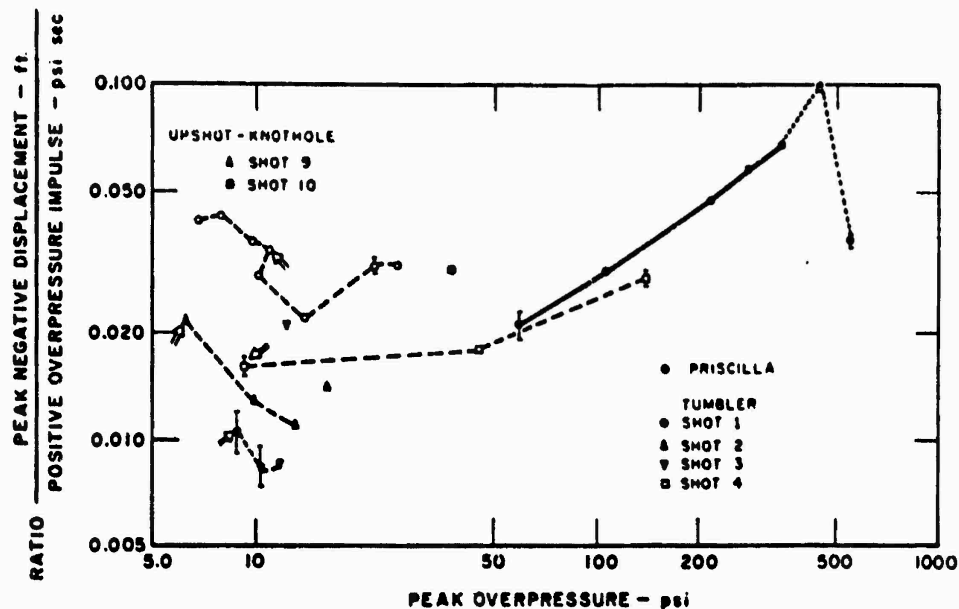


Figure 4.33 Summary of vertical displacement, Nevada Test Site (e indicates estimated value).

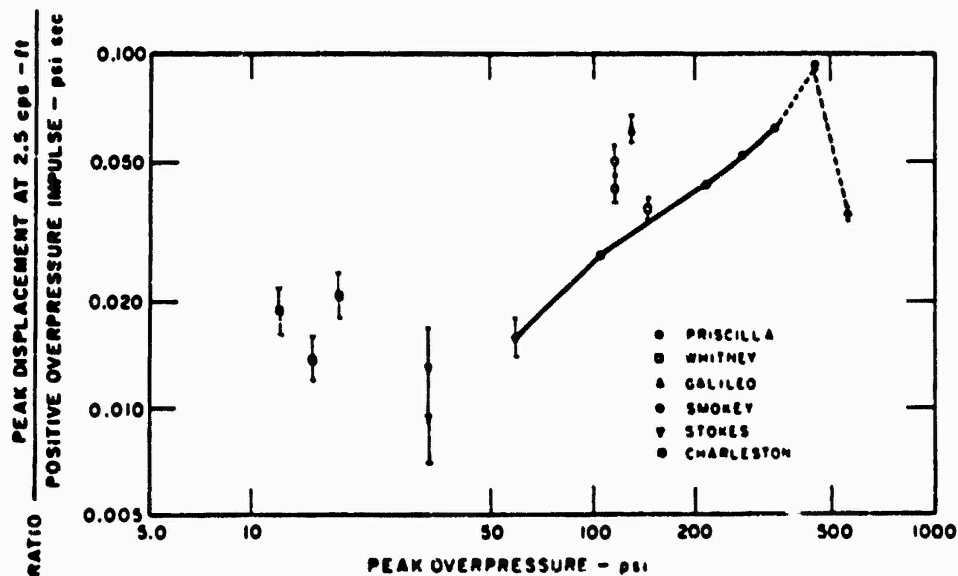


Figure 4.34 Summary of reed-gage data (displacement spectra), Nevada Test Site (e indicates estimated value).

tain fixed time duration. Additional work in this area is required before any conclusions can be presented.

In any analysis of vertical displacement, examination of the validity of the double integration of acceleration is worthwhile effort. As previously mentioned, most first integrations of acceleration lead to nonzero velocities at the end of the record. Provided the velocity baseline shift is linear and one is able to make a reliable estimate of the time of zero velocity, the second integration affords little difficulty. Prior to Priscilla, however, data did not exist which would serve as an independent check on the results obtained. The Priscilla long-span strain gage data now provide this opportunity. In Table 4.4 a comparison is made between the Sandia long-span strain gage results and the Stanford Research Institute double integrations. Only near-surface data are compared since strain gage data at depth have not yet been reduced. The agreement between these two independent measurements is surprisingly good, except at 1,350-foot range. One can speculate that the Sandia anchor at 200 feet at this station would be most influenced by remote source signals, thereby reducing the apparent near-surface peak displacement. However, this type of reasoning is dangerous without more complete data. It should be noted, however, that the capability of the integration method to lead to valid permanent displacements is severely limited.

4.4.4 Strain (and Overpressure). Reference to Figure 4.18 indicates quite a different peak strain attenuation with depth at the two stations instrumented (750- and 1,050-foot ground range). The reason for this difference may be traced to the different character of the inputs at the two

TABLE 4.4 COMPARISON OF MAXIMUM TRANSIENT-VERTICAL DISPLACEMENT, SHOT PRISCILLA

Ground Range, ft	Maximum Displacement	
	SRI, 5 ft *	Sandia, 3 ft †
650	0.84	0.82
850	> 0.40 ‡	0.52
1,050	0.27	0.23
1,350	0.24	0.11

* Double integration of acceleration.

† Long-span displacement gage.

‡ Cable break; displacement estimated.

stations. At Station 4 (750-foot ground range), the precursor pressure of about 25 psi precedes a rise (in about 5 msec) to 228-psi peak overpressure. By contrast, the input at Station 6 indicates a precursor pressure of 20 psi and rises to only 104-psi peak in about 15 msec.

Probably the rise time associated with the input overpressure assumes the greatest importance when considering earth strain, particularly near the ground surface. Measurements of seismic velocity indicate that the weathered layer at Frenchman Flat extended to depths of 5 or more feet. It is feasible that an overpressure-time input such as 4B (Figure 3.1) would produce large strains in such a layer, whereas the 6B input would not. The few strain measurements obtained by Project 1.4 severely limit firm conclusions concerning the phenomenology.

4.5 RESPONSE SPECTRUM OF GROUND MOTION

4.5.1 Theory. The response spectrum is defined as the maximum response of a linear, single degree of freedom, spring mass system, relative to the motion of ground. Such a system is shown in Figure 4.35.

The equation of motion, in terms of the relative displacement, x , is (dot superscript denotes differentiation with respect to time,)

$$\ddot{x} + 2n\dot{x} + \omega^2 x = -a(t)$$

Where: n is the ratio of damping to critical damping
 ω = undamped natural frequency, $\omega^2 = k/m$
 m = mass of system
 k = spring rate of system
 a = ground acceleration
 t = time

Development of this equation may be found in any standard text on dynamic motion, or in References 22 and 23.

Let $\dot{y} = x$ and integrate once, resulting in

$$\ddot{y} + 2n\omega\dot{y} + \omega^2 y = -u(t)$$

Where u is ground particle velocity. Let $\dot{z} = y$ and integrate once again,

$$\ddot{z} + 2n\omega\dot{z} - \omega^2 z = -s(t)$$

Where s is ground displacement.

These equations demonstrate that the response may be calculated from knowledge of any one of the ground motion parameters, acceleration, velocity, or displacement.

Three response spectra may be defined:

$|x|_{\max}$, the displacement (response) spectrum

$\omega|x|_{\max}$, the velocity (response) spectrum

$\omega^2|x|_{\max}$, the acceleration (response) spectrum

The velocity spectrum is proportional to the maximum strain energy per unit mass for an instantaneous applied force and no damping,

$$\frac{E}{m} = \frac{k|x|_{\max}^2}{2m} = \frac{1}{2} \cdot \omega^2|x|_{\max}^2$$

For a small amount of damping, $n \sim 0$, the acceleration spectrum equals the maximum absolute acceleration of the mass, \ddot{q} .

One has

$$x = q - s \text{ or } \ddot{x} = \ddot{q} - a$$

From the equation of motion ($n = 0$)

$$\ddot{x} + a = -\omega^2 x.$$

Hence

$$|\ddot{q}|_{\max} = \omega^2|x|_{\max}.$$

A few characteristics of response spectrum may now be illustrated. Take the second form of the equation of motion. The ground particle velocity may be characterized by a peak value, u_m , and a duration T , as in Figure 4.36, i.e., $u/u_m = \phi(\tau)$ and $t = T\tau$.

Let $Y = (y/u_m)T^2$ and $\Omega = \omega T$, then $\ddot{Y} + 2n\Omega\dot{Y} + \Omega^2 Y = -\phi(\tau)$.

The velocity spectrum, $\Omega|\dot{Y}|_{\max}$, is a single valued function of Ω only.
But

$$\Omega|\dot{Y}|_{\max} = \omega T + \frac{1}{T} \frac{|x|_{\max}}{u_m},$$

Hence $(\omega|x|_{\max})/u_m$ is also a single valued function of ωT as in Figure 4.37a.

In Figure 4.37b the velocity spectrum of Figure 4.36 is displayed for large T , large yield devices and small t , small yield devices. The peak value of $\omega|x|_{\max}$, does not change provided the peak particle velocity does not vary, i.e., constant overpressure. However, the curve shifts toward the lower frequencies as the yield increases. These statements are true only if $\Phi(\tau)$ is invariant.

In the same manner it may be shown that

$$\frac{|x|_{\max}}{d_m} = f_1(\omega T)$$

$$\frac{\omega^2|x|_{\max}}{a_m} = f_2(\omega T)$$

Where d_m and a_m are the peak ground displacement and acceleration, respectively.

As the frequency ω (or more rigorously ωT) approaches zero, the response $|x|_{\max}$ approaches the peak ground displacement. At large values of ω (ωT) the response approaches the peak acceleration divided by ω^2 . Hence as $\omega \rightarrow 0$

$$|x|_{\max} \sim d_m + u_m T \int_0^1 \frac{u}{u_m} d\tau$$

and

$$\frac{\omega|x|_{\max}}{u_m} \sim C_1 \omega T$$

where

$$C_1 = \int_0^1 \frac{u}{u_m} d\tau$$

As $\omega \rightarrow \infty$

$$\omega^2|x|_{\max} \sim a_m = \frac{u_m}{T} \left| \frac{d(u/u_m)}{d\tau} \right|_{\max}$$

and

$$\frac{\omega|x|_{\max}}{u_m} \sim \frac{C_2}{\omega T}$$

where

$$C_2 = \left| \frac{d(u/u_m)}{d\tau} \right|_{\max}$$

The conditions under which the velocity spectrum may be scaled as in Figure 4.37b, require

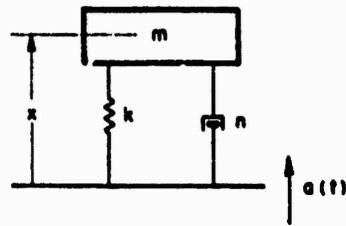


Figure 4.35 A linear, single-degree-of-freedom system.

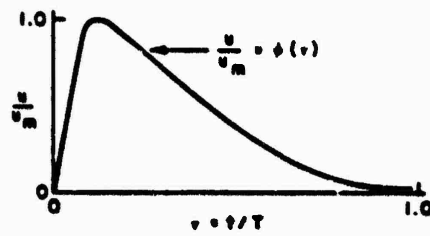


Figure 4.36 Schematic diagram of ground particle velocity.

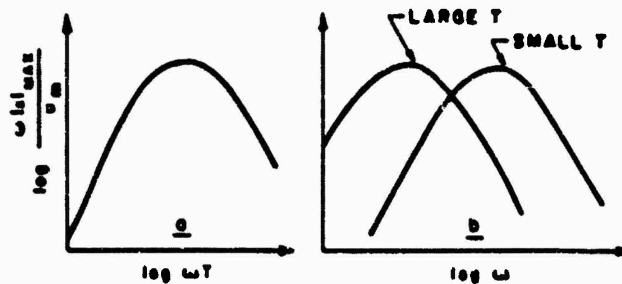


Figure 4.37 Schematic diagram of velocity spectrum.

that the maximum displacement at constant overpressure (u_m is proportional to overpressure) vary as T and that the peak acceleration at constant overpressure vary as T^{-1} . That is, all details of the velocity time history must scale in a consistent manner.

4.5.2 Measurements. The displacement spectrum may be determined either by direct measurement with reed gages, by numerical calculation of the response of a linear system to the ground motion, or through use of the electrical-mechanical analogy by converting the measured ground motion into an electrical signal (Reference 24). All methods will produce identical results provided certain precautions are taken. An excellent example of equivalent results obtained by direct measurement and the analog calculation is presented in Reference 25.

Reed gages should be constructed so that their springs remain linear up to the maximum response measured. The damping should be linear, i.e., viscous, up to the maximum response. The percent of critical damping should be known and preferably should be small and approximately the same for each spring of the set.

The accuracy of numerical or analog calculations of the response depends first on the accuracy of measurement of the ground motion, i.e., the accelerogram. As discussed in Appendix C an accelerometer-galvanometer system will yield faithful results if its natural frequency is more than twice the fundamental frequency observed in the ground motion, and hence it is unwise to calculate response spectrum for frequencies greater than half the accelerometer or galvanometer frequency, whichever is smaller.

Secondly, the accuracy of numerical calculation depends on the fineness of the calculation network, i.e., the time interval between successive readings of the record, in relation to the sophistication of the integration program. The time interval is usually limited by the precision of the time base on the original record (0.5 msec on Priscilla, 1 msec on previous operations). The integration program selected is a compromise between the cost of running a complex computation and the maximum frequency to which the computations are carried. For example, the simplest program, using the particle velocity as the input, appears to give reliable results for the majority of the Priscilla records to a frequency of 250 radians/sec (40 cps). To compute the response of a 100-cps system, a more complex (and costly) program must be written.

This second consideration is not usually a limiting factor in analog calculations. However a necessary condition for both calculations is that the velocity at the end of the pulse be zero. This is of major importance at low frequencies and becomes less important as the frequency increases (Reference 26). The importance of correcting for the baseline shift discussed in Appendix C is now further emphasized.

Response spectra for all the Priscilla ground motion data, excepting Stations 2V5, 5V5, and 5V10 have been calculated to a frequency of 150 radians/sec (24 cps) and about half these have been extended to 250 radians/sec (40 cps). Station 2V5 was eliminated due to a spurious electrical signal, and 5V5 and 5V10 were eliminated because of cable breaks. Displacement response spectra are shown in Figures 4.38 and 4.39 and the corresponding velocity response spectra in Figures 4.40 and 4.41. In Figures 4.40 and 4.41 are shown the asymptotic values as $\omega \rightarrow 0$ (Curve A) and as $\omega \rightarrow \infty$ (Curve B). In Figure 4.42 are shown a selected number of acceleration spectra. The calculations have obviously not been carried to frequencies high enough to determine the maximum of the acceleration spectra.

The results of Figure 4.38 indicate a flat response to 10 radians/sec (1.6 cps). A reed gage frequency of 2.5 cps would respond generally within 10 percent error in maximum transient vertical and horizontal displacements. The spectra are smooth out to and including Station 4 (275 psi). The spectra at Station 6 (100 psi) begin to assume a jagged character which becomes more pronounced at Station 7 (60 psi) as the frequency increases.

The overpressure wave forms from Station 3 (340 psi) on were precursor Type 1, Appendix A. The only significant difference in the shape of the overpressure-time curve was increased precursor duration and rise time of the main overpressure pulse at the larger ground ranges. Hence, it does not appear that the change in character of the response can be associated with the local ground wave but rather that it results from interference of the refracted ground-transmitted wave.

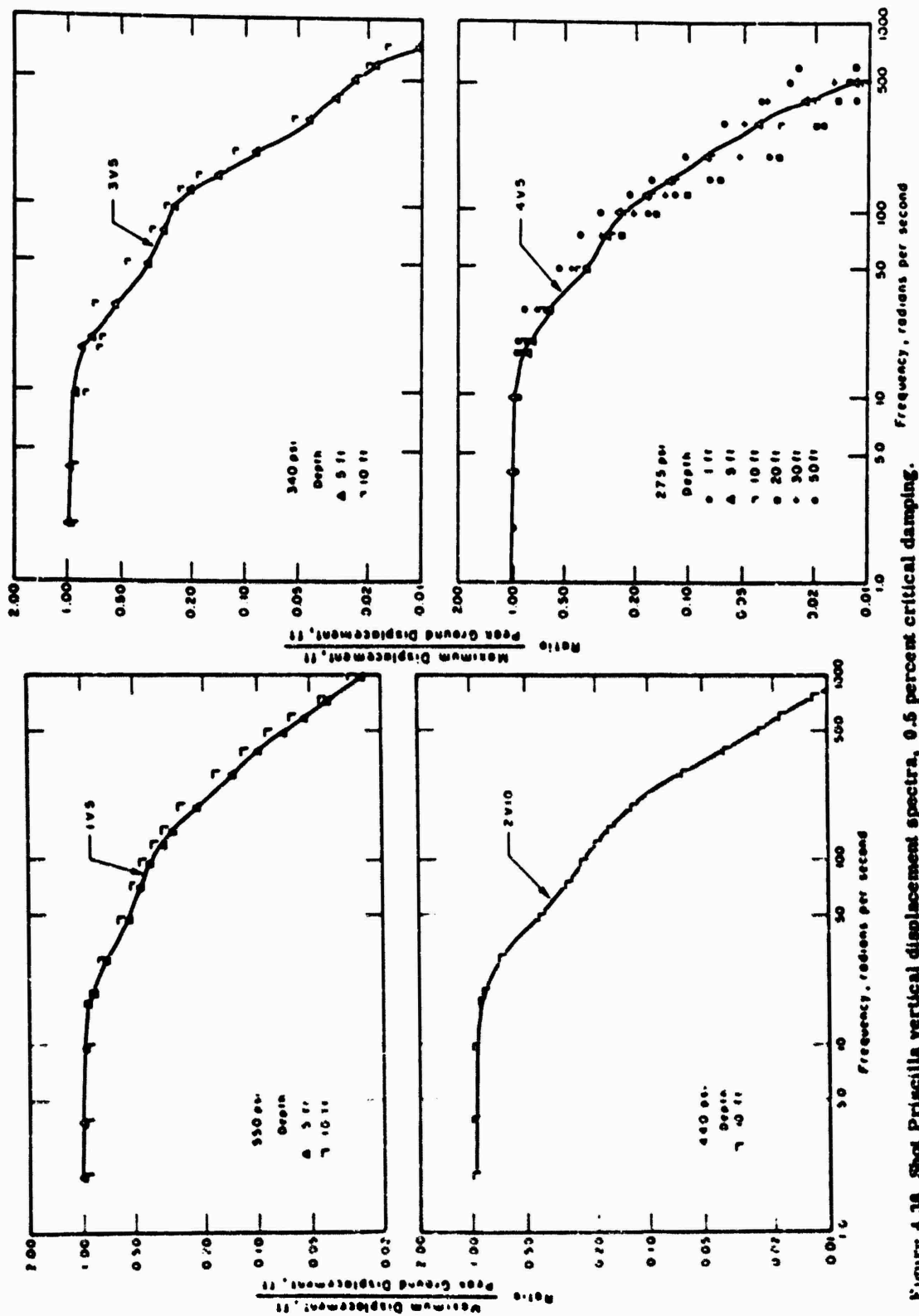


Figure 4.38 Shot Priscilla vertical displacement spectra, 0.5 percent critical damping.

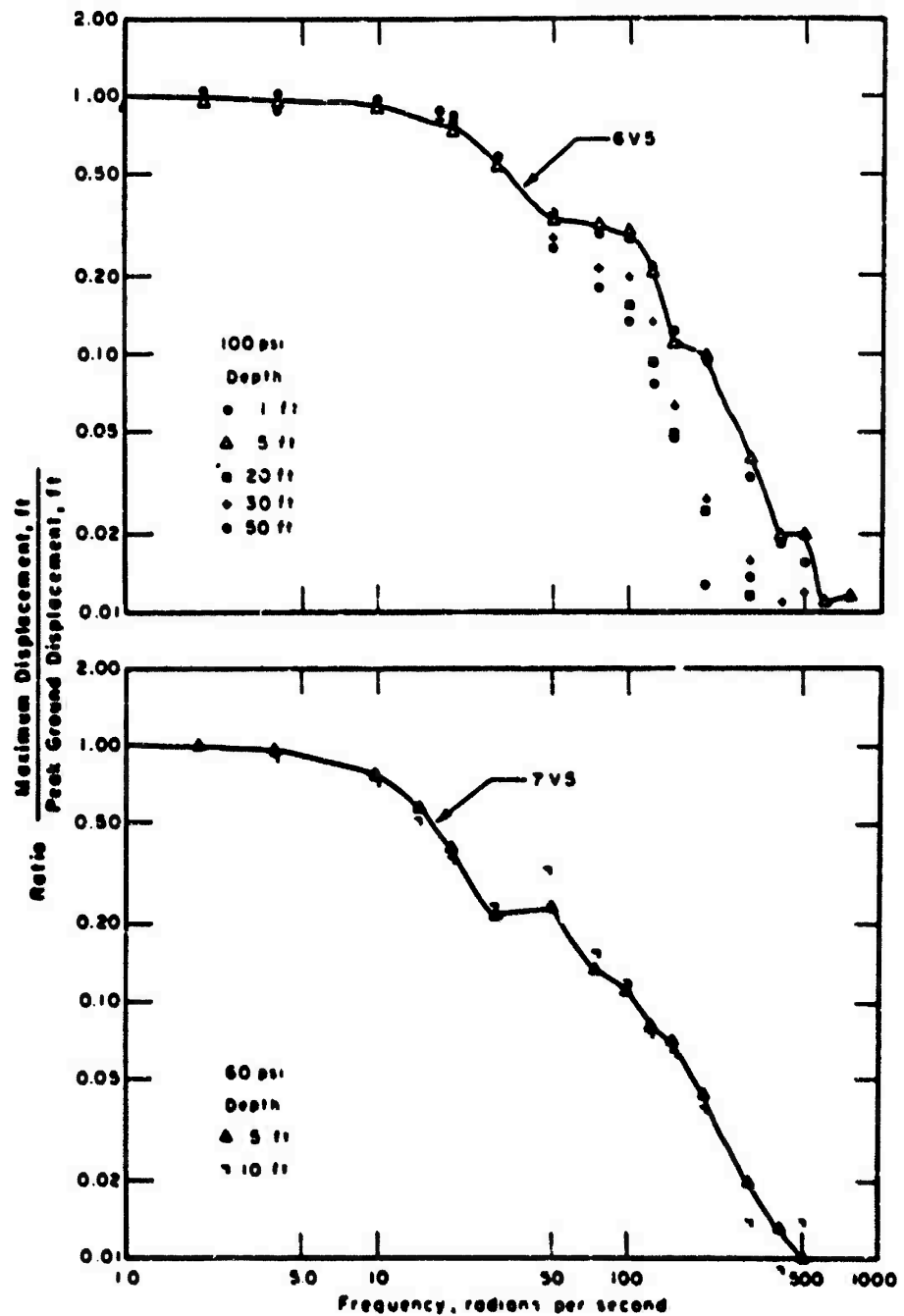


Figure 4.38 Continued.

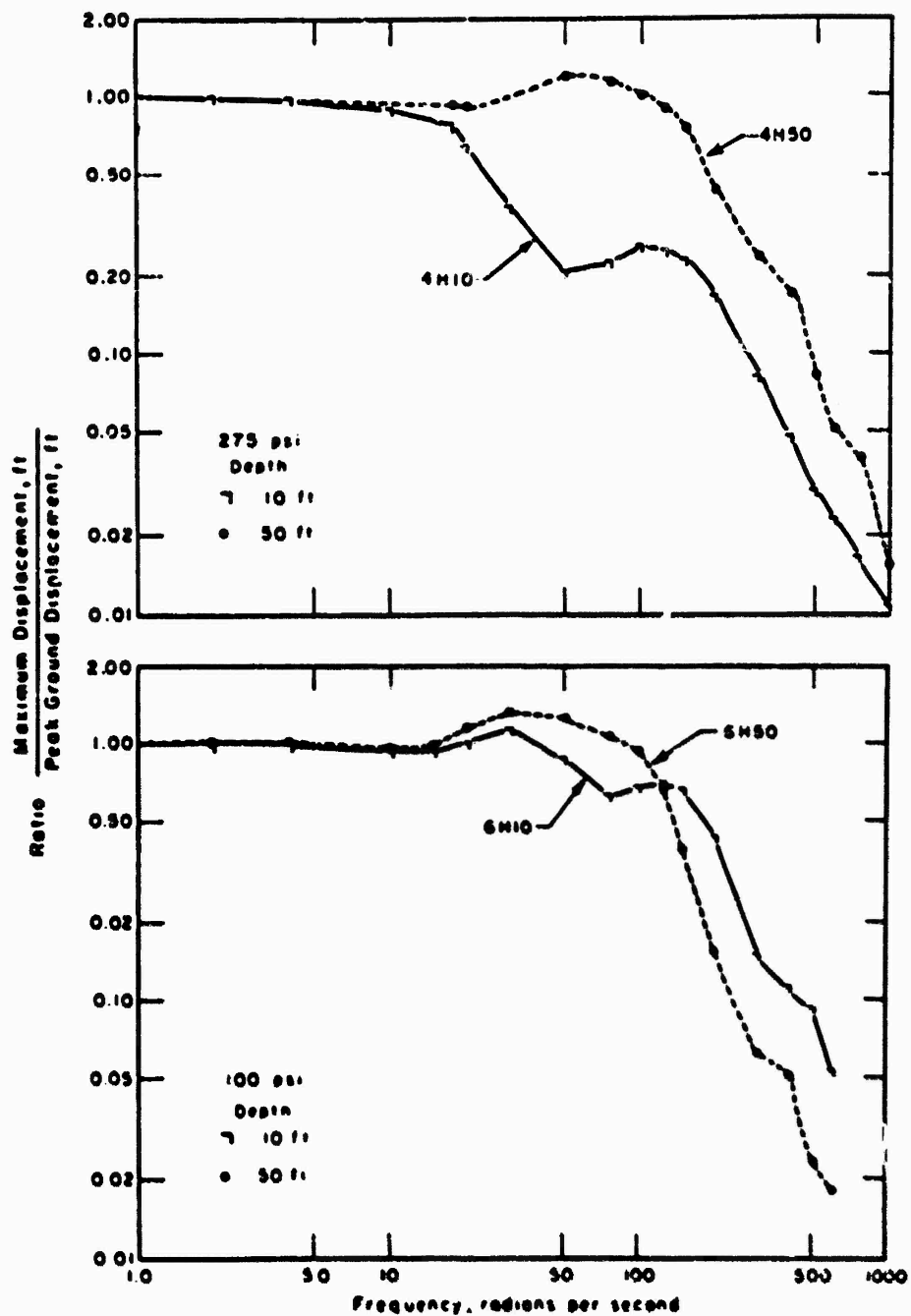


Figure 4.39 Shot Priscilla horizontal displacement spectra, 0.5 percent critical damping.

This conclusion is supported by close examination of the acceleration records. At Station 4 (275 psi), the ground wave has not yet outrun the main air-blast wave but arrives slightly behind the direct signal. The interference is most pronounced at the 20- and 30-foot depths. At Stations 6 (100 psi) and 7 (60 psi), the ground wave appears to be outrunning the main blast wave but not the precursor. This is possible since the precursor propagation velocity at these ground ranges is roughly twice the main wave velocity.

This example illustrates one of the inherent advantages of accelerograms over reed-gage data in that significant information may be lost when an attempt is made to reduce primary data

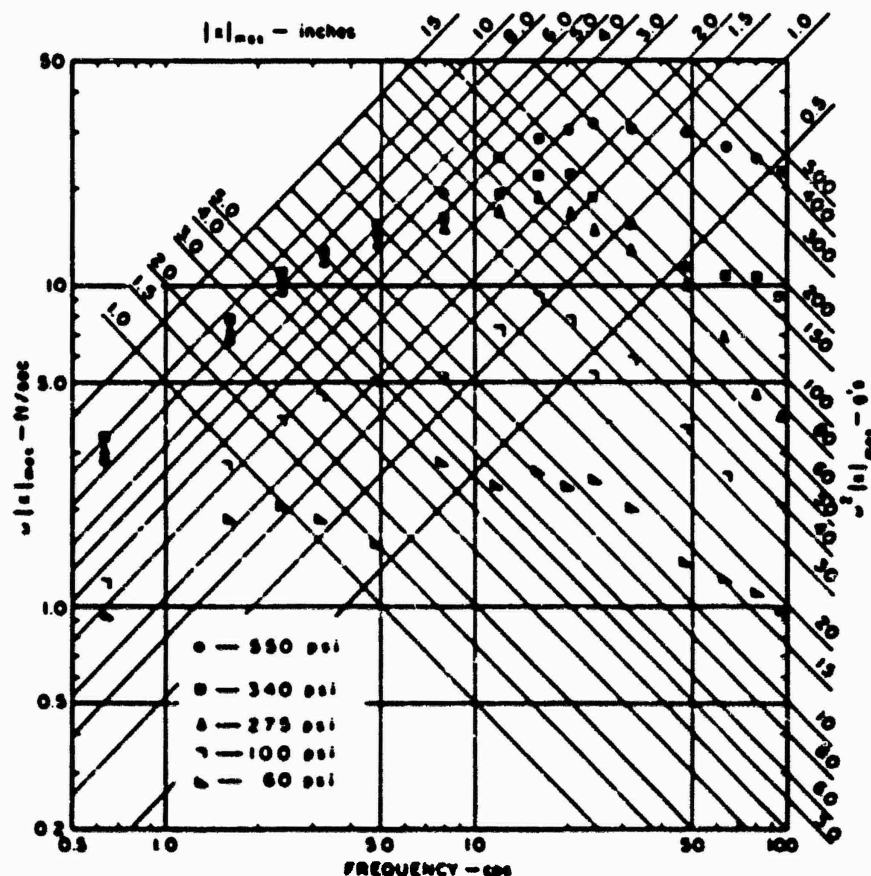


Figure 4.40a Vertical velocity spectra, 5-foot depth, Shot Priscilla.

at the instrument itself. However, the reed gage, or preferably a displacement-time meter, has the advantage of being insensitive to the type of baseline correction which appears necessary to the integration of accelerograms. These comments point out that neither accelerometers nor reed gages (or other displacement meters) are completely self sufficient and that the most advantageous instrumentation probably will consist of both types placed as a pair rather than as separate entities.

4.5.3 Correlation and Scaling. The question of correlation and scaling of the response spectra is now considered. In Figures 4.43 and 4.44 are shown the vertical velocity spectra for 5- and 10-foot depth normalized in the manner indicated in the section on theory. Data for the 100- and 60-pai stations are not shown due to the interference of the ground wave, and data for the 550-pai station are not shown due to the anomalous (low) values of peak displacement at this station.

The velocity spectra were chosen over the displacement and acceleration spectra since the maximum, i.e., the maximum energy per unit mass, is one of the principal factors in design of

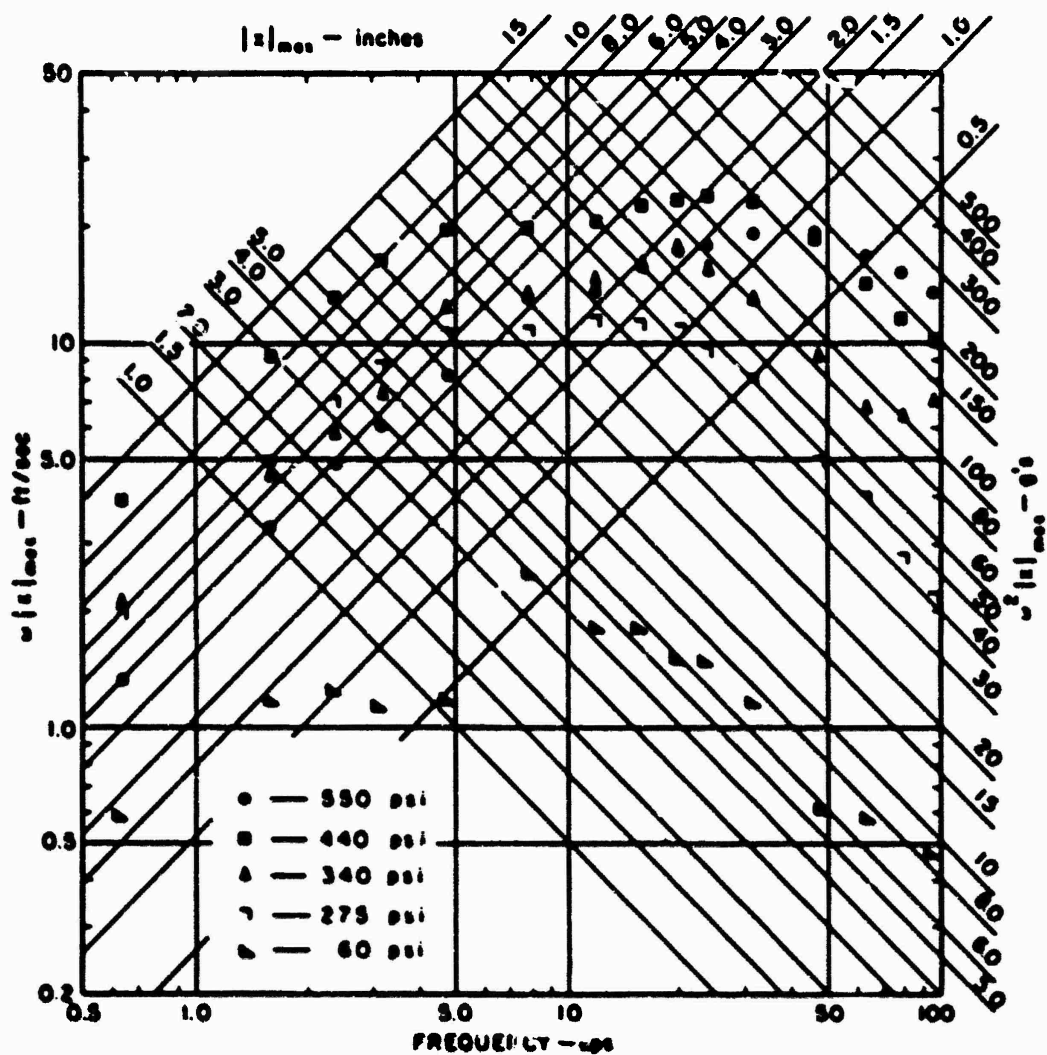


Figure 4.40b Vertical velocity spectra, 10-foot depth, Shot Priscilla.

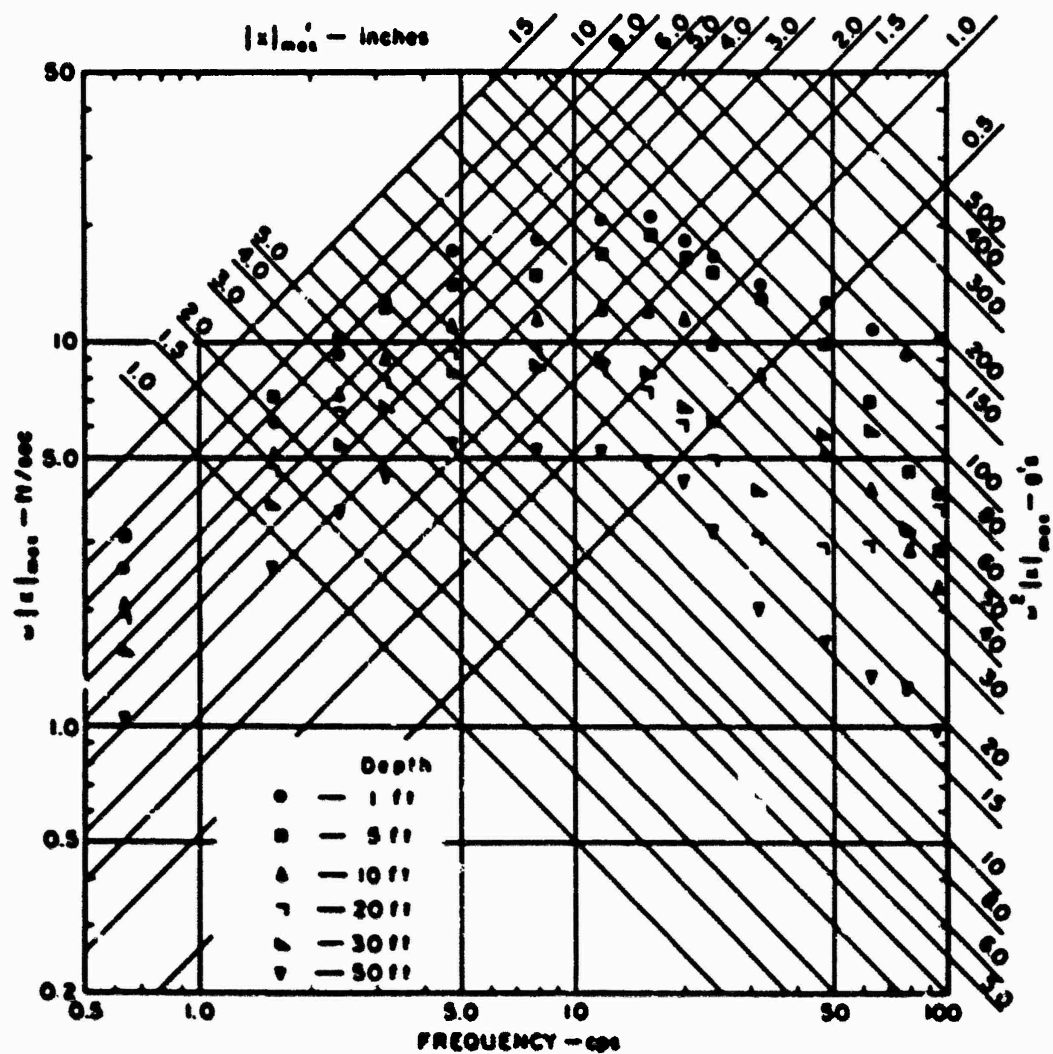


Figure 4.40c Vertical velocity spectra, 375 psi, Shot Priscilla.

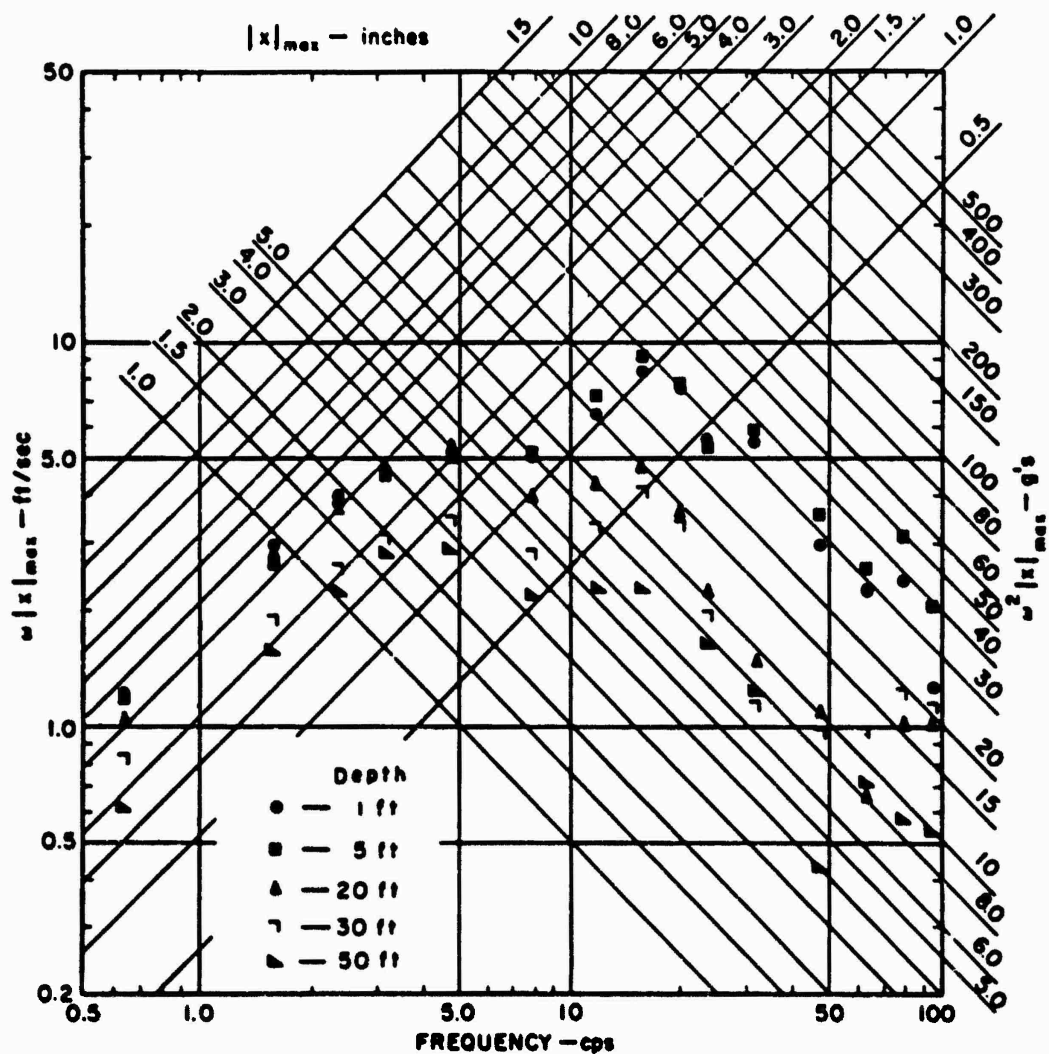


Figure 4.40d Vertical velocity spectra, 100 psi, Shot Priscilla.

shock isolation equipment. Since the displacement and acceleration are both known functions of the velocity, they may be easily derived from Figures 4.43 and 4.44. For T, the normalizing factor for ω (Section 4.5.1), the overpressure positive phase duration is used, again as a matter of convenience, rather than the duration of the velocity pulse. Whether or not this serves to correlate the data constitutes a test of the validity of the procedure. Furthermore, the overpressure duration is a known quantity independent of the ground motion, a factor necessary for scaling to larger yields.

The smoothed curves of Figures 4.43 and 4.44 are identical, which is encouraging; however, the variation in T is only 25 percent and hardly constitutes a valid test.

The normalized velocity spectra for 50-foot depths are shown in Figure 4.45 and compared

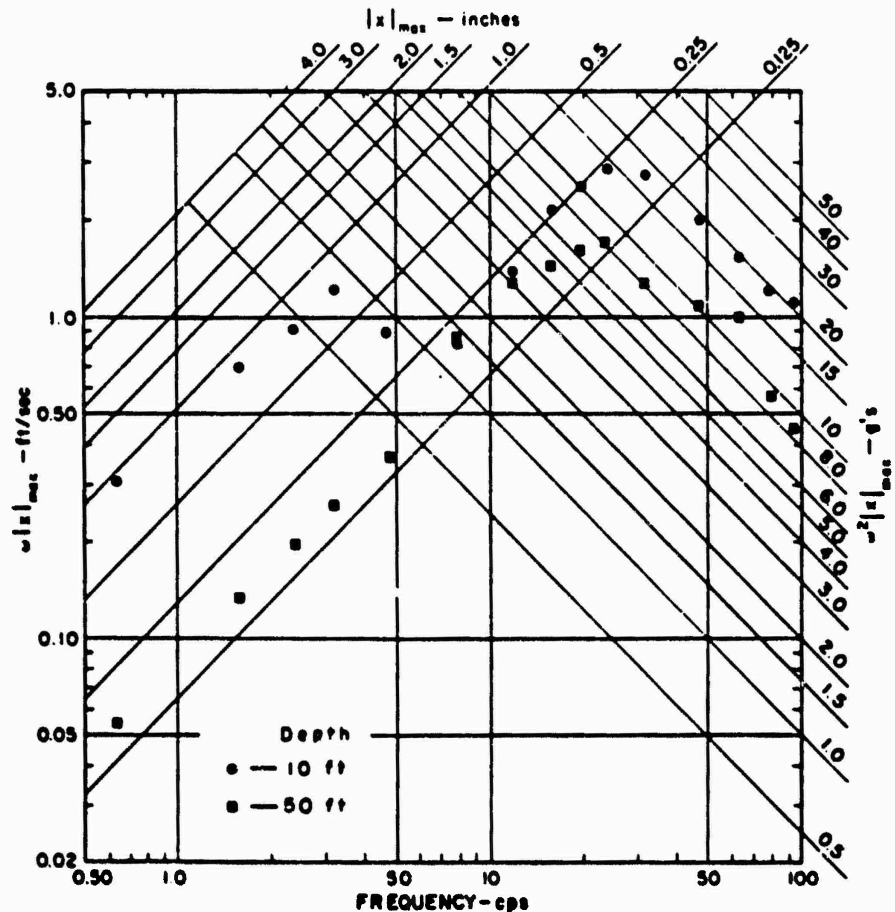


Figure 4.41a Horizontal velocity spectra, 275 psi, Shot Priscilla.

with the spectra for 5- and 10-foot depths. The normalized value does not change significantly although the frequency at which this maximum occurs decreases. Table 4.5 summarizes the maximum ratios for all gages. The average ratio for all vertical gages except Station 7 (60 psi) is approximately 1.2; at Station 7 the ratio is greater than 2 due to the ground wave. Note that for all horizontal gages the maximum value of the normalized velocity is greater than two.

The normalized horizontal spectra for the 10- and 50-foot depths are shown in Figures 4.46 and 4.47. The 100- and 275-psi, 50-foot depth and the 100-psi, 10-foot depth spectra are similar while the 275-psi, 10-foot depth exhibits marked differences.

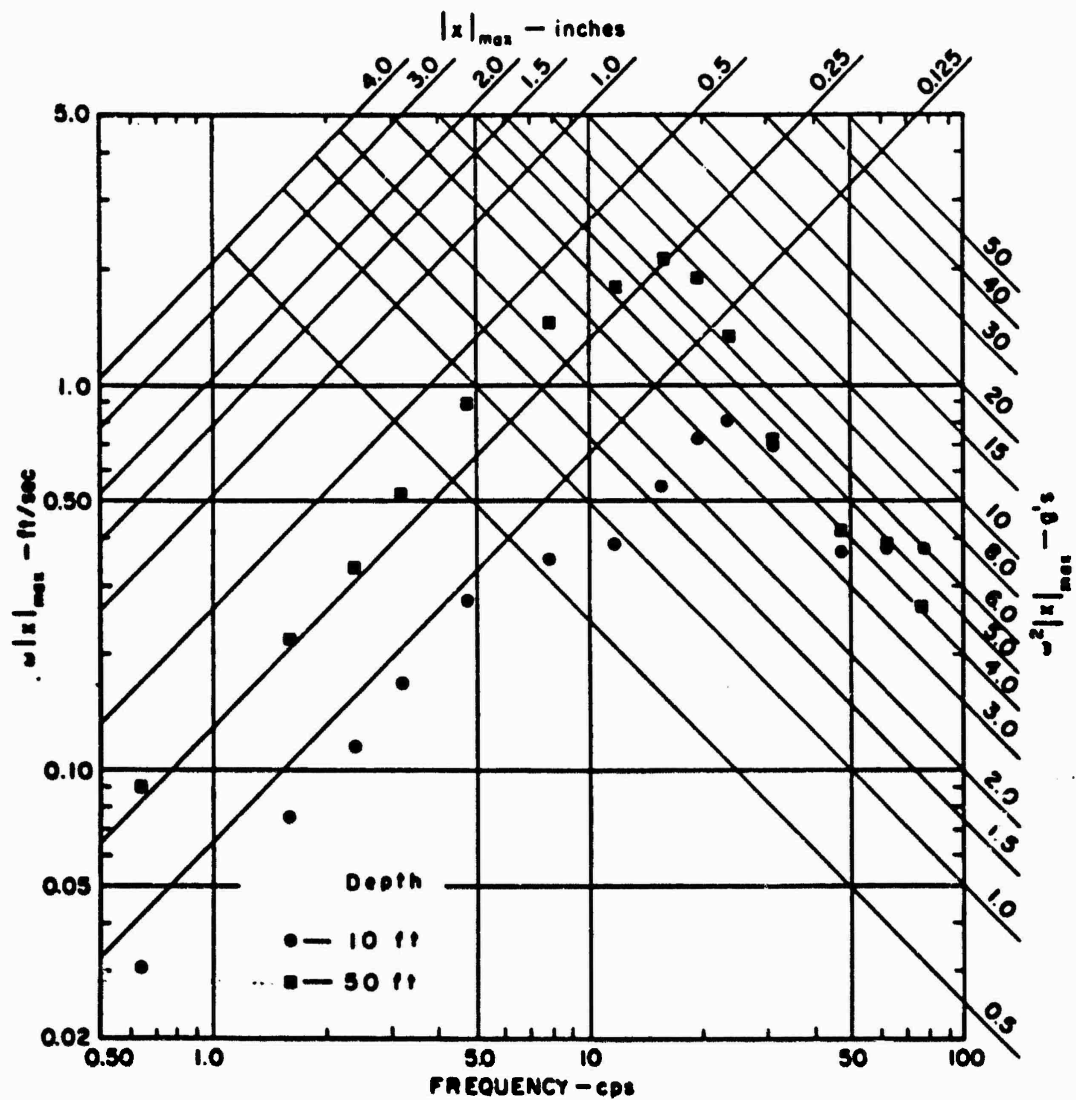


Figure 4.41b Horizontal velocity spectra, 100 psi, Shot Priscilla.

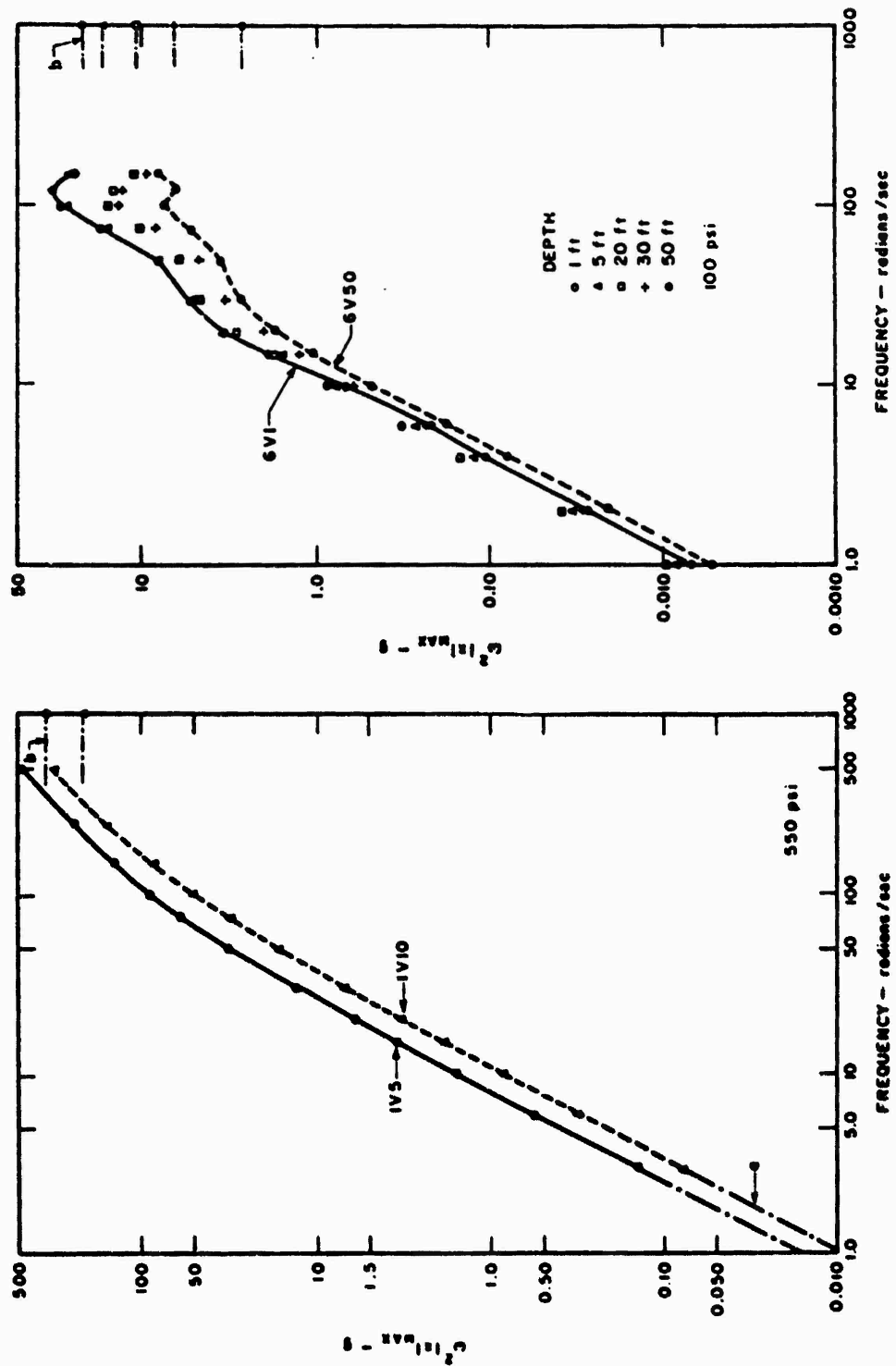


Figure 4.42 Shot Priscilla vertical acceleration spectra, 0.5 percent critical damping.

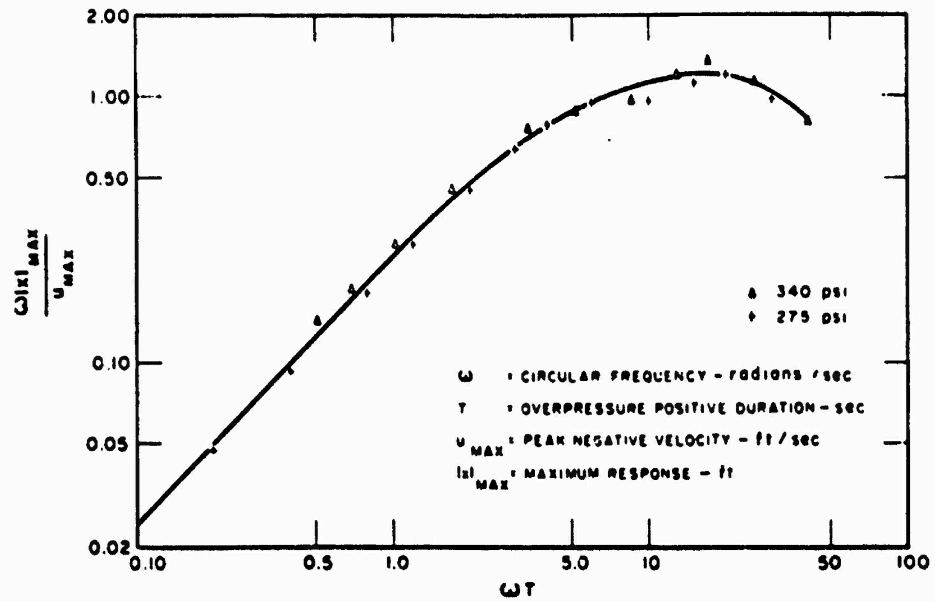


Figure 4.43 Normalized vertical velocity spectra, Priscilla 5-foot depth, 0.5 percent critical damping.

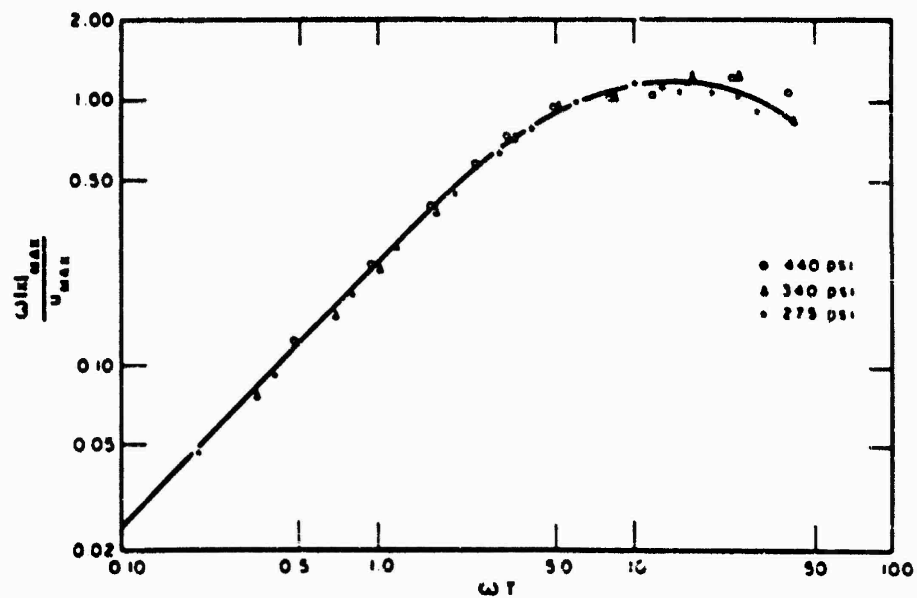


Figure 4.44 Normalized vertical velocity spectra, Priscilla 10-foot depth, 0.5 percent critical damping.

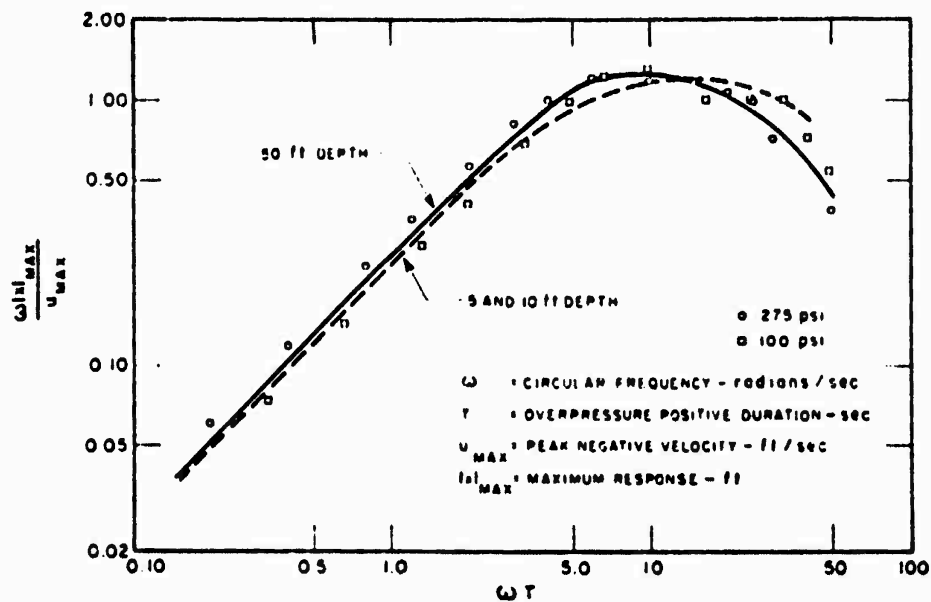


Figure 4.45 Normalized vertical velocity spectra, Priscilla 50-foot depth, 0.5 percent critical damping.

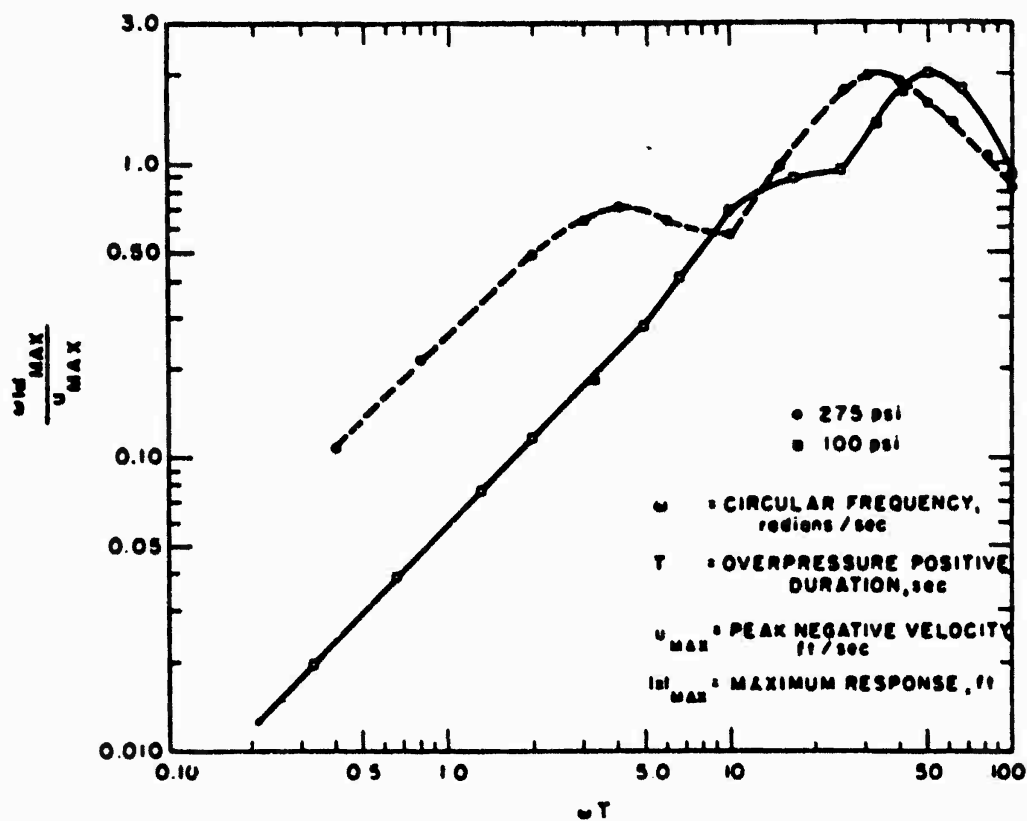


Figure 4.46 Normalized horizontal velocity spectra, Priscilla 10-foot depth, 0.5 percent critical damping.

4.6 SOIL STRESS-STRAIN CONSIDERATIONS

4.6.1 Soil Survey Tests. As a part of Project 3.8 carried out by Waterways Experiment Station (Reference 14), the compressibility characteristics of the undisturbed foundation were determined using four types of tests. A modulus of deformation was determined from consolidation test data using the slope of the stress-strain curve in the first cycle of loading at applied stresses of 50 psi and 100 psi. The modulus of compression was determined using the maximum slope of the stress-strain curve from constant ratio of applied stress triaxial tests. A compressive modulus was determined from soniscope test data using conventional procedures. A modu-

TABLE 4.6 MAXIMUM OF NORMALIZED VELOCITY SPECTRUM, SHOT PRISCILLA

Depth ft	Overpressure psi	$\omega x _{\max} \div u_{\max}$	
		Vertical	Horizontal
1	275	1.32	—
	100	1.29	—
5	550	1.22	—
	340	1.34	—
	275	1.22	—
	100	1.50	—
	60	0.98	—
10	550	1.30	—
	440	1.18	—
	340	1.33	—
	275	1.08	2.0
	100	—	2.0
	60	1.52	—
20	275	1.23	—
	100	1.31	—
30	275	1.46	—
	100	1.18	—
50	275	1.17	1.9
	100	1.28	2.3

lus of elasticity was determined using data from field plate bearing tests. The data from the above tests which are pertinent to Project 1.4 are summarized in Table 4.6.

Looking at Table 4.6, based upon the consolidation test, it may be noted that the modulus of deformation for the natural soil generally increased with an increase in applied stress. It was higher also for stresses applied parallel to the stratification than for stresses applied normal to the stratification. It is also noted that the modulus for the compacted backfill assumed values somewhat higher than for the natural soil.

Variation in soil modulus for different types of tests is to be expected. The rate of application and duration of load undoubtedly influence the magnitude of the soil modulus. The consolidation, triaxial, and load-bearing tests are relatively slow tests, whereas the soniscope test is analogous to a rapid test wherein the load is applied for a short period of time. Other factors such as side wall friction for the consolidation test specimens and the distribution of stress in the triaxial test specimens also undoubtedly influence the test results.

Figures 4.48 and 4.49 present typical examples of stress-strain diagrams taken from the Project 3.8 report. The consolidation test results (Figure 4.49) show a characteristic slow take-off at low stress on the first compression cycle; the second cycle loading curve does not display this behavior to the same degree. This behavior might be due to some sample-apparatus

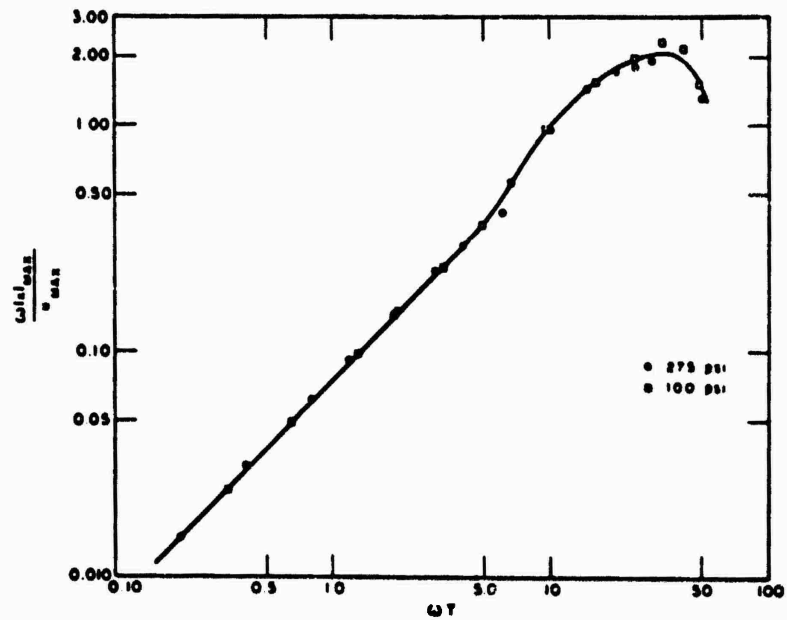


Figure 4.47 Normalized horizontal velocity spectra, Priscilla 50-foot depth, 0.5 percent critical damping.

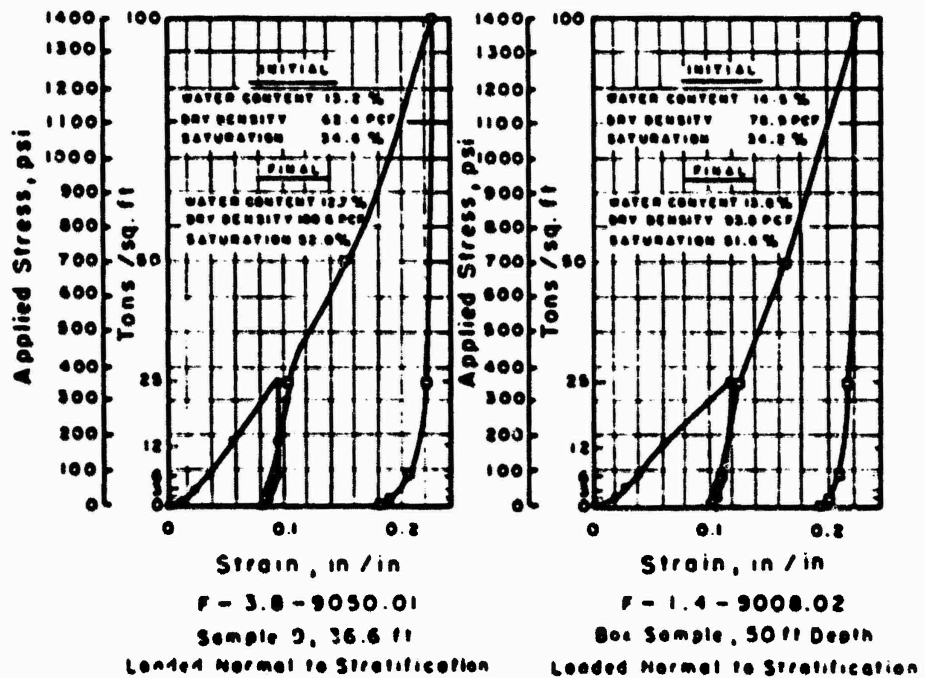


Figure 4.48 Stress-strain curves, undisturbed soil, Frenchman Flat. (Reprinted from Reference 14.)

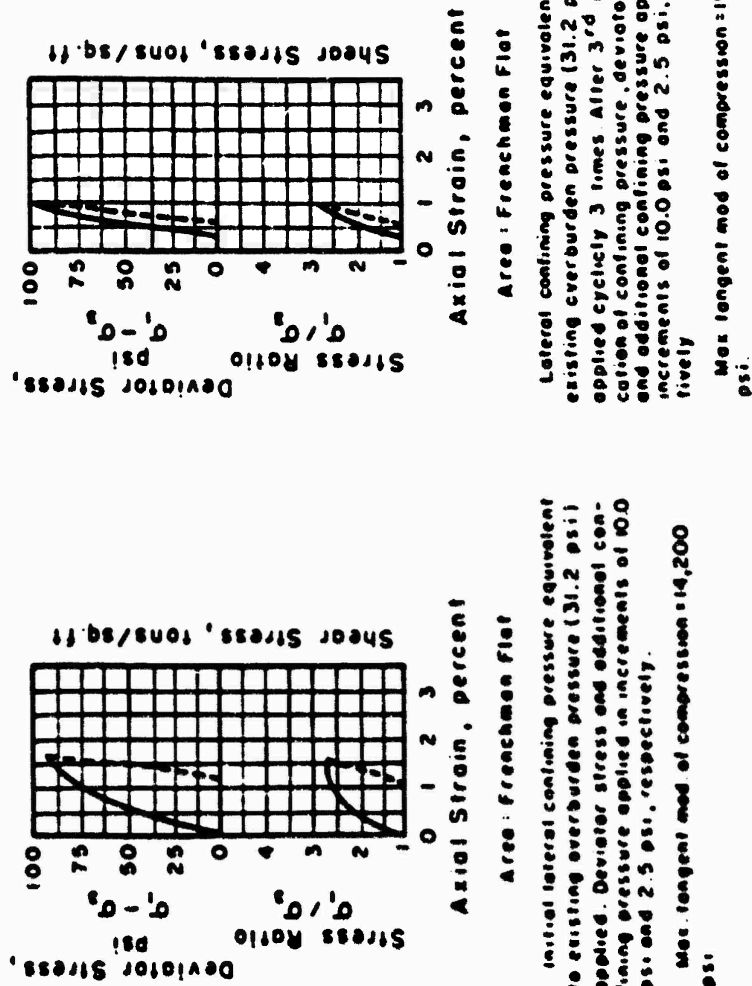


Figure 4.49 Project 1.4 constant ratio of applied stress, triaxial tests, undisturbed soil, 50-foot depth. (Reprinted from Reference 14.)

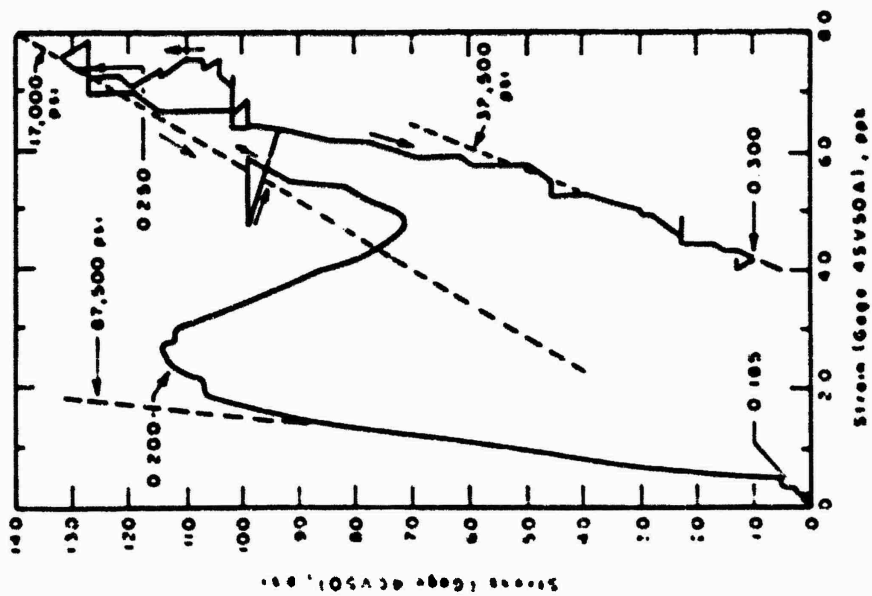


Figure 4.50 Stress-strain diagram, Station 4 (Ct: 750 feet), Shot Priscilla.

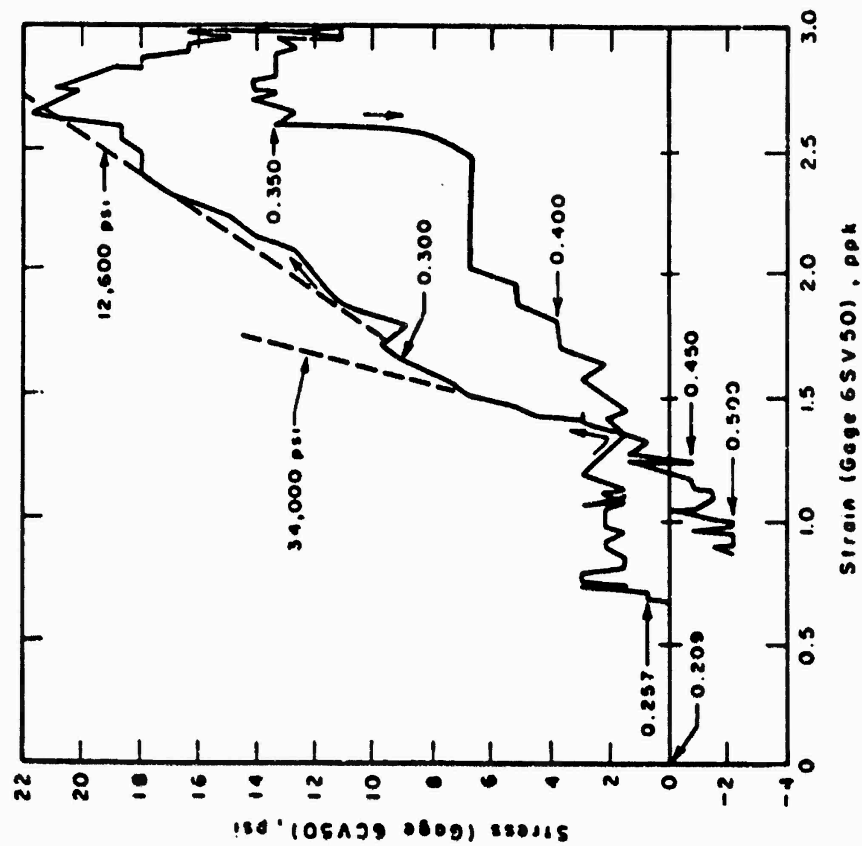


Figure 4.51 Stress-strain diagram, Station 6 (GR: 1,050 feet), Shot Priscilla.

coupling alignments which must be affected before the reliable measurement is taken. Also, it should be noted that the tests indicate strains in excess of 4 percent for 100-psi applied stress in the first cycle; the second cycle produces only about 1 percent strain for the same applied stress. The triaxial results of Figure 4.49 indicate 1 to 1.5 percent strains for lateral stresses approaching 100 psi.

4.6.2 Deduced Stress-Strain. Since stress and strain were measured independently at various depths in Frenchman Flat soil (Project 1.4), it would be possible to construct a measured stress-strain diagram. This possibility is severely limited by the fact that so many of the strain-

TABLE 4.6 PROJECT 3.8 SOIL SURVEY RESULTS

Item	Natural Soil			Compacted Backfill		
	Ranged		Average	Ranged		Average
	From	To		From	To	
Modulus of deformation (consolidation test)						
Normal to stratification						
50 psi	2,140	12,150	5,300	3,580	20,700	6,630
100 psi	3,000	13,900	6,180	4,000	20,700	8,665
Parallel to stratification						
50 psi	11,580	16,800	14,500	—	—	—
100 psi	10,330	26,780	18,550	—	—	—
Modulus of compression (triaxial test)	9,050	19,050	13,300	—	—	—
Compressive modulus (scaloscope test)	31,000	155,000	96,200	—	—	—
Modulus of elasticity (plate bearing test)						
50 psi	4,100	6,800	6,450	—	—	—
100 psi	4,900	3,900	4,400	—	—	—

time records were either lost or are in question. However, it is possible to construct such diagrams for the 50-foot depths at both Stations 4 and 6; these deduced stress-strain diagrams are shown in Figures 4.50 and 4.51.

The form of the stress-strain picture of Figure 4.50 is quite different from the Project 3.8 curves of Figure 4.48. This is due probably, to the rather abrupt increase of stress (4CV50) at this station, and it results in a tangent modulus of about 87,500 psi in the early portion of the curve. Calculation of the modulus corresponding to the peak strain yields 17,300 psi, and the unloading modulus is about 32,500 psi. Also significant is the fact that the soil attains a strain of less than 1 percent (about 0.8 percent) at a stress of 130 psi, which means that the Project 3.8 triaxial tests approximated the working range of dynamic soil response more exactly than did the compaction tests. The residual strain (after unloading) of about 0.4 percent also agrees with the triaxial test residual magnitudes.

The situation at Station 6 is also atypical but for the opposite reason from that at Station 4. At Station 6, the stress appears to increase unusually slow while the strain is attaining readable values. The best choice of tangent modulus corresponding to peak stress and strain computes to 12,600 psi, a value which again agrees best with the modulus obtained from the Project 3.8 triaxial tests. The curve also indicates a small residual strain at this depth.

It would be unwise to draw any firm conclusions from the small amount of data available. Tentatively, it can be said that, as presently conceived, the laboratory triaxial tests are more useful in correlation with blast results than are the compaction tests. Still to be resolved is the question of the relationship between the tangent modulus so computed and the modulus determined from measurements of seismic velocity.

Chapter 5

CONCLUSIONS and RECOMMENDATIONS

5.1 CONCLUSIONS

5.1.1 Instrument Performance. For Operation Plumbbob Project 1.4, full length records were obtained on 75 percent of the total gage channels and partial records on an additional 12 percent. The failures were caused principally by a jammed oscillograph recorder and cable trouble on the strain gage installations.

Five out of the ten short-span strain gages installed on the sides of the two deep holes failed to give useful data, and three of the five useful records were incomplete. It is concluded that the reliability of these gages could be enhanced by improving the method of coupling to the soil and by redesign of the cable connector at the gage end.

5.1.2 Acceleration and Velocity Wave Forms. For ground shock accelerations induced by air blast, there is no ideal wave form. The integral of vertical acceleration, vertical particle velocity in the soil, is the more familiar of ground motion parameters since it bears a direct relationship to the overpressure. It is possible to separate the predominant earth acceleration and velocity wave forms into six groups associated with the character of the input; namely,

1. Air-blast wave ideal and overpressure high, traveling supersesimically.
2. Same as Item 1 above, except lower overpressure.
3. Air-blast wave traveling transesimically, first indication of outrunning.
4. Air-blast wave in early stages of precursor development, peak overpressures high, traveling supersesimically.
5. Air-blast wave extremely disturbed, in most violent precursor region, traveling super- or transesimically.
6. Complete outrunning, refracted ground wave arrives before local induced effect, air wave traveling subsesimically.

Even though the blast wave may be traveling with supersesimic velocity, i.e., no outrunning, the signal produced by the refracted wave may be sufficient to modify the velocities in the later portions of the ground shock disturbance. At depth, outrunning occurs earlier than at the surface.

5.1.3 Signals from Remote Sources. When the propagation velocity of the air-blast wave front is larger than the compression wave velocity in the soil, signals will not be observed underground prior to the arrival of the air wave over the gage. As the air wave velocity decreases with distance from ground zero, the information given to the earth will eventually arrive before the arrival of the local signal. This may occur either when a near-surface seismic velocity is greater than the air-blast velocity or by transmission through the soil along a curved path which dips into the higher-velocity lower earth strata, i.e., seismic refraction.

For Shot Priacilla, it was concluded that outrunning occurred at the ground surface at about 2,500-foot ground range, due to a signal originating at about 1,900-foot ground range. However, it is possible for outrunning to occur at closer ranges for deeper measurements, and refracted signals may be evident on records after the arrival of the local effects. Although Project 1.4 acceleration results (measurements to 1,350-foot ground range) showed no outrunning, they showed presence of refracted signals from remote sources, particularly at the deeper gages.

The remote source disturbances, whether outrunning or not, are extremely bothersome when one is attempting to integrate the acceleration-time records to obtain velocity-time and displace-

ment-time. Any criteria used for determining the time of zero velocity may be useless in the presence of remote source signals.

5.1.4 Attenuation of Ground Shock with Depth. Maximum downward acceleration data indicate that between 5- and 10-foot depths the attenuation varies between 30 to 45 percent, except at the 550- and 650-foot ground ranges where the attenuation is practically negligible. The results at greater depths, taken into consideration with the measured seismic profile at Frenchman Flat, suggest that the wave theory concerning energy transfer at an interface between two materials may be valid. The theory states that:

1. If an accelerometer is located at or near the transition from a hard to a soft material, the peak acceleration is increased.

2. If an accelerometer is located at or near the transition from a soft to a hard material, the peak acceleration is decreased.

The peak outward horizontal acceleration at the 10- and 50-foot depths shows less attenuation with depth than does the corresponding peak downward acceleration; numerically, the attenuation is about 40 percent for the outward component and about 80 percent for the downward.

When all pertinent data are included, it is found that power law decay with depth of peak downward acceleration agrees best with the experimental results.

For peak downward velocity (or velocity-jump data), an exponential decay law appears to represent the data better than a power law. On Shot Priscilla, at the two stations where measurements were obtained to 50-foot depth, the attenuation of peak downward velocity is similar and is apparently little influenced by the underlying soft layer documented in the refraction seismic survey.

The peak outward velocity data from Shot Priscilla showed somewhat less attenuation with depth than the downward component at 275-pai overpressure; at the larger ground range (100-pai overpressure), the outward peak velocity at 50-foot depth was twice that at 10 feet. This effect was traced to the influence of signals from remote sources closer to ground zero.

The vertical velocity-time curve is similar to the overpressure-time curve when the air-blast wave is supersonic. The velocity peak is, however, more rounded and progressively lags the wave front by an increasing amount as the depth increases. Below 10-foot depth, the rise time to peak velocity increases significantly, even for rapid air-pressure onset.

The attenuation of peak displacement, obtained from successive integration of the acceleration-time data, corresponds closely to the attenuation of peak velocity. However, the larger than expected displacements below 5 feet at the 100-pai overpressure station can be explained by a refracted ground wave superimposed on the motion induced by the main air-blast wave. It should be noted that the double integration method of obtaining displacement-time is probably not reliable for times beyond the peak value.

The attenuation of maximum vertical stress, as determined by Carlson-type gages, is slight between the surface and 5-foot depth; the attenuation at shallow depths is probably a function of the duration of the overpressure input pulse, the shorter the input pulse the greater the attenuation with depth.

For the deeper stress measurements, the pattern of attenuation follows the rule of halving the peak stress for each 10-foot increase in depth. However, the increase in stress at 50 feet tends to deny the validity of this rule.

Although several possibilities are offered to explain the seeming anomalous stress results at 50-foot depth, it is probable that the measurements are influenced to some degree by all the suggested mechanisms. That is, the stress measured at 50 feet may be a function of the soil layering structure, the character of the backfill, and inequalities of planting or tamping methods in the vicinity of the gages.

In general, the stress-time wave forms compare well with the air overpressure input; below 10-foot depths, the time-to-peak increases noticeably over that observed on the surface air-blast pressure.

It is difficult to determine the relative validity of the free-field stress results obtained on Project 1.4. The control of backfill operations during Priscilla was considered optimum, and

extraordinary care was taken in the placement of gages; still the stress measurements appeared internally inconsistent. It is concluded that, unless an alternative measurement method can be devised, stress must be derived from other primary measurements such as strain and acceleration, which are more independent of hole size and character of the backfill.

In addition to the short-span strain gage results, it is possible to compute the average vertical strain between accelerometer positions from the double integrations (i.e., displacement-time plots). At the 275-psi overpressure station, the peak strain suffers a pronounced decrease between 1- and 30-foot depths. At greater depths, the vertical strain levels off to a constant value. On the other hand, the data obtained at the 100-psi overpressure station show practically no change in vertical strain with increasing depth. This difference in behavior is probably traceable to the character of the input overpressure; the rise times associated with the 100-psi input are significantly longer than at the high pressure station.

5.1.5 Ground Shock and Overpressure. When the ratio of peak acceleration to peak overpressure is plotted versus peak overpressure, the values at high overpressures (above 200 psi) are high, decreasing as the overpressure drops and as the precursor wave develops, finally increasing somewhat below 10 psi when the precursor has dissipated. The effect of device yield, if any, does not appear to be discernible. No systematic variation with height of burst is to be found; also, the trend toward higher ratios at extreme ground ranges may be associated with outrunning of the ground wave.

In conformity with elastic theory, subsequent to outrunning of the ground wave, the velocity-jump peak overpressure ratios increase with decreasing pressure (i.e., increasing ground range). There appears to be no systematic variation with either yield, overpressure level or wave form, or test area. The experimental ratios agree well with the theoretical result, particularly if the velocity of propagation of the ground wave is determined from measured accelerometer arrival times.

The fact that the finite amplitude stress waves appear to propagate slower than the seismic waves suggests plastic flow conditions in the soil; also, relative significance of the soil modulus determined from seismic velocity is not, as yet, completely clear.

Consideration of the peak vertical displacement-overpressure impulse ratios indicates a definite increase in the ratio with increasing peak overpressure in the range of 50 to 300 psi. However, the wide scatter in displacement data precludes any firm conclusions. Comparisons between the Project 1.4 peak displacement data (obtained by integration of accelerograms) and the Project 1.5 long-span strain results show good agreement between these two independent measurements.

5.1.6 Response Spectrum of Ground Motion. The response spectrum is defined as the maximum response of a linear, single degree of freedom, spring mass system, relative to the motion of the ground. The displacement spectrum may be determined either by direct measurement with read gages, by numerical calculation of the response of a linear system (e.g., accelerometer) to the ground motion, or through the use of the electrical-mechanical analogy. An accelerometer-galvanometer system will yield faithful results if its natural frequency is more than twice the fundamental frequency observed in the ground motion.

From the results of the displacement response spectra, it does not appear that the change in character of the response can be associated with the local ground wave, but this change probably is due to interference of the refracted ground-transmitted wave.

Using overpressure positive phase duration as a normalizing factor, it is possible to show correlation of response spectra obtained under different input conditions. The normalized velocity spectra for 30-foot depth when compared with spectra at 5- and 10-foot depths show similar maxima although the frequency at which this maximum occurs decreases with increasing depth.

Weighing the relative advantages and disadvantages of the read gages and accelerometers for determination of response spectra, one concludes that neither gage result is completely sufficient for definitive spectra; the most advantageous instrumentation probably will consist of both types placed as a pair.

5.1.7 Soil Stress-Strain Considerations. Since stress and strain were measured independently (versus time) at various depths in Frenchman Flat soil, it is possible to construct a measured soil stress-strain diagram. Such diagrams may be constructed for the 50-foot depths at Stations 4 (275-psi input) and 6 (100-psi input).

The deduced stress-strain relations appear to agree best with the laboratory triaxial tests performed upon Frenchman Flat soil samples by Waterways Experiment Station (Project 3.8). The consolidation test results yield soil moduli which are much lower than those indicated by the deduced stress-strain curves. Tentatively, it can be concluded that the laboratory triaxial tests are more useful in correlation with blast results than are the compaction tests. However, still to be resolved is the question of the relationship between the tangent modulus so computed and the modulus determined from measurements of seismic velocity.

5.2 RECOMMENDATIONS

It is recommended that future work on the problem of ground motion induced by air blast include the following:

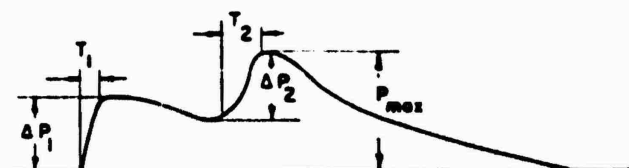
1. In conjunction with any future ground motion measurements, means should be provided for determination of the seismic signal arrivals at each measurement position; a geophone would serve this purpose.
2. Attention should be given to devising laboratory soil test methods which give promise of correlating with field test results.
3. Work should continue for the development of a reliable gage (or gages) which will measure directly velocity-time and/or displacement-time of ground motion. These measurements would almost completely eliminate the present uncertainty associated with integrated acceleration data.
4. The theoretical aspects of the problem should be pursued vigorously, from the standpoint of pure elasticity and, also, to include the dissipative and layered aspects of the soil medium.
5. In ground motion measurements an independent measurement of the motion of the ground relative to some fixed point in the earth made by a mechanical gage is useful in checking displacement results from integrations of accelerograms.

Appendix A

SYMBOLS and OVERPRESSURE WAVE FORM CLASSIFICATION

A.1 SYMBOLS

- A** = acceleration, g (vertical)
P = density, lb/cu ft
E = Youngs' modulus, psi
S = strain, vertical
P = applied air pressure, psi
 ΔP_1 = total rise of first peak of input pressure wave
 ΔP_2 = total rise of second peak of input pressure wave
C = stress, vertical, psi
 σ = Poissons' ratio
 T_R = total rise time of stress (or velocity) wave at a particular depth (assuming half-cosine wave form of rise), sec
 T_1 = rise time of first peak of input pressure wave
 T_2 = rise time of second peak of input pressure wave
 T_y = rise time of stress (or velocity) wave produced by travel to depth y
V = particle velocity (vertical), fps
 V_0 = seismic (compressional) wave velocity, fps
x = range, ft
y = depth, ft
 $\phi = \sqrt{\frac{1 - \sigma}{(1 + \sigma)(1 - 2\sigma)}}$

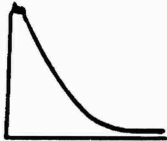
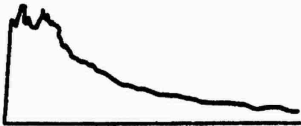
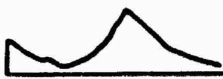
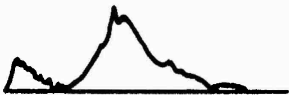
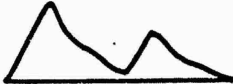
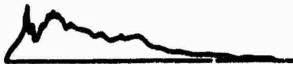
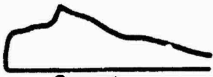



AIR BLAST WAVE FORM, PRECURSOR TYPE I



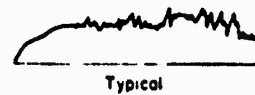
AIR BLAST WAVE FORM, GENERALIZED

A.2 OVERPRESSURE-WAVE-FORM CLASSIFICATION

Type	Description of Form	Relation to Previous Type
0	A sharp rise to a double-peaked maximum; peaks close together in time and approximately equal in amplitude.	In its ideal form, it is the classical single-peaked shock wave but is usually recorded as a double-peaked wave.
	 <p>General</p>	 <p>Typical</p>
1	A sharp rise to first low peak followed by either a plateau or a slight decay, then a higher second peak preceding the rapid decay. Time interval between first and second peaks can vary significantly; shock-like rises are evident.	The first low peak indicates the existence of a disturbance which travels faster than the main wave. This type is distinctly nonclassical.
	 <p>General</p>	 <p>Typical</p>
2	Same as Type 1 except that second peak is less than first.	The second peak has decayed to a lower value than the first and has become more rounded and less distinct. Second peak finally disappears.
	 <p>General</p>	 <p>Typical</p>
3	A first large, rounded maximum followed by decay; then a later, usually smaller, second peak. Pressure rises may be slower than for Type 2.	The first peak of Type 3 has developed to become the rounded maximum, while the second peak has decreased in magnitude with respect to the first.
	 <p>General</p>	 <p>Typical</p>

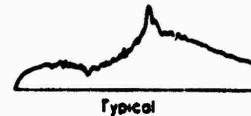
- 4 A long-rise-time flat-topped form which exhibits a long decay time and much hash.

The relatively sharp pressure rise of Type 3 has been replaced by a slow rise and the second peak has disappeared.



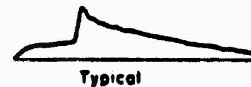
- 5 A pressure rise to a rounded plateau which is followed by a slow rise to a second, higher peak.

The single-peaked hashy form of Type 4 seems to develop a compression-type second peak, which may be the first indication of the return of the main wave.



- 6 A clear-cut double peak form with a rise to a plateau which slopes upward, then a shock rise to a peak.

This is clearly a cleaned-up Type 5, with the compression-type second peaks becoming sharp.



- 7 A shock rise to a peak followed by either a slight gentle rise, a plateau, or in later examples, a slow decay.

The second peak of Type 6 has overtaken the first peak, resulting in a wave form which is close to classical; sharp, single peak is not evident.



- 7R Refers to Type 7 in region of regular reflection where a second (reflected) shock front is evident.

Second rise due to reflected wave.



- 8 A classical wave form.

Sharp single-peaked form, followed by classical decay.



- 8R Refers to classical wave form in region of regular reflection.

Second rise due to reflected wave.



Appendix B

CATALOG of GROUND MOTION MEASUREMENTS

**TABLE B-1 SUMMARY OF NEVADA SURFACE AND AIR NUCLEAR BURSTS
ON WHICH STRONG GROUND MOTION WAS MEASURED**

Y, Yucca Flat; and FF, Frenchman Flat.

Operation	Shot	Yield	Height of Burst	Date	Area
		kt	ft		
Buster-Jangle	8	1.19	3.5	November 1951	NTS-Y
Tumbler-Snapper	1	1.05	793	April 1952	NTS-FF
	2	1.15	1,109	April 1952	NTS-Y
	3	30	3,447	April 1952	NTS-Y
	4	19.6	1,040	May 1952	NTS-Y
Upshot-Knothole	1	16.2	300	March 1953	NTS-Y
	9	26.0	2,423	May 1953	NTS-FF
	10	14.9	524	May 1953	NTS-FF
Plumbbob	Priscilla	39	700	June 1957	NTS-FF
	Whitney	19.2	500	September 1957	NTS-Y
	Galileo	11	500	September 1957	NTS-Y
	Smokey	43	700	August 1957	NTS-Y
	Stokes	19	1,500	August 1957	NTS-Y
	Charleston	11.5	1,500	September 1957	NTS-Y

TABLE B.2 NUMBER OF GROUP. OTION MEASUREMENTS, NTS
Y, Yacca Flat; FF, Freshman Flat; H, horizontal direction; and V, vertical direction.

Operation	Overpressure psi	Depth, ft										Source of Data *
		Surface	1	5	10	20	30	50	60	100	200	
Jangle, Y	> 50				3H	1H	1H					
					3V	1V	1V					
	> 10				7H	2H	2H					WT-414
	Total				7V	2V	2V					WT-388
Tumbler, FF					11H	4H	4H					
					11V	4V	4V					
	> 10			1H				1H				WT-514
	Total			4V				1V				WT-514
Tumbler, Y				2H				2H				
				10V				2V				
	> 50			1V								WT-514
	Total			7V				4H				WT-517
Upshot-Knothole, FF				6V	30V			4H				
				1V	2H			6V				
	> 50			8H								WT-782
	Total			9V	2V							WT-711
Upshot-Knothole, Y				14V	2V							WT-716
				1H								WT-712
	> 10			1H								WT-716
												ITR-1403
Plumbbob, FF		2H			4H		1H	2H	3H	4H		ITR-1404
		3V	2V	7V	12V	2V	5V	2V	4V	3V	1V	ITR-1405
	> 50											ITR-1487
	Total											ITR-1487

* First source is air blast.

† Reed gage data.

TABLE B.3 NUMBER OF GROUND MOTION MEASUREMENTS, EPG
H, horizontal direction; and V, vertical direction.

Operation	Depth	Overpressure	Number	Source of Data *
	ft	psi		
Greenhouse	1 to 6 †	> 50	4H	
			4V	
		> 10	11H	WT-53
			10V	WT-69
		Total	13H 13V	
Ivy	17	> 50	1H	
			1V	
		> 10	3H	WT-602
			3V	WT-9002
		Total	4H 5V	
Castle	15 to 17	> 10	3H	WT-920
			2V	WT-9002
Redwing	2.5	> 50	1H	ITR-1302
			6V	ITR-1364
Hardtack	1 to 100	> 50	17H	ITR-1613
			19V	

* First source is air blast.

† Varies with station.

TABLE B.4 SUMMARY OF MOLE ROUNDS (256-POUND TNT)

Height of Burst, ft	0	0.83	1.65	3.18	6.35
λ (scaled height of burst for HE)	0	0.13	0.26	0.50	1.0
Test Area					
Utah dry clay	1	1	1	2	1
Nevada gravel and sand mix	1	1	2	2	1
California wet sand	1	1	-	-	-
California moist clay	-	1	-	-	-

TABLE B.5 NUMBER OF GROUND MOTION
MEASUREMENTS, JANGLE HIE-4

Charge	Height of Burst	Overpressure	Number of Observations, 5 ft
	ft	psi	
3,500-lb/TNT	2	> 50	4H
			4V
		> 10	9H
			8V
		Total	10H
			10V

Appendix C

RECORD INTEGRATION and INSTRUMENT RESPONSE

Ground motion instrumentation has been confined, except for the long-span displacement gages used on Shot Priscilla, to accelerometers. Determination of velocity and displacement requires numerical integration of these records. Prior to Shot Priscilla, this was usually done with a planimeter as a two-step process. Integration of Priscilla records has been performed numerically using the IBM 650. Acceleration records were read at $\frac{1}{4}$ -msec intervals throughout the portion of maximum fluctuation. As the records smoothed out, this time interval was lengthened successively to 1, 2, and 4 msec, mainly as an economy measure. Records were read to the end of the air-blast positive phase or past the point of apparent signal, whichever was longer.

C.1 ACCELERATION BASELINE SHIFT

It is an indisputable fact that the ground motion due to air-blast pressure must cease at some time after the passage of the blast wave. Most integrations indicate, in varying degree, that the velocity at the end of the integration is not zero. This result can be interpreted as an acceleration record baseline shift, which is affected during recording or during reading of the record. If it can be assumed that there are no frequency response problems (see Section C.2), the source of the difficulty can be traced to the character of the acceleration-time wave form. Reference to Figure 4.1a shows that the duration of the first acceleration peak is a small fraction of the total record length. Therefore, a small error, perhaps only one or two percent of the peak acceleration, will accumulate as time increases to result in a significant error in velocity at the end of the integration.

Speaking instrumentally, there are many possible ways the acceleration record baseline (zero signal reference) could shift. However, in this analysis the shift is considered as a reading error, a conclusion which is substantiated by the fact that the amount of correction that is necessary to achieve zero velocity at the end of the record is frequently within the least count of the reading equipment (see Table C.1).

Figure C.1 shows some typical examples of velocity-time wave forms obtained from types a, b, or c acceleration-time wave forms (Figure 4.1). It is thought that a good criterion for zero velocity in such cases is that the velocity equals zero at a time after signal arrival equal to the duration of the air-blast input positive phase. For this criterion, Figure C.1 indi-

cates how the baseline would be shifted on the velocity-time plots; subsequently, the velocity-time plots relative to the shifted baselines would be integrated to obtain the corrected displacement-time plots. It should be pointed out that, in the case of gages buried deeper than 50 feet in a soil whose seismic velocity varies significantly with depth, it would be unwise to apply the above criterion for zero velocity even for ideal overpressure inputs. Each record would have to be regarded as a special case.

As the peak acceleration decreases, the problems of accurate record reading diminish with the exception of ground waves from remote sources, which result in exceptionally complicated records. A typical example (type f) is shown in Figure C.2, where the upper portion of the figure illustrates the original integration without correction. Beyond 600 msec the velocity increases (negatively) linearly. The linear baseline shift required to correct the velocity to zero at the end of the ground motion is shown as well as the corrected velocity. However, it is at once apparent that the criterion of zero velocity at the end of the air-blast pressure pulse is not applicable when signals from remote sources are present. For these, each uncorrected velocity must be plotted and a best judgment made as to the time zero velocity is attained; thus it is important that the acceleration-time record be read to times beyond which the signal apparently has settled down to small amplitudes. In complex cases, the practice has been adopted that the baseline be adjusted to maximize the resulting peak displacement. The displacement-time records will then indicate a residual displacement equal to the peak displacement. If more than one choice of baseline shift appears reasonable, the extremes are calculated.

If the velocity records appear to require other than a single linear correction; e.g., a series of linear corrections attached end-to-end, the data are considered suspect and not corrected or tabulated.

Table C.1 includes a summary of the magnitude of the corrections made in the integrations of the Priscilla acceleration-time records. In terms of the peak acceleration, the baseline shifts varied between 0.06 and 4.4 percent, which corresponds to between 0.1 and 5 counts on the electromechanical reader (Oscar). The reader is set up so that one count equals slightly less than $\frac{1}{100}$ -inch deflection on the gage record and the reproducing accuracy of a single reader is approximately ± 2 counts. Thus it appears that the need for a

TABLE C.1 BASELINE CORRECTIONS, SHOT PRISCILLA

(1) and (2) indicate alternate baseline choices.

Gage	A Uncor	A Cor	$\frac{\Delta A}{A \text{ Cor}}$	Oscar Counts in ΔA	V Uncor	V Cor	$\frac{\Delta V}{V \text{ Cor}}$	D Uncor	D Cor	$\frac{\Delta D}{D \text{ Cor}}$
	g	g	pct		ft/sec	ft/sec	pct	ft	ft	pct
1V5	363.7	357.7	1.64	3	26.7	25.3	5.34	2.14	0.693	208.
1V10	221.9	225.9	1.74	3	13.9	14.8	6.11	0.298	0.343	13.1
2V5	174.9	173.4	3.17	4.5	20.7	17.9	14.98	1.47	0.586	150.2
2V10	150.6	151.9	0.87	1.5	19.6	20.2	2.95	0.718	0.964	25.5
3V5	120.5	120.9	0.27	0.3	16.1	16.3	1.18	0.717	0.839	14.5
3V10	129.6	129.3	0.22	1	13.3	13.1	1.50	0.631	0.555	13.7
4V1	189.3	188.3	0.54	1	17.0	15.9	7.20	0.898	0.644	35.2
4V5	53.9	54.7	1.35	2	14.4	15.3	5.53	0.543	0.768	29.3
4V10	38.5	39.2	1.69	2	10.1	10.9	7.13	0.373	0.521	28.4
4V20A	46.0	46.6	1.13	6	6.91	7.64	9.65	0.326	0.486	32.5
4V30A	37.9	38.1	0.35	2	7.72	7.92	2.54	0.345	0.388	11.1
4V50	13.2	13.5	2.27	3	4.51	4.96	9.13	0.221	0.311	28.9
4V50A	12.5	12.8	2.16	5	4.25	4.66	8.73	0.207	0.289	28.4
4H10	14.2	14.3	1.06	2	1.27	1.42	11.1	0.016	0.078	79.5
4H50	5.08	5.07	0.10	0.3	0.890	0.885	0.56	0.011	0.014	—
5V5	24.3	—	—	—	—	—	—	—	—	—
5V10	16.7	—	—	—	—	—	—	—	—	—
6V1 (1)	21.8	21.5	1.23	1	6.72	6.12	9.87	0.300	0.218	37.6
(2)	21.8	21.7	0.34	0.1	6.72	6.55	2.63	0.348	0.299	16.4
6V5 (1)	16.7	16.7	0.08	0.1	6.05	6.02	0.53	0.274	0.267	2.62
(2)	16.7	16.8	0.33	0.4	6.05	6.18	2.17	0.273	0.307	11.1
6V20 (1)	10.5	10.5	0.23	0.2	4.13	4.07	1.55	0.322	0.306	5.23
(2)	10.5	10.5	0.20	0.2	4.13	4.06	1.37	0.323	0.307	5.21
6V20A (1)	9.80	9.93	1.32	2	3.61	3.96	8.76	0.221	0.275	19.6
(2)	9.80	9.97	1.68	2	3.61	4.06	10.9	0.220	0.293	24.9
6V30	6.49	6.53	0.64	0.5	3.49	3.59	2.78	0.191	0.214	10.6
6V30A	6.32	6.40	1.28	3	3.32	3.56	6.67	0.166	0.209	20.6
6V50 (1)	2.62	2.72	3.71	4	1.97	2.30	14.2	0.125	0.169	26.0
(2)	2.62	2.74	4.39	4	1.97	2.36	16.4	0.126	0.182	30.8
6H10	1.30	1.31	0.53	0.3	0.383	0.400	4.25	0.006	0.006	25.0
6H30	2.53	2.54	0.71	2	0.677	0.920	4.67	0.620	0.022	9.09
7V5	9.23	9.16	0.85	1	3.09	2.84	8.65	0.376	0.239	57.3
7V10 (1)	4.84	4.84	0.65	0.1	1.50	1.49	0.80	0.086	0.090	4.44
(2)	4.84	4.78	1.21	2	1.50	1.67	10.11	0.178	0.154	15.6
Average			1.17	1.9			6.25			32.30

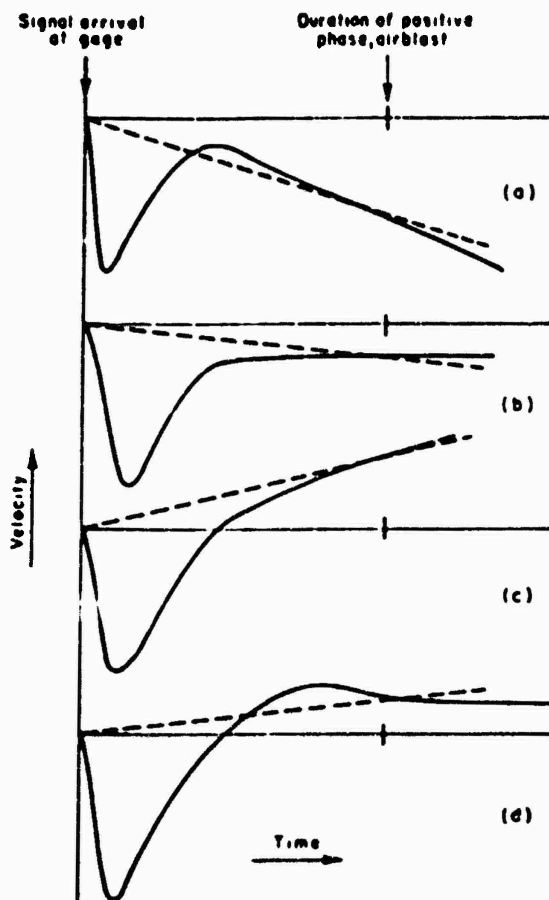


Figure C.1 Typical velocity-time wave forms from Types a, b, or c acceleration-time wave forms.

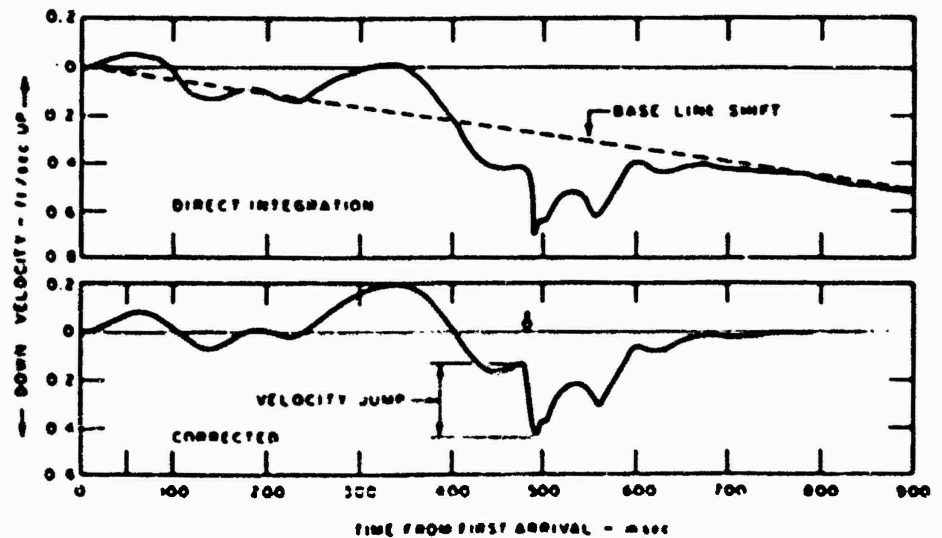


Figure C.2 Uncorrected and corrected vertical velocities.

baseline shift in the integration process can be traced, with few exceptions, to reading errors. This fact puts a great emphasis upon accurate record reading, if point-by-point integration is to be attempted. It is also apparent from the table that the corrections in terms of average percent of peak amplitude were smallest for acceleration (1.17 percent), larger for velocity (6.25 percent), and largest for displacement (32.2 percent).

In some cases, particularly on records obtained at Stations 6 and 7, two independent baseline corrections

were made, for damping between 0.5 and 0.6 critical, transient pulses are reproduced fairly well for pulse frequencies of one sixth the gage frequency. When the pulse frequency becomes equal to or greater than one half the gage frequency, considerable error in gage response along with phase distortion may be expected. For the half sine pulse, the errors are approximately 20 percent. If the damping is only 0.4 critical, overshoots of 50 to 100 percent occur.

In general, the frequency response of accelerometers used in weapons effects experiments has in-

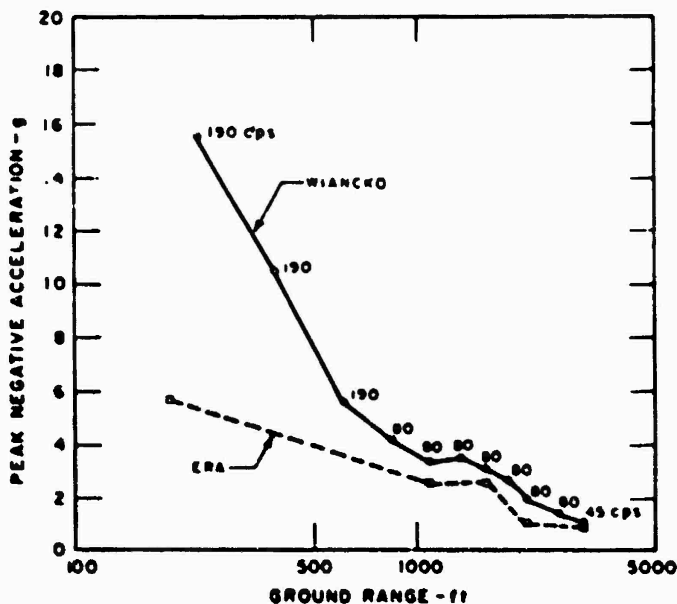


Figure C.3 Comparison of ERA and Wiancko accelerometer data, Tumbler Shot 1, 5-foot depth (numbers adjacent to data indicate accelerometer natural frequencies).

were made and the integrations carried through using both. Deviations in peak velocity from the two choices varied between 2.5 and 10.8 percent, whereas the peak displacements were separated by as much as 41.5 percent. The largest deviations between the two baseline choices were observed on the TV10 record; it is probably more than coincidence that this record displays the most complex wave form due to ground shock signals from remote sources. This result leads to the conclusion that integration of acceleration-time records possessing complex wave forms involves a good deal of judgment and is necessarily less accurate than integration of simple records, i.e., those with local effects only.

C.2 INSTRUMENT RESPONSE

The complex pattern of the ground accelerations makes a precise statement of error due to frequency response intractable. A few general remarks can be made, however, for simple inputs such as a half sine

wave, for damping between 0.5 and 0.6 critical, transient pulses are reproduced fairly well for pulse frequencies of one sixth the gage frequency. When the pulse frequency becomes equal to or greater than one half the gage frequency, considerable error in gage response along with phase distortion may be expected. For the half sine pulse, the errors are approximately 20 percent. If the damping is only 0.4 critical, overshoots of 50 to 100 percent occur.

In general, the frequency response of accelerometers used in weapons effects experiments has increased markedly since Operation Greenhouse. The natural frequency of accelerometers used on Operation Jangle varied between 10 and 140 cps, (Reference 19), on Operation Tumbler between 80 and 190 cps, (Reference 2), and on Operation Upshot-Knothole all vertical accelerometers had frequencies of 450 cps, (Reference 9). In the latter, the frequency response was limited by the galvanometer circuit at a slightly lower value. Shot Priscilla response characteristics were similar to those of Operation Upshot-Knothole.

A graphic illustration of inadequate frequency response is found in the comparison of ERA accelerometer results (Reference 20) and Wiancko accelerometer results on Tumbler (Reference 2). ERA accelerometers with natural frequencies of the order of 40 to 50 cps were used to back up the primary instrument line. Figure C.3 compares the two sets of data on Tumbler Shot 1. For accelerations greater than 5 g, the ERA equipment fails to give satisfactory results.

Appendix D

SCALING of POSITIVE OVERPRESSURE IMPULSE and DURATION

Figures D.1 and D.2 present the major portion of available data on impulse and duration for overpressures greater than 10 psi. As a guide in extrapolating previously presented correlations, (Reference 29), results of the theoretical solution for the point source explosion in real air (Reference 30) are included in the figures, modified by 2W theory (surface bursts).

Impulse data on Priscilla are in agreement with the theoretical curve at high pressures. At intermediate pressures (10 to 100 psi) measured impulse is from 0 to 50 percent greater (due to precursor formation) than 2W theory predicts. While it is understood that 2W theory does not apply theoretically to air bursts, it is believed that impulse resulting from 2W theory will be a lower limit. Impulse predictions used throughout the report are based on this postulate, applying a 50 percent correction as an upper limit.

Data on duration do not follow the theoretical calculations for overpressures greater than 100 psi. It is suspected that this may be a limitation of the instrumentation. In order that the maximum overpressure does not over-range the gage or recording instrumentation, the sensitivity of the system must be reduced at high pressures. A check of the SRI system indicates that when consideration is given to the absolute accuracy of reading camera records, the accuracy of reading pressure amounts to approximately 5 percent of the peak overpressure. Using this criterion, the theoretical duration curve has been constructed for the duration at which the overpressure reached 5 percent of its peak value. This curve deviates markedly from the theoretical phase duration (associated with zero overpressure) as the pressure increases. However, over 95 percent of the total positive overpressure impulse is included before the overpressure drops to 5 percent of the peak overpressure. Hence, the theoretical curve of Figure D.2 is believed to be a legitimate guide in the high pressure region provided allowance is made for the increased duration of the positive phase in the 10- to 100-psi region due to precursor formation.

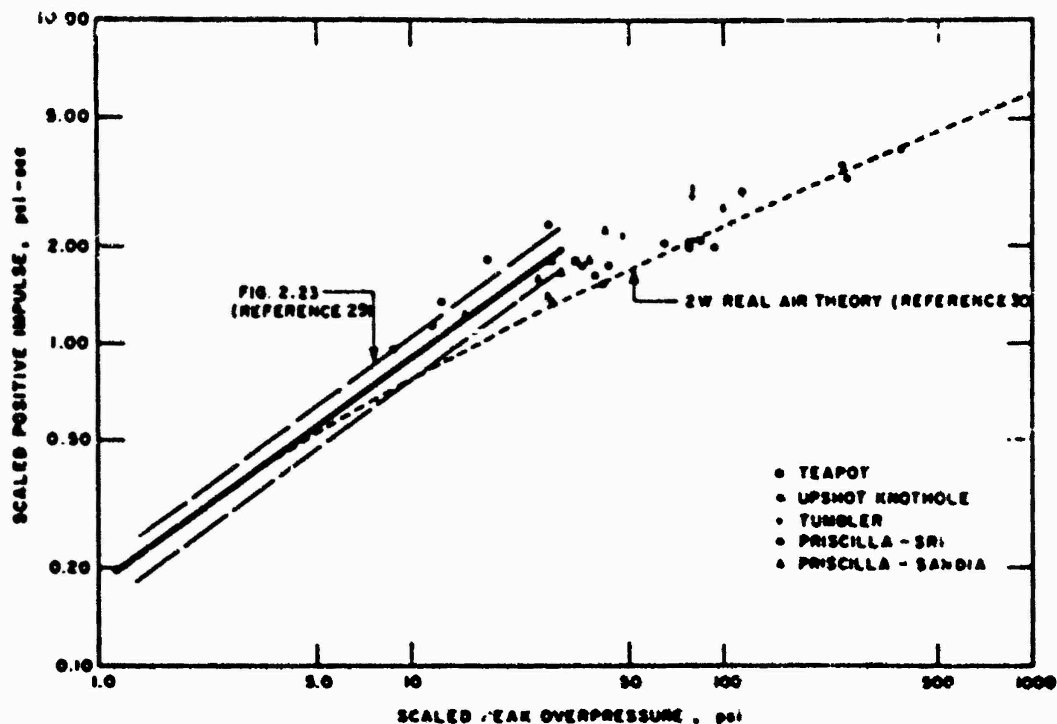


Figure D.1 Positive overpressure impulse versus peak overpressure.

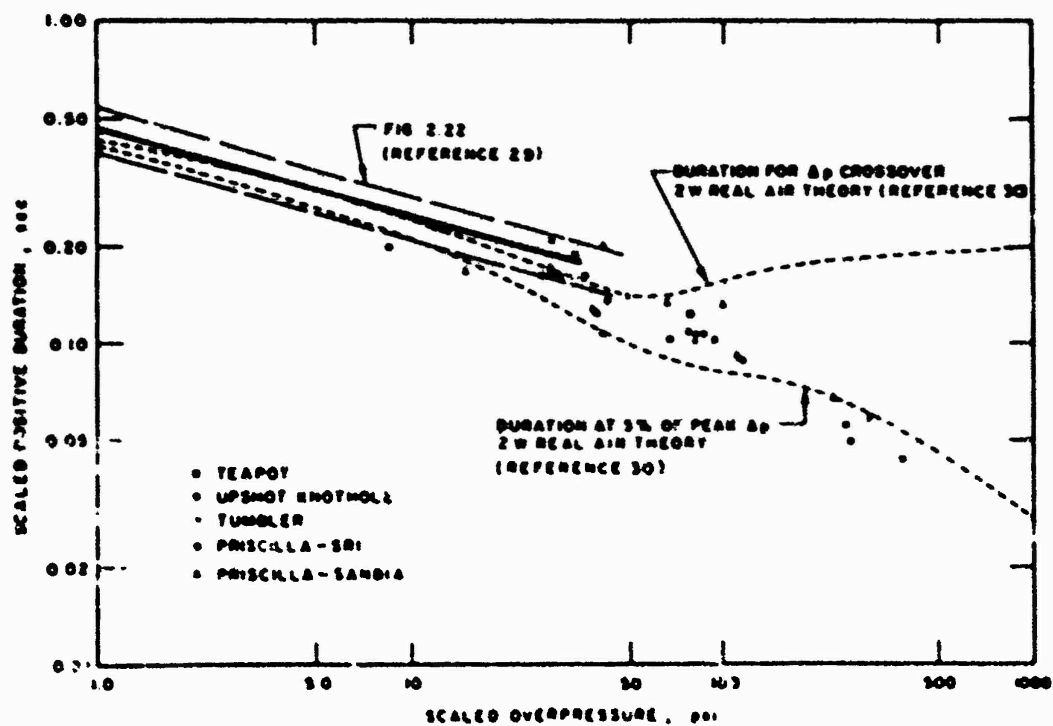


Figure D.2 Positive overpressure duration versus peak overpressure.

DISTRIBUTION

Military Distribution Category 11

ARMY ACTIVITIES

- 1 Deputy Chief of Staff for Military Operations, D/A, Washington 25, D.C. ATTN: Dir. of JAG
- 2 Chief of Research and Development, D/A, Washington 25, D.C. ATTN: At-Staff Div.
- 3 Assistant Chief of Staff, Intelligence, D/A, Washington 25, D.C.
- 4 Chief of Engineers, D/A, Washington 25, D.C. ATTN: ENCHB
- 5 Chief of Engineers, D/A, Washington 25, D.C. ATTN: ENCHB
- 6 Chief of Engineers, D/A, Washington 25, D.C. ATTN: ENCHB
- 7-9 Office, Chief of Engineers, D/A, Washington 25, D.C. ATTN: ENCHB
- 10-11 Commanding General, U.S. Continental Army Command, Ft. Monmouth, N.J.
- 12 Director of Special Weapons Development Office, Headquarters CSMAC, Ft. Belvoir, Mo. ATTN: Cont. Chapter 1, Personnel
- 13 President, U.S. Army Artillery Board, Ft. Sill, Okla.
- 14 President, U.S. Army Air Defense Board, Ft. Belvoir, Mo.
- 15 Commandant, U.S. Army Command & General Staff College, Ft. Leavenworth, Kansas. ATTN: AGENCIES
- 16 Commandant, U.S. Army Air Defense School, Ft. Belvoir, Mo. ATTN: Command & Staff Dept.
- 17 Commandant, U.S. Army Artillery School, Ft. Sill, Okla.
- 18 Commandant, U.S. Army Artillery and Missile School, Ft. Sill, Okla. ATTN: Combat Development Department
- 19 Commandant, U.S. Army Aviation School, Ft. Rucker, Ala.
- 20 Commandant, U.S. Army Infantry School, Ft. Benning, Ga. ATTN: G-3
- 21 Commandant, U.S. Army Ordnance School, Aberdeen Proving Ground, Md.
- 22 Commandant, U.S. Army Ordnance and Guided Missile School, Aberdeen Arsenal, Md.
- 23 Commanding General, Chemical Corps Training Center, Ft. Belvoir, Mo.
- 24 Commanding General, The Engineer Center, Ft. Belvoir, Mo. ATTN: Asst. Chief, Engr. School
- 25 Director, Armed Forces Institute of Pathology, Walter Reed Army Med. Center, 4950 Judd St., Wt. Washington 25, D.C.
- 26 Commanding Officer, Army Medical Research Lab., Ft. Detrick, Md.
- 27 Commandant, Walter Reed Army Inst. of Res., Walter Reed Army Medical Center, Washington 25, D.C.
- 28-29 Commanding General, 4th Inf. Div., 4th Inf. Div., Fort. Belvoir, Mo. ATTN: G-3 Liaison Officer
- 30-31 Commanding Officer, Chemical Warfare Lab., Ft. Belvoir, Mo. ATTN: Tech. Library
- 32 Commanding General, Engineer Research and Dev. Lab., Ft. Belvoir, Mo. ATTN: Chief, Tech. Support Section
- 33 Director, Chemical Warfare Laboratory, Ft. Belvoir, Mo. ATTN: Library
- 34 Commanding Officer, Biological Research, Ft. Detrick, Md. ATTN: G-3
- 35 Commanding Officer, Biological Research, Ft. Detrick, Md. ATTN: G-3
- 36-37 Commanding General, Aberdeen Proving Ground, Md. ATTN: Director, Biological Research
- 38 Commandant, Army School of Guided Missile Research, Aberdeen Proving Ground, Md. ATTN: Tech. Library
- 39 Commanding General, Aberdeen Proving Ground, Md. ATTN: Director, Biological Research
- 40-41 Commanding General, Aberdeen Proving Ground, Md. ATTN: Director, Biological Research
- 42-43 Commanding General, Aberdeen Proving Ground, Md. ATTN: Director, Biological Research
- 44-45 Commanding General, Aberdeen Proving Ground, Md. ATTN: Director, Biological Research
- 46-47 Commanding General, Aberdeen Proving Ground, Md. ATTN: Director, Biological Research
- 48-49 Commanding General, Aberdeen Proving Ground, Md. ATTN: Director, Biological Research
- 50-51 Commanding General, Aberdeen Proving Ground, Md. ATTN: Director, Biological Research
- 52-53 Commanding General, Aberdeen Proving Ground, Md. ATTN: Director, Biological Research
- 54-55 Commanding General, Aberdeen Proving Ground, Md. ATTN: Director, Biological Research
- 56-57 Commanding General, Aberdeen Proving Ground, Md. ATTN: Director, Biological Research
- 58-59 Commanding General, Aberdeen Proving Ground, Md. ATTN: Director, Biological Research
- 60-61 Commanding General, Aberdeen Proving Ground, Md. ATTN: Director, Biological Research
- 62-63 Commanding General, Aberdeen Proving Ground, Md. ATTN: Director, Biological Research
- 64-65 Commanding General, Aberdeen Proving Ground, Md. ATTN: Director, Biological Research
- 66-67 Commanding General, Aberdeen Proving Ground, Md. ATTN: Director, Biological Research
- 68-69 Commanding General, Aberdeen Proving Ground, Md. ATTN: Director, Biological Research
- 70-71 Commanding General, Aberdeen Proving Ground, Md. ATTN: Director, Biological Research
- 72-73 Commanding General, Aberdeen Proving Ground, Md. ATTN: Director, Biological Research
- 74-75 Commanding General, Aberdeen Proving Ground, Md. ATTN: Director, Biological Research
- 76-77 Commanding General, Aberdeen Proving Ground, Md. ATTN: Director, Biological Research
- 78-79 Commanding General, Aberdeen Proving Ground, Md. ATTN: Director, Biological Research
- 80-81 Commanding General, Aberdeen Proving Ground, Md. ATTN: Director, Biological Research
- 82-83 Commanding General, Aberdeen Proving Ground, Md. ATTN: Director, Biological Research
- 84-85 Commanding General, Aberdeen Proving Ground, Md. ATTN: Director, Biological Research
- 86-87 Commanding General, Aberdeen Proving Ground, Md. ATTN: Director, Biological Research
- 88-89 Commanding General, Aberdeen Proving Ground, Md. ATTN: Director, Biological Research
- 90-91 Commanding General, Aberdeen Proving Ground, Md. ATTN: Director, Biological Research
- 92-93 Commanding General, Aberdeen Proving Ground, Md. ATTN: Director, Biological Research
- 94-95 Commanding General, Aberdeen Proving Ground, Md. ATTN: Director, Biological Research
- 96-97 Commanding General, Aberdeen Proving Ground, Md. ATTN: Director, Biological Research
- 98-99 Commanding General, Aberdeen Proving Ground, Md. ATTN: Director, Biological Research

- 61 Director, Chemical Warfare Laboratory, Ft. Belvoir, Mo.
- 62 Commanding General, U. S. OGD Special Weapons Development Command, Denver, D.C.
- 63 Commander-in-Chief, U.S. Army Europe, AFM 603, New York, N.Y. ATTN: Opt. Div., Weapons Br.

NAVY ACTIVITIES

- 14 Chief of Naval Operations, N/V, Washington 25, D.C. ATTN: OP-0300
- 17 Chief of Naval Operations, N/V, Washington 25, D.C. ATTN: OP-73
- 18-19 Chief of Naval Research, N/V, Washington 25, D.C. ATTN: Code 411
- 20-21 Chief, Bureau of Aeronautics, N/V, Washington 25, D.C.
- 22 Chief, Bureau of Ordnance, N/V, Washington 25, D.C.
- 23 Chief, Bureau of Ships, N/V, Washington 25, D.C. ATTN: Code 423
- 24 Chief, Bureau of Yards and Docks, N/V, Washington 25, D.C. ATTN: Code 430
- 25 Director, U.S. Naval Research Laboratory, Washington 25, D.C. ATTN: Mr. Nathaniel S. Case
- 26-27 Commander, U.S. Naval Ordnance Laboratory, White Oak, Silver Spring 19, Md.
- 28 Commanding Officer and Director, Navy Electronics Laboratory, San Diego 16, Calif.
- 29 Commanding Officer, U.S. Naval Mine Defense Lab., Panama City, Fla.
- 30-31 Commanding Officer, U.S. Naval Anthropological Research Laboratory, San Francisco, Calif. ATTN: Tech. Info. Div.
- 32-33 Commanding Officer and Director, U.S. Naval Civil Engineering Laboratory, Port Hueneme, Calif. ATTN: Code 131
- 34 Commanding Officer, U.S. Naval Submarine Command, U.S. Naval Station, Treasure Island, San Francisco, Calif.
- 35-36 Commandant, U.S. Naval Postgraduate School, Monterey, Calif.
- 37 Officer-in-Charge, U.S. Naval School, CMC Officers, U.S. Naval Construction Engr. Center, Port Hueneme, Calif.
- 38 Commanding Officer, Surface Weapons Training Center, Atlantic, U.S. Naval Base, Norfolk 17, Va. ATTN: Surface Weapons Dept.
- 39 Commanding Officer, Surface Weapons Training Center, Pacific, Naval Station, San Diego, Calif.
- 40 Commanding Officer, U.S. Naval Mine Defense Lab., Panama City, Fla.
- 41-42 Commanding Officer, Naval Air Materiel Center, Philadelphia 12, Pa. ATTN: Technical Data Br.
- 43-44 Commander, Officer U.S. Naval Air Materiel Center, Philadelphia, Pa. ATTN: ASD, Library
- 45-46 Commanding Officer, U.S. Naval Medical Research Institute, Naval Medical Center, Bethesda, Md.
- 47-48 Commanding Officer and Director, Naval U. Taylor Naval School, Washington 25, D.C. ATTN: Library
- 49-50 Commanding Officer and Director, U.S. Naval Engineering Experiment Station, Annapolis, Md.
- 51-52 Commander, U.S. Naval Engineering, Ft. Belvoir, Mo. ATTN: Technical Support to Research Division
- 53-54 Commander, U.S. Naval Corps, Washington 25, D.C. ATTN: Code 423
- 55-56 Director, Marine Corps Training Center, Quantico, Va.
- 57-58 Commanding Officer, U.S. Naval Civil Engineering, Ft. Belvoir, Mo. ATTN: Tech. Info. Div.
- 59-60 Chief, Bureau of Naval Weapons, Navy Department, Washington 25, D.C. ATTN: Code 423

UNCLASSIFIED

UNCLASSIFIED

AIR FORCE ACTIVITIES

- 82 Assistant for Atomic Energy, HQ, INET, Washington 25, D.C. ATTN: DCS/O
- 83 Hq. USAF, ATTN: Operations Analysis Office, Office, Vice Chief of Staff, Washington 25, D.C.
- 84-85 Air Force Intelligence Center, Hq. USAF, ACSI (AFCIN-JVI) Washington 25, D.C.
- 86 Director of Research and Development, DCS/D, Hq. USAF, Washington 25, D.C. ATTN: Guidance and Weapons Div.
- 87 The Surgeon General, Hq. USAF, Washington 25, D.C. ATTN: Bio-Def. Pre. Med. Division
- 88 Commander, Tactical Air Command, Langley AFB, Va. ATTN: Doc. Security Branch
- 89 Commander, Air Defense Command, Ent AFB, Colorado. ATTN: Assistant for Atomic Energy, ADLDC-A
- 90 Commander, Hq. Air Research and Development Command, Andrews AFB, Washington 25, D.C. ATTN: RDRWA
- 91 Commander, Air Force Ballistic Missile Div. Hq. AFMDC, Air Force Unit Post Office, Los Angeles 45, Calif. ATTN: VDOOT
- 92-93 Commander, AF Cambridge Research Center, L. G. Hanscom Field, Bedford, Mass. ATTN: CRAC-2
- 94-98 Commander, Air Force Special Weapons Center, Kirtland AFB, Albuquerque, N. Mex. ATTN: Tech. Info. & Intel. Div.
- 99-100 Director, Air University Library, Maxwell AFB, Ala.
- 101 Commander, Lowry Technical Training Center (TW), Lowry AFB, Denver, Colorado.
- 102 Commandant, School of Aviation Medicine, USAF, Randolph AFB, Tex. ATTN: Research Secretariat
- 103 Commander, 1000th Sp. Wpns. Squadron, Hq. USAF, Washington 25, D.C.
- 104-106 Commander, Wright Air Development Center, Wright-Patterson AFB, Dayton, Ohio. ATTN: WCACT (For WCACT)
- 107-108 Director, USAF Project RAND, VIA: USAF Liaison Office, The RAND Corp., 1700 Main St., Santa Monica, Calif.
- 109 Commander, Rome Air Development Center, AFPC, Griffiss AFB, N.Y. ATTN: Documents Library, RCSEL-1
- 110 Commander, Air Technical Intelligence Center, USAF, Wright-Patterson AFB, Ohio. ATTN: AFCIN-451a, Library
- 111 Assistant Chief of Staff, Intelligence, Hq. USAF, APO 611, New York, N.Y. ATTN: Directorate of Air Targets
- 112 Commander-in-Chief, Pacific Air Forces, APO 991, San Francisco, Calif. ATTN: PFCIN-40, Base Recovery

OTHER DEPARTMENT OF DEFENSE ACTIVITIES

- 113 Director of Defense Research and Engineering, Washington 25, D.C. ATTN: Tech. Library
- 114 Chairman, Armed Services Explosives Safety Board, DOD, Building T-7, Gravelly Point, Washington 25, D.C.
- 115 Director, Weapons Systems Evaluation Group, Room 1B880, The Pentagon, Washington 25, D.C.
- 116-119 Chief, Defense Atomic Support Agency, Washington 25, D.C. ATTN: Document Library
- 120 Commander, Field Command, DASA, Sandia Base, Albuquerque, N. Mex.
- 121 Commander, Field Command, DASA, Sandia Base, Albuquerque, N. Mex. ATTN: PCTG
- 122-126 Commander, Field Command, DASA, Sandia Base, Albuquerque, N. Mex. ATTN: PCMT
- 127 Commander, JTF-7, Arlington Hall Station, Arlington 12, Va.
- 128 Commander-in-Chief, Strategic Air Command, Offutt AFB, Neb. ATTN: OAMS
- 129 Commander-in-Chief, EUCOM, APO 128, New York, N.Y.

ATOMIC ENERGY COMMISSION ACTIVITIES

- 130-132 U.S. Atomic Energy Commission, Technical Library, Washington 25, D.C. ATTN: For DMA
- 133-134 Los Alamos Scientific Laboratory, Report Library, P.O. Box 1661, Los Alamos, N. Mex. ATTN: Helen Feldman
- 135-139 Sandia Corporation, Classified Document Division, Sandia Base, Albuquerque, N. Mex. ATTN: H. J. Smyth, Jr.
- 140-142 University of California Lawrence Radiation Laboratory, P.O. Box 808, Livermore, Calif. ATTN: Cloris G. Craig
- 143 Essential Operating Records, Division of Information Services for Storage and ENE-M. ATTN: John S. Rans, Chief, Headquarters Records and Mail Service Branch, U.S. AEC, Washington 25, D.C.
- 144 Weapon Data Section, Technical Information Service Extension, Oak Ridge, Tenn.
- 145-179 Technical Information Service Extension, Oak Ridge, Tenn. (Surplus)
- ADDITIONAL DISTRIBUTION
- 180 Stanford Research Institute, Menlo Park, Calif. ATTN: Mr. R. B. Valle

SUPPLEMENTARY

INFORMATION



SSTL

Defense Nuclear Agency
6801 Telegraph Road
Alexandria, Virginia 22310-3398

ERRATA

14 September 1995

AD-491310

MEMORANDUM TO DEFENSE TECHNICAL INFORMATION CENTER
ATTN: OCD/Mr Bill Bush

SUBJECT: Change of Distribution Statement

The following documents have been downgraded to Unclassified
and the distribution statement changed to Statement A:

WT-1307, AD-311926
POR-2011, AD-352684
WT-1405, AD-611229
WT-1420, AD-B001855
WT-1423, AD-460283
WT-1422, AD-615737
WT-1225, AD-460282
WT-1437, AD-311158
WT-1404, AD-491310
WT-1421, AD-691406
WT-1304, AD-357971

WT-1305, AD-361774
WT-1303, AD-339277
WT-1408, AD-344937
WT-1417, AD-360872
WT-1348, AD-362108
WT-1349, AD-361977
WT-1340, AD-357964

If you have any questions, please call MS Ardith Jarrett, at
325-1034.

FOR THE DIRECTOR:

Ardith Jarrett
for JOSEPHINE WOOD
Chief
Technical Support

ERRATA

151.20/8